The Journal of Gemmology

Volume 35 / No. 2 / 2016

SSEF SCHWEIZERISCHES GEMMOLOGISCHES INSTITUT SWISS GEMMOLOGICAL INSTITUTE INSTITUT SUISSE DE GEMMOLOGIE

Gem-A THE GEMMOLOGICAL ASSOCIATION OF GREAT BRITAIN

The Gemmological Association of Great Britain

Gem-A

THE GEMMOLOGICAL ASSOCIATION OF GREAT BRITAIN

SPECIAL STUDENT RATE FOR 2016

Gem-A Conference

5–6 November 2016

The Gem-A Conference will be held at the prestigious **Royal Institute of British Architects (RIBA)** in Marylebone, London.

This year will feature talks from the following renowned gem experts:

- Jim Clanin, mining engineer
- Pat Daly, valuer and Gem-A Tutor
- David Fisher, De Beers
- Ian Harebottle, Gemfields
- Bill Larson, Palagems.com
- Helen Molesworth, Gübelin Academy
- Danny Sanchez, photomicrographer
- Robert Weldon, GIA
- Dr Michael Wise, Smithsonian Institution

To keep up to date with the latest from the Conference and for information on how to book please visit the Gem-A website.

Creating gemmologists since 1908

Join us.

The Gemmological Association of Great Britain, 21 Ely Place, London, EC1N 6TD, UK. T: +44 (0) 20 7404 3334 F: +44 (0) 20 7404 8843.
Registered charity no. 1109555. A company limited by guarantee and registered in England No. 1945780. Registered Office: 3rd Floor, 1-4 Argyll Street, London W1F 7LD.

The Journal of Gemmology
Volume 35 / No. 2 / 2016

COLUMNS

ARTICLES

Feature Articles

Gemmological Brief

Cover Photo: These Cu-bearing tourmalines are from Mozambique (13.93 ct cushion and ~5 ct stone in ring) and from Paraíba, Brazil (3.5 mm gems in bracelet and 4.02 ct oval). Courtesy of Collectorfinejewelry.com, Palagems.com (13.93 ct stone) and Leslie Hindman Auctioneers, Chicago, Illinois, USA (4.02 ct gem); photo by Orasa Weldon.

The Journal is published by Gem-A in collaboration with SSEF and with the support of AGL and GIT.

The Journal of Gemmology

Content Submission

The Editor-in-Chief is glad to consider original articles, news items, conference/excursion reports, announcements and calendar entries on subjects of gemmological interest for publication in *The Journal of Gemmology*. A guide to the various sections and the preparation of manuscripts is given at www.gem-a.com/publications/journal-of-gemmology/submit-an-article.aspx, or contact the Production Editor.

Subscriptions

Gem-A members receive *The Journal* as part of their membership package, full details of which are given at www.gem-a.com/membership.aspx. Laboratories, libraries, museums and similar institutions may become Direct Subscribers to *The Journal* (see www.gem-a.com/publications/subscribe.aspx).

Advertising

Enquiries about advertising in *The Journal* should be directed to the Marketing Consultant. For more information, see www.gem-a.com/publications/journal-of-gemmology/advertising-in-the-journal.aspx.

Database Coverage

The Journal of Gemmology is covered by the following abstracting and indexing services: Australian Research Council academic journal list, British Library Document Supply Service, Chemical Abstracts (CA Plus), Copyright Clearance Center's RightFind application, CrossRef, EBSCO (Academic Search International, Discovery Service and TOC Premier), Gale/Cengage Learning Academic OneFile, GeoRef, Mineralogical Abstracts, ProQuest, Scopus and the Thomson Reuters' Emerging Sources Citation Index (in the Web of Science).

Copyright and Reprint Permission

The Journal of Gemmology is published quarterly by Gem-A, The Gemmological Association of Great Britain. Any opinions expressed in *The Journal* are understood to be the views of the contributors and not necessarily of the publisher.

Printed by DG3 (Europe) Ltd.

ISSN: 1355-4565

Gem-A
THE GEMMOLOGICAL ASSOCIATION OF GREAT BRITAIN

21 Ely Place
London EC1N 6TD
UK

t: +44 (0)20 7404 3334
f: +44 (0)20 7404 8843
e: information@gem-a.com
w: www.gem-a.com

Registered Charity No. 1109555
Registered office: Palladium House, 1–4 Argyll Street, London W1F 7LD

Understanding Gems™

What's New

INSTRUMENTS AND TECHNIQUES

ASDI Device Updated

In 2015, SSEF twice updated its own Automated Spectral Diamond Inspection (ASDI) device, and these changes will be included on future orders of the instrument. The system is used to rapidly screen colourless round melee for imitations, HPHT-treated diamonds and synthetic (CVD and HPHT) diamonds. More information is available on SSEF's Swiss Analytical Testing Tools website at www.sattgems.com. *CMS*

D-Secure Synthetic Diamond Detection Instrument

From DRC Techno of Gujarat, India, and unveiled in September 2015, D-Secure is designed to be a cost-effective instrument for detecting colourless to near-colourless synthetic diamonds of all shapes, including rough, ranging from 0.003–10 ct (or larger with a special attachment). The 3-inch scan area establishes the parcel size possible for analysis, and also accommodates some mounted diamonds. Visit www.dsecure.com. *CMS*

Dialite MasterGrader

Available since early 2016, the Dialite MasterGrader from System Eickhorst (Hamburg, Germany) was developed jointly with the Natural Color Diamond Association to provide a standardized grading environment especially for fancy-colour diamonds and other coloured gems. The instrument includes standardized daylight illumination (per ISO/PAS and CIBJO), switchable lighting (LED, UV, and incandescent), diffuse illumination for photography and a neutral grey background. The unit measures 34 × 40 × 15 cm, and a voltage converter and adapter plug are available separately for various regions. Visit http://eickhorst.com/en/gemmological-instruments/dialite-mastergrader/features. *CMS*

GemLab Instrument Updates

In May 2016, GemLab (Vancouver, British Columbia, Canada) announced changes to two of its instruments. The 2016/17 model of the GL Gem Raman PL532 features an upgraded spectrometer, a faster processor and version 3.0 of its GLGemSpec software. The unit is available in two models, TEC (5400–100 cm^{-1}) and PL (530–750 nm). Also included is a band-pass filter to suppress fluorescence in Raman mode. The 2016/17 model of the GL Gem Spectrometer also incorporates a new processor and GLGemSpec 3.0 software. The portable UV-Vis-NIR spectrometer can be operated using a Windows laptop via a USB 2.0 connection. The spectral range is 300–1000 nm, in transmission mode with 1.5 nm resolution. The unit measures 17 × 10 × 5 cm and comes with a specimen holder. Optional accessories include a fibre-optic probe, a cosine corrector kit and a Xenon flashlight kit. Visit www.cigem.ca/research-technology/gl-gem-raman and www.cigem.ca/research-technology/gl-gem-spectrometer. *CMS*

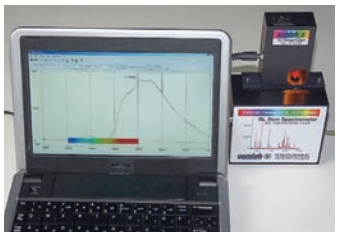

NEWS AND PUBLICATIONS

De Beers' 2015 Diamond Jewellery Demand and Outlook for 2016

Released in April 2016, this De Beers Group report includes statistics on diamond jewellery sales for 2015 compared to 2014. Consumer demand rose 2%, but sales (in US$) declined 2% due to the strength of the US dollar. Growth based on polished wholesale prices was greatest in the USA, followed by China. The report concludes with the outlook for 2016. PDFs and MP4 videos are available for download, along with the online report, at www.debeersgroup.com/en/reports/insight/flash-data/flash-data-Apr2016.html. *CMS*

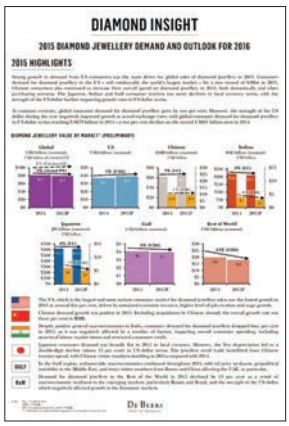

GIT Laboratory Updates

The Gem and Jewelery Institute of Thailand (GIT) released a Lab Update on 1 March 2016 regarding a specimen of 'ruby in marble' containing a polished rod of synthetic ruby embedded in a hole drilled into a piece of marble. After insertion, the exposed portion of the synthetic ruby was polished to create an appearance of natural faces. On 11 May 2016, GIT posted a Gemstone Update on purple garnet from Mozambique that describes the standard gem properties, inclusions and chemical composition of this attractive material. To download these and previous GIT reports, visit www.git.or.th/2014/articles_technic_en.html. *CMS*

GIT Trade Review 2015

Posted in February 2016, this GIT publication reviews Thailand's gem and jewellery import-export performance in 2015. The overall export value

increased 9.27% over 2014, with the main markets being Hong Kong, Switzerland, USA and Cambodia. The import value of gems and jewellery grew 4.38%, with the main sources being Switzerland, Japan, Australia and Hong Kong. Download the report at www.git.or.th/2014/git_trade_publication_en. html. *BML*

IAA Newsletter

The March 2016 issue of *Bursztynisko*, the bilingual (Polish and English) newsletter of the International Amber Association (IAA), can be downloaded at www.amber.org.pl/index.php/download_file/view/474. Articles in this 20th anniversary issue cover the history of IAA, description of the IAA Gallery in Gdańsk, amber classification, amber craft and goldsmiths in 16th–18th century Gdańsk, palaeontological inclusions in amber, mapping of old amber mines in Poland, amber mining in Ukraine, Burmite and recent Baltic amber prices. A report on observations in the IAA Amber Laboratory over the past year describes various simulants seen and methods of testing performed at the lab. *CMS*

ICGL *Newsletter*

Issue 1 for 2016 of the newsletter from the International Consortium of Gem-Testing Laboratories focuses on rubies, with articles on 'blood red' rubies from Madagascar, 'pigeon-blood' coloration and asterism caused by 'tialite' needles in rubies from India. Download the newsletter at http://icglabs.org. *CMS*

IGDA News and Overview of the Lab-Grown Diamond Industry 2015–2016

In February 2016, leading synthetic diamond producers, distributors and retailers formed the International Grown Diamond Association (IGDA).

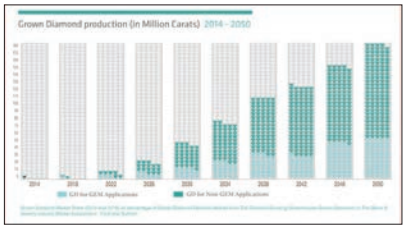

Selected news stories about synthetic diamonds are posted in the Market News section of the IGDA website at http://theigda.org/news, and a report titled 'Overview of the Lab-Grown Diamond Industry in 2015–16' reviews the production of synthetic diamonds beginning in 2014 (around 360,000 carats) and projects growth through 2050 (anticipated to be ~2 million carats). For the full report, visit http://theigda.org/education/an-overview-of-the-grown-diamond-industry-in-2015-16. *CMS*

JGGL *Gem Information*

The latest *Gem Information* (in Japanese, Vol. 43, 2015) from the Japan Germany Gemmological Laboratory in Kofu, Japan, covers demantoid from Pakistan, colour terminology in the gem trade, melee-size synthetic diamonds from India and China, black opal and green amber from Ethiopia, and a report on the 2015 Tucson gem shows. English-language abstracts (posted in December 2015) are available at www.sapphire.co.jp/jggl/978.htm. *CMS*

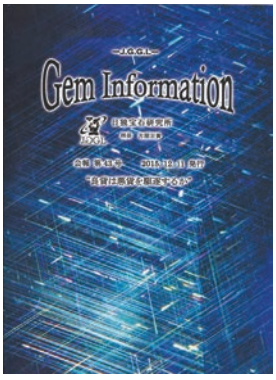

Kyawthuite, a New Mineral from Mogok, Myanmar

A new mineral has been discovered as a faceted gemstone from Mogok, Myanmar. Kyawthuite ($BiSbO_4$) is named after Dr Kyaw Thu of Macle Gem Trade Laboratory, Yangon, Myanmar. The original pebble was recovered in 2010 and suspected to be scheelite. When Dr Thu faceted the 1.61 ct reddish orange gemstone, he recognized it as something unusual. The full description of kyawthuite will be published in an article by A. R. Kampf, G. R. Rossman, C. Ma and P. A. Williams in *Mineralogical Magazine* (download the preprint at www.ingentaconnect.com/content/minsoc/mag/pre-prints/content-minmag-1285). *BML*


G. Rossman

Margaritologia Pearl Newsletter

In December 2015, *Margaritologia* No. 2/3 was released by Gemmologisches Institut Hamburg, Germany. This latest issue features cultured pearls from Lake Kasumigaura, Japan, beginning with the import of mussels from Lake Biwa in 1931. The report covers the history of development, culturing methods, breeding of mussels, marketing, description of the pearls and development of 'Kasumigaura-type' cultured pearls in China. To subscribe to the newsletter, visit www.gemmologisches-institut-hamburg.de. *CMS*


MARGARITOLOGIA
CULTURED PEARLS FROM LAKE KASUMIGAURA

PDAC Diamond Abstracts

Abstracts are available for download from the 2016 conference of the Prospectors & Developers Association of Canada, held in Toronto, Ontario, Canada. A session titled 'Diamonds in Southern Africa: Back to the Beginning' consisted of five presentations: (1) a summary of diamond resources by Mike de Wit of Tsodilo Resources, (2) information on Petra Diamonds by Jim Davidson, (3) the Karowe mine by John Armstrong of Lucara Diamond Corp., (4) the future of the international diamond business by John Bristow of Global Diamond Network and (5) the status of the diamond industry by Chaim Even-Zohar of Tacy Ltd. Download the abstracts at www.pdac.ca/convention/programming/technical-program/sessions/technical-program/diamonds-in-southern-africa-back-to-the-beginning. *CMS*

Photomicrographs of Fossils in Amber

Two articles by Drs David Penney and David Green in *Deposits Magazine* dated 11 and 15 December 2015 focus on 'Biodiversity of fossils in amber' and 'Preparation and study of fossils in amber'. The first lists important amber deposits worldwide with examples of exceptional insect fossils and typical source-identification characteristics. The second article explores how to prepare amber samples to reveal the fossils within, and how to photograph these inclusions using conventional photomicrography and computed tomography. Visit https://depositsmag.com/2015/12/11/biodiversity-of-fossils-in-amber and https://depositsmag.com/2015/12/15/preparation-and-study-of-fossils-in-amber. *CMS*

Precious Stones Multi-Stakeholder Working Group Study

Available online April 2016, a report from the Precious Stones Multi-Stakeholder Working Group dated 16 July 2015 was commissioned by Jewelers of America and authored by members of Sustainable & Responsible Solutions Ltd. and Estelle Levin Ltd.

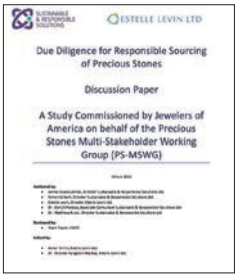

It examines the status of due diligence approaches in the gem industry and addresses the need for future developments within that supply chain. The issues focus on social responsibility based on the UN Guiding Principles on Business and Human Rights, from sourcing of gems through retail practices. Download the report at www.dmia.diamonds/wp-content/uploads/2014/11/PS-MSWGPreciousStonesReportFinal.pdf. *CMS*

Santa Fe Symposium Proceedings

Released in April 2016 are 23 presentations from the 2015 Santa Fe Symposium (held in Albuquerque, New Mexico, USA), with abstracts online and PDFs of the full presentations available for download. Topics include methods of preparing various metals for jewellery making, innovative alloys, manufacturing methods and more. Visit www.santafesymposium.org/2015-santa-fe-symposium-papers/?category=2015. *CMS*

OTHER RESOURCES

AIGS Gem Dictionary App

The Asian Institute of Gemological Sciences (AIGS) updated its searchable Chinese-English Gem Dictionary app in October 2015. Adapted by AIGS from Akira Chikayama's *Dictionary of Gemstones & Jewelry*, the app is suitable for both amateur and professional gemmologists. Terms can be searched in both English and Chinese, and translations between the two languages are also available. For more information, including links to download iOS and Android versions, visit www.aigsthailand.com/gem_dictionary.aspx. *CMS*

Corporate Social Responsibility Course

In April 2016, CIBJO's World Jewellery Confederation Education Foundation (WJCEF) launched an online educational course titled 'CSR for the Jewellery Professional'. The course consists of six lessons: 'Practical Definitions of CSR', 'Major CSR Issues Affecting the Jewellery Industry', 'The Business Case for CSR', 'Tools and Approaches for Implementing CSR', 'Making "Green" Claims and Consumer Protection Law' and 'Professional CSR Accreditation'. Students who complete the course requirements will receive a Level 1 Certificate of Accreditation from WJCEF. For more information and course registration, go to http://cibjo-csr.btassurance.com. *CMS*

What's New provides announcements of new instruments/technology, publications, online resources and more. Inclusion in What's New does not imply recommendation or endorsement by Gem-A. Entries are prepared by Carol M. Stockton (CMS) or Brendan M. Laurs (BML).

The Fire Within

"For in them you shall see the living fire of the ruby, the glorious purple of the amethyst, the sea-green of the emerald, all glittering together in an incredible mixture of light."

– Roman Elder Pliny, 1st Century AD

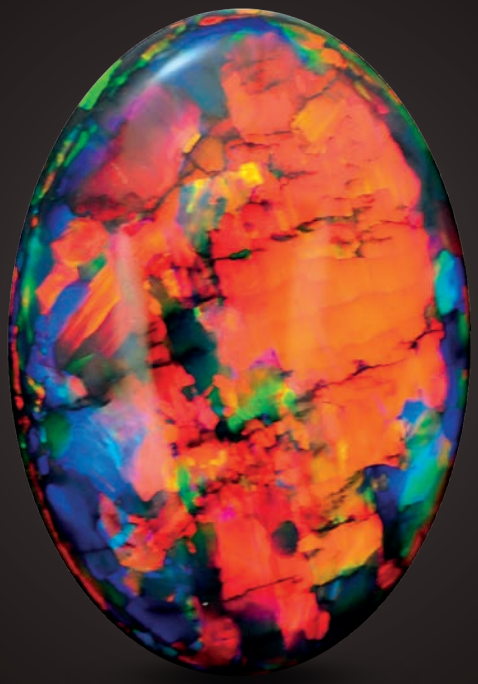

Black Opal 15.7 Carats

Suppliers of Australia's finest opals to the world's gem trade.

CODY OPAL

Level 1 - 119 Swanston Street Melbourne Australia

T. +61 3 9654 5533 E. INFO@CODYOPAL.COM

WWW.CODYOPAL.COM

INTERNATIONAL COLORED GEMSTONE ASSOCIATION MEMBER

JOG

Gem Notes

COLOURED STONES

Axinite from Shigar Fort, Northern Pakistan

While on a buying trip to Pakistan in October 2014, one of the authors (DB) saw an old friend in Skardu who had financed a mining venture to work an alpine cleft deposit (series of hydrothermal veins) located above Shigar Fort, a historical site on the outskirts of Shigar town. This area is the gateway to the Shigar Valley, which is famous for producing well-formed crystals of aquamarine, topaz, garnet and other minerals (e.g. Agheem et al., 2014). The dealer had about 3.5 kg of axinite from the Shigar Fort deposit, mostly as broken or poorly formed crystals ranging from 2.5 to 7.0 cm long. Approximately 1 kg of the more transparent pieces were purchased by this author, and many contained silky string-like inclusions that produced a slight schiller effect. Twenty-one pieces weighing 135.4 g were sent to the cutting factory, resulting in 40 faceted stones totalling 25.03 carats (ranging from 0.12 to 3.44 ct each), and two cabochons weighing a total of 12.36 carats. The cutters were instructed to produce clean faceted stones with proper depth, and for the cabochons it was hoped that a cat's-eye effect would result from the silky inclusions. The yield was small due to the presence of fractures and the silky inclusions, as well as the typically thin dimensions of the platy rough material.

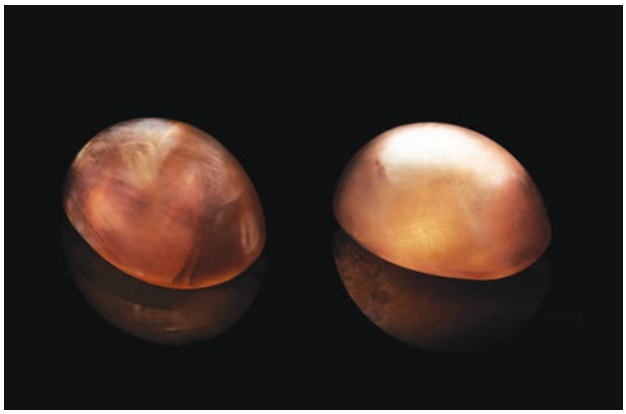

Figure 1: Weighing 6.57 and 5.79 ct, these axinite cabochons are from near the historic Shigar Fort in northern Pakistan. Photo by Bilal Mahmood and Alex Mercado.

Figure 2: Coarse irregular tubules form abundant inclusions in the Pakistan axinite. Photomicrograph by B. Clark; magnified 40×.

The two cabochons (Figure 1) were characterized by one of the authors (BC) for this report. They weighed 6.57 and 5.79 ct, and both were reddish brown, with moderate pleochroism of light brown and purple-brown. The spot RI values of both stones were 1.67–1.69, yielding a birefringence of 0.02. Hydrostatic SG values for the two samples were 3.28 and 3.29. These values are similar to those of axinite from elsewhere in Pakistan (Baluchistan: Fritz et al., 2007), except that the birefringence from these spot readings was somewhat higher. Both stones were inert to long- and short-wave UV radiation. They contained similar inclusion features, consisting of abundant long irregular tubules throughout the stones as well as partially healed fissures and clouds of fine particles (Figure 2).

The identification as axinite was confirmed with Raman spectroscopy using a 514 nm laser. Spectra collected with a multi-channel ultraviolet-visible–near infrared (UV-Vis-NIR) spectrometer revealed weak absorptions at 490 and 515 nm, as well as a broad transmission window at around 780 nm. Energy-dispersive X-ray fluorescence (EDXRF) chemical analysis showed major amounts of Al, as well as traces of Fe, Mn and Mg, consistent with O'Donoghue's (2006) observation that axinite is a mineral group that may contain a combination of the various end members within a single stone (similar to garnet). Agheem et al. (2014) reported an Fe-dominant composition for similar axinites from nearby deposits (Hashupa and Alchuri, located 15–20 km upriver from Shigar Fort), classifying them as ferroaxinite, now called axinite-(Fe).

Axinite is both pyroelectric and piezoelectric, meaning that it will develop a temporary electrical charge when heat or pressure is applied (e.g. Martin, 1931). Although no voltage reading was seen using a basic multimeter when both of the present samples were heated, they were warmed only slightly during this experiment to avoid damaging them.

Bryan Clark (bclark@aglgemlab.com)
American Gemological Laboratories
New York, New York, USA

Dudley Blauwet
Dudley Blauwet Gems, Louisville, Colorado, USA

References

Agheem M.H., Shah M.T., Khan T., Murata M., Arif M. and Dars H., 2013. Shigar Valley gemstones, their chemical composition and origin, Skardu, Gilgit-Baltistan, Pakistan. *Arabian Journal of Geosciences*, **7**(9), 3801–3814, http://dx.doi.org/10.1007/s12517-013-1045-8.

Fritz E.A., McClure S.F., Shen A.H., Laurs B.M., Simmons W.B. and Falster A.U., 2007. Gem News International: Color-zoned axinite from Pakistan. *Gems & Gemology*, **43**(3), 254–255.

Martin A.J.P., 1931. On a new method of detecting pyroelectricity. *Mineralogical Magazine*, **22**, 519–523, http://dx.doi.org/10.1180/minmag.1931.022.133.04.

O'Donoghue M., Ed., 2006. *Gems*, 6th edn. Butterworth-Heinemann, Oxford, 386.

Cat's-eye Diaspore from Turkey

Gem-quality diaspore appeared on the market in the mid-1980s, but its availability remained small and sporadic until a deposit in southwestern Turkey started being mined—mainly for gem rough—in the mid-2000s by Zultanite Gems LLC (Hatipoglu and Chamberlain, 2011). Significant quantities of gem diaspore, commonly showing a somewhat alexandrite-like colour change, became more widely available. The deposit has yielded transparent material suitable for faceted stones, and also some cabochons have been cut, but only rarely have they been mentioned as showing a cat's-eye effect (e.g. Kammerling et al., 1995). Therefore, it was interesting to see several chatoyant diaspore cabochons—some of them quite large—exhibited at the 2016 Tucson gem shows. Gem dealer Leonardo Silva Souto (Gems in Gems, Teófilo Otoni, Brazil) had approximately 50 cabochons weighing up to 335 ct. Most of the gems were yellowish green in daylight and yellowish brown in incandescent light. Some of the smaller gems displaying sharper eyes were purchased by Mauro Pantò (The Beauty in the Rocks, Sassari, Italy), who loaned a 4.60 ct sample for this report (Figure 3).

The sample showed a slight colour change, from greyish yellowish green (in daylight) to pale brown (in incandescent light). The polariscope revealed the stone was biaxial, and spot RI readings of 1.68–1.72 were obtained with the refractometer, yielding a birefringence of 0.04. The hydrostatic SG was 3.28. These properties are comparable to those reported for diaspore by O'Donoghue (2006). The stone was inert to both long- and short-wave UV radiation. Inclusions consisted of numerous coarse tubules throughout the stone (Figure 4), which were responsible for the cat's-eye effect. EDXRF spectroscopy revealed major Al as well as traces of Fe, Ti and Ga. Analysis with a multi-channel UV-Vis-NIR spectrometer revealed absorption bands at 385, 438 and 560 nm, which differed from those at

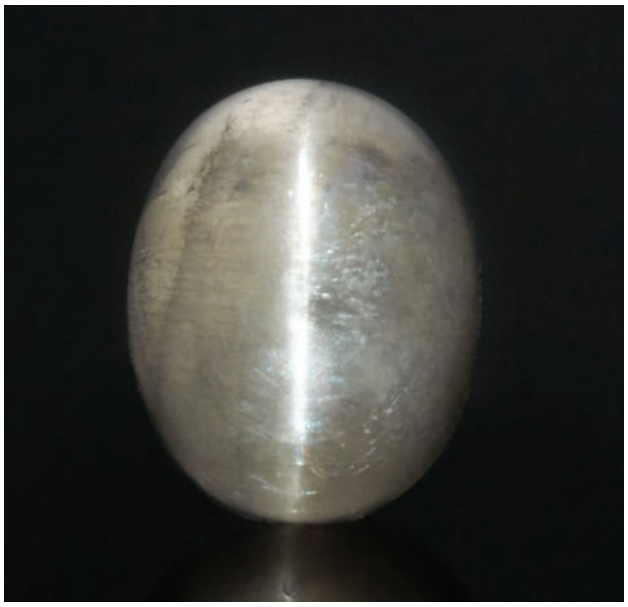

Figure 3: This chatoyant 4.60 ct diaspore from Turkey displays a sharp 'eye'. Photo by Bilal Mahmood.

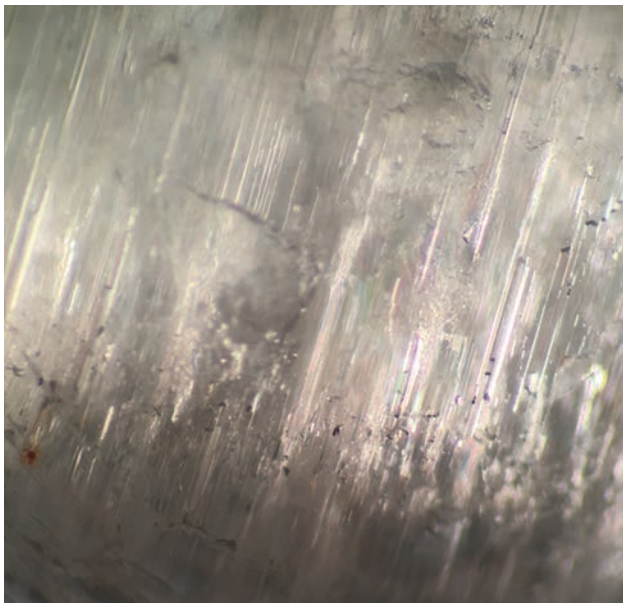

Figure 4: Coarse, parallel growth tubules are responsible for the cat's-eye effect in the diaspore. Photomicrograph by B. Clark; magnified 50×.

454, 463 and 471 nm reported for some diaspore by O'Donoghue (2006).

According to Mauro Pantò, much of the Turkish diaspore he has encountered is heavily included, and some of this material contains abundant tubules that could produce chatoyancy. Therefore it would not be surprising to see more cat's-eye diaspore enter the market in the future.

Bryan Clark

References

Hatipoglu M. and Chamberlain S.C., 2011. A gem diaspore occurrence near Pinarcik, Mugla, Turkey. *Rocks & Minerals*, **86**(3), 242–249, http://dx.doi.org/10.1080/00357529.2011.568304.

Kammerling R.C., Koivula J.I. and Fritsch E., Eds., 1995. Gem News: Diaspore from Turkey. *Gems & Gemology*, **31**(1), 60.

O'Donoghue M., Ed., 2006. *Gems*, 6th edn. Butterworth-Heinemann, Oxford, 404.

Polymer-filled Star Enstatite from Norway

Fe-rich enstatite with a brassy brown colour was first called *bronzite* by Karsten (1808); it is part of the enstatite-ferrosilite $(Mg,Fe)_2(Si_2O_6)$ pyroxene solid-solution series. Star enstatite is rare, but has been known for decades. Eppler (1967) described a dark brown, six-rayed star enstatite from southern India, with asterism reportedly caused by thin oriented rutile needles intersecting one another at 51° and 64°. Henn and Bank (1991) documented a brown six-rayed star 'bronzite' that contained oriented hollow channels as the cause of the star effect. Brown enstatite with star and cat's-eye phenomena due to rutile needles and fibrous sillimanite were described in Gübelin and Koivula (2008). This report characterizes star enstatite from a reportedly new find in south-west Norway.

The sample was loaned by Michael Wild (Werner Wild, Idar-Oberstein, Germany), and consisted of a 20.89 ct brassy-brown cabochon showing a weak four-rayed star (Figure 5, left). Also supplied for our research were two slices that were reportedly cut from the same piece of rough as the cabochon. Refractive indices measured on one of the slices were $n_x = 1.685$, $n_y = 1.693$ and $n_z = 1.697$, yielding a birefringence of 0.012. The hydrostatic SG of the cabochon

A. Kleiman & Co.

Simply...
Pure...
Quality

Natural and Untreated

+1-415-982-3500

Tucson AGTA GemFair

Hong Kong March Gem Show at the Asia World Expo

BASELWORLD

Las Vegas AGTA GemFair

Hong Kong September Gem Fair at the Asia World Expo

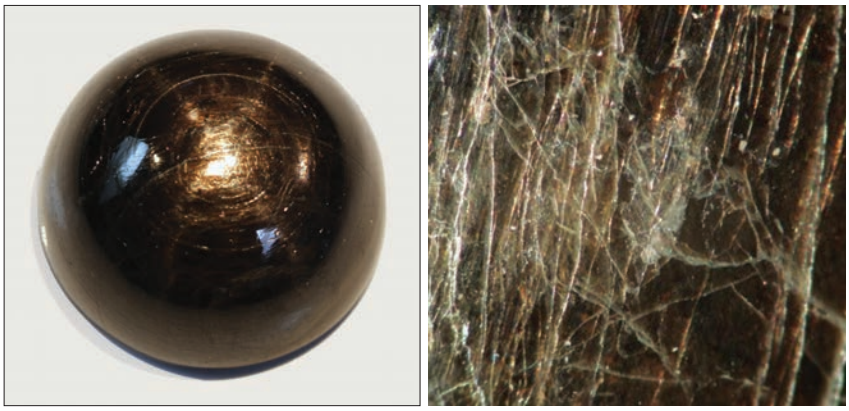

Figure 5: This star enstatite from Norway weighs 20.89 ct (left). Whitish areas in the enstatite cabochon reveal the presence of fractures filled with epoxy resin (right, magnified 30×). Photos by F. Schmitz.

was 3.35. These values are within the expected range for iron-rich enstatite. Chemical analysis of one of the slabs with a Jeol JXA-8200 electron microprobe yielded the formula $(Fe_{0.50}Mg_{1.43}Al_{0.10}Ca_{0.01}Mn_{0.006})(Si_{1.85}Al_{0.15})O_6$.

Examination with a gemmological microscope revealed slightly whitish areas on the surface of the cabochon that corresponded to filled fissures (Figure 5, right). Raman analysis with a Renishaw inVia spectrometer (514 nm laser) showed that the filler consisted of an artificial polymer (epoxy resin), which apparently was used to enhance the surface lustre and stabilize the stone. Microscopic examination also showed oriented inclusions consisting of needles and platelets (Figure 6, left) that apparently were responsible for the star effect. Measured at the top of the cabochon, the inclusions intersected one another at approximately 64°, which also is the angle displayed by the rays of the star when observed from above. This is not consistent with the orthorhombic crystal form of enstatite, but rather a pseudo-hexagonal symmetry that was apparently induced by the cutting orientation. The stone was probably cut slightly oblique to the c-axis, resulting in the appearance of a four-rayed star.

Chemical analysis of the oriented inclusions in one of the slices (using the microprobe's energy-dispersive system) revealed that they were ilmenite. The width of the ilmenite needles and platelets varied between 5 and 50 µm (e.g. Figure 6, right), and they were up to 0.5 mm long. In addition to these inclusions, it is possible that oriented cracks, fissures and/or exsolution areas in the enstatite also contributed to the asterism. Some additional inclusions (not related to the asterism) analysed with the microprobe consisted of rutile and apatite, as well as an unidentified phase. The presence of ilmenite and rutile inclusions in this enstatite is consistent with the existence of titanium deposits in southern Norway (Diot et al., 2003).

Fabian Schmitz (f.schmitz@dgemg.com),
Tom Stephan and Stefan Müller
German Gemmological Association, Idar-Oberstein

Figure 6: The star enstatite contains oriented needles and platelets that were identified as ilmenite (left, magnified 30×). Backscattered-electron imagery (right) clearly reveals the oriented ilmenite inclusions (bright areas) against the enstatite matrix. Analysis of the medium grey area at the end of the central ilmenite inclusion gave only a carbon signal, suggesting that it may consist of a void filled by the epoxy resin used to treat the stone. Images by F. Schmitz.

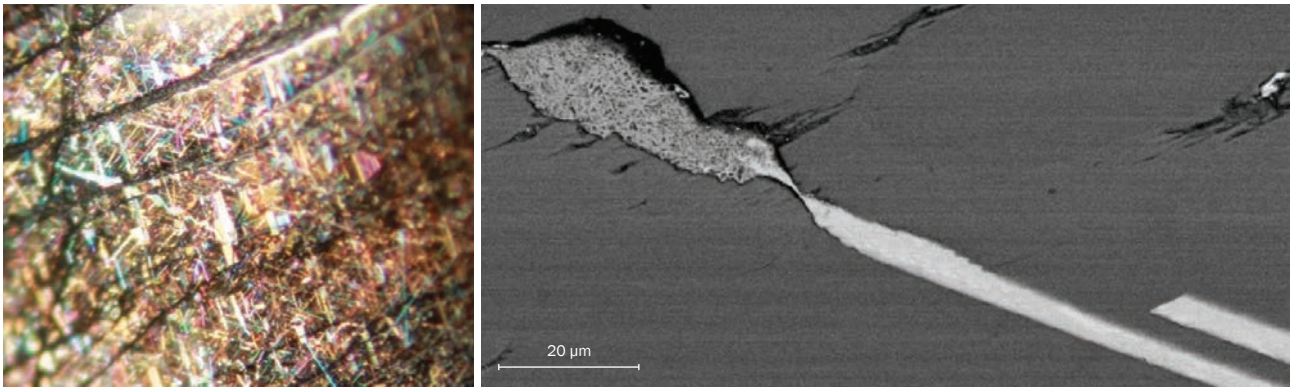

References

Diot H., Bolle O., Lambert J.-M., Launeau P. and Duchesne J.-C., 2003. The Tellnes ilmenite deposit (Rogaland, south Norway): Magnetic and petrofabric evidence for emplacement of a Ti-enriched noritic crystal mush in a fracture zone. *Journal of Structural Geology*, **25**, 481–501, http://dx.doi.org/10.1016/s0191-8141(02)00050-0.

Eppler W.F., 1967. Star-diopside and star-enstatite. *Journal of Gemmology*, **10**(6), 185–188, http://dx.doi.org/10.15506/jog.1967.10.6.185.

Gübelin E.J. and Koivula J.I., 2008. *Photoatlas of Inclusions in Gemstones*, Vol. 3. Opinio Publishers, Basel, Switzerland.

Henn U. and Bank H., 1991. Sternbronzit aus Sri Lanka. *Zeitschrift der Deutschen Gemmologischen Gesellschaft*, **40**(2/3), 145–148.

Karsten D.L.G., 1808. *Mineralogische Tabellen*. Heinrich August Rottmann, Berlin, Germany.

Garnet Mining near Mahenge, Tanzania

In late 2015, a new alluvial garnet deposit was discovered near Mahenge, Tanzania, that has produced attractive pyrope-almandine-spessartine (Williams and Williams, 2016). For two days in April 2016, rough stone dealer Sir-Faraz 'Farooq' Hashmi (Intimate Gems, Glen Cove, New York, USA) visited the deposit while on a buying trip to Tanzania. He was told that he was the first foreigner to enter the mining area.

The journey was difficult due to wet and muddy conditions caused by the rainy season. From the town of Mahenge, Hashmi was taken by motorcycle to Mbella near the village of Epanko. The ~17 km trip was expected to take 40 minutes, but it actually took one hour and 40 minutes on the narrow rough roads. This was followed by a two-hour walk for 2–3 km on a steeply uphill trail to the mining area. Only a few simple houses were seen during the beginning of the hike in this largely uninhabited area.

The garnets were being mined along a ~2-km-long drainage surrounded by hills that were locally forested (Figure 7). Multiple landowners farm the area where the garnets were discovered, and they sold mining privileges to people who funded digging operations in the valley. Hundreds of pits have been dug in a somewhat chaotic pattern. In each pit, after the garnet-bearing gravel layer was exhausted a new adjacent pit was started. Blue-tarped shelters were constructed by the miners near some of the pits. Hashmi indicated that several dozen people were actively digging during his visit, although he was told that many more miners were present before the start of the

Figure 7: This image (taken in April 2016) shows a portion of the garnet-mining area near Mahenge, Tanzania. Photo by Farooq Hashmi.

rainy season. In addition, several of them recently left the area to try their luck at a new garnet area located about three hours away by foot.

The mines consisted of small hand-dug pits that were filled with various amounts of water (e.g. Figure 8). Hashmi saw only one gasoline-powered pump in operation during his visit. Water from the pump was used to wash the gem-bearing gravels, which were placed into wood-framed screens (Figure 9, right). Most of the gravel washing was done using metal pans, and then the garnets were hand-picked from the screens (e.g. Figure 9, left). Garnet is the only gem found in the gravels; this area has not produced any spinel, tourmaline or other gem minerals known from the Mahenge region.

Hashmi saw only a few of the 'Mahenge malaya' garnets while visiting the mining area, and in Mahenge town he observed ~½ kg of rough material (e.g. Figure 10). The colours ranged from pinkish orange (referred to by the traders as *champagne*) to pink to purple (*rhodolite*). Most of the pieces weighed ~½ g, and Hashmi estimates that the deposit has yielded a total of 30–40 kg of garnet since mining began in November 2015. The largest pieces known to him weighed up to

Figure 8: The garnet-bearing alluvial material is excavated from small water-filled pits using simple hand tools. Photo by Farooq Hashmi.

Figure 9: The mined material is washed with metal pans (left) or with pumped water (right), and then the garnets are hand-picked from the screens. Photos by Farooq Hashmi.

Figure 10: This parcel, seen in Mahenge, shows the colour range of the 'Mahenge malaya' garnet. The pieces range from ~0.5 to 5 g. Photo by Farooq Hashmi.

12 g (pinkish orange) and 15–20 g (purple); most of the larger stones have been sent to Germany for cutting.

Brendan M. Laurs

Reference

Williams C. and Williams B., 2016. Gem Notes: Garnet from Mahenge, Tanzania. *Journal of Gemmology*, **35**(1), 10–12.

Kyanite from Pakistan

During a buying trip to northern Pakistan in June 2015, author DB was shown gem-quality blue kyanite at the home of a local miner in Doko village in the Basha Valley of the Haramosh Mountains. He obtained the entire production at the time—3.78 kg—which consisted of crystals and fragments ranging from 2.5 to 6.0 cm long that were heavily encrusted with iron-stained mica schist. The kyanite deposit is reportedly accessed by climbing 7–8 hours south of Doko village.

Upon returning home, author DB cleaned some of the crystals using a high-pressure water gun, which exposed small transparent areas of the kyanite that ranged from light greyish blue to an attractive violetish blue. He sent 10 pieces weighing 116.1 g to his cutting factory, and instructed them to cut only clean stones. In January 2016, the cutting factory returned 24 stones totalling 15.07 carats; at 0.15–0.85 ct, most of the gems were rather small. More of the kyanite will be cut in the future.

For this report, author WMM characterized a pair of oval modified-brilliant-cut kyanites measuring 6.76 × 4.84 × 3.47 and 6.89 × 5.18 × 3.17 mm; each weighed 0.85 ct. Also examined was a 9.84 g piece of rough material measuring 46.93 × 14.19 × 7.50 mm (Figure 11). Seen in the face-up position with the naked eye, both of the faceted stones were evenly coloured with a bright and pleasant blue hue, and they were transparent with a vitreous lustre. When viewed in the microscope with diffuse transmitted light, both gems showed subtle blue and colourless zoning. The rough was mostly opaque with just a few transparent areas, and displayed colour zoning (in blue and white), local iron staining and a pearly lustre. The RIs of both faceted stones were 1.710–1.728, giving a birefringence of 0.018. Both gems were biaxial positive, which is unusual for kyanite but consistent with material from Nepal (Fritsch, 2002; Henn and Schollenbruch, 2012). The hydrostatic SG value

Figure 11: These faceted (each 0.85 ct) and rough (9.84 g) kyanite samples are from a new deposit in the Haramosh Mountains of Pakistan. Photo by Bilal Mahmood.

of one of the faceted samples was 3.86, well above the typical range for kyanite (e.g. 3.65–3.68: Henn and Schollenbruch, 2012). This may be due to the presence of dark included crystals (one of them was fairly large); similar inclusions in Nepalese kyanite were speculated as ilmenite (SG = 4.7) by Henn and Schollenbruch (2012). The SG of the other faceted sample was 3.54, and although some minute dark inclusions were also present in that stone, this low value was likely caused by a large hollow tube-like inclusion. Other internal features observed in the two faceted stones consisted of parallel whitish growth tubes that were oriented in a single direction, and cleavage fractures evident as several parallel shiny breaks. The rough displayed two directions of white growth tubes (or fibrous inclusions) intersecting at 90°.

All three stones showed identical spectra with a CCD-array UV-Vis spectrophotometer, and the features were consistent with those shown by Nepalese kyanite. Weak peaks at approximately 380 and 385 nm, as well as at 435 and 445 nm, are caused by Fe^{3+} substituting for Al^{3+}, and a broad absorption at approximately 600 nm (the cause of the blue colour) is due to Fe^{2+}–Ti^{4+} intervalence charge transfer (Henn and Schollenbruch, 2012). Small peaks at 690 and 710 nm indicated trace amounts of chromium, which was also the cause of very weak red long-wave UV fluorescence seen in the two gems. It should be noted that the UV-Vis spectra were quite similar to those of blue sapphire, with a subtle shift in the position of the absorption bands that is probably related to differences in the crystal structure of the minerals (corundum is hexagonal, and kyanite is triclinic). Mid-infrared spectroscopy of the two samples using a Thermo Scientific Nicolet 6700 FT-IR produced spectra that were consistent with kyanite.

Although the initial production of this kyanite has been rather small, Pakistan now joins Nepal as a source of facetable blue kyanite from the Himalayan region. Kyanite from the two localities is quite similar, except that stones from Nepal are typically larger. Additional production of the Pakistani kyanite will probably be limited by the rigorous climb to the remote, high-altitude mining area, as well as the relatively low value of the material, making it likely that the local miners will pursue other gem materials in the area.

Wendi M. Mayerson (wmayerson@aglgemlab.com)
American Gemological Laboratories
New York, New York, USA

Dudley Blauwet

References

Fritsch E., 2002. Gem News International: Blue, biaxial positive kyanite from Nepal. *Gems & Gemology*, **38**(1), 96–99.

Henn U. and Schollenbruch K., 2012. Saphirblauer Disthen (Kyanit) aus Nepal. *Gemmologie: Zeitschrift der Deutschen Gemmologischen Gesellschaft*, **61**(3-4), 91–98.

Mayer & Watt

Download the Mayer and Watt
App for iOS/Droid.

We *Deal* in inspiration...Naturally.

US#: 606.564.3400 | www.mayerandwatt.com

Black Star Sapphires from Liberia

Black star sapphires are well-known from Thailand and Australia (e.g. Wüthrich and Weibel, 1981; Moon and Phillips, 1984). During the 2016 Tucson gem shows, Eric Braunwart (Columbia Gem House, Vancouver, Washington, USA) had black star sapphires from a new locality: Liberia. He indicated that this material has been produced since approximately mid-2015, commonly as large crystals (approaching 250 g). The rough is processed by first identifying its crystallographic orientation, then slicing it into slabs, and finally looking for areas that are likely to show asterism when cutting cabochons. Approximately 1,000 cabochons have been cut so far, ranging from 8 × 6 mm to 30 ct (e.g. Figure 12).

Braunwart loaned a 7.01 ct cabochon for examination, and the stone was confirmed as corundum using a GemmoRaman-SG spectrometer. The six-rayed star was slightly off centre and consisted of one strong band and two weaker bands. Its colour appearance was similar to other black star material, and its slightly translucent edges showed a medium greyish 'golden' brown body colour. Magnetic susceptibility was moderately strong, with the sample easily dragged by an N-52 neodymium magnet.

Microscopic observation revealed a consistent cross-hatched texture due to repeated parallel parting planes in two directions. Scattered short, dark stick-like inclusions (Figure 13) were identified as hematite by an Enwave 785 micro-Raman spectrometer. With 40× magnification, fine, short, silvery-gold needles created 'silk' in the stone that was responsible for the asterism. EDXRF spectroscopy with an Amptek X123-SDD unit revealed high contents of Fe and Ti—even higher than in Thai black star sapphires in these authors' experience. Calcium was nearly three times the concentration of the Thai stars, suggesting a possible metamorphic influence.

The back of the cabochon was smooth and well-polished, showing no signs of delaminating parting planes (as is commonly seen in Thai black stars, requiring stabilization with a polymer). As reserves of black star sapphires are depleted, this additional West African source is welcome news. Braunwart is stockpiling additional rough material, and the deposit appears to show good potential for future production.

Cara Williams FGA and Bear Williams FGA
(info@stonegrouplabs.com)
Stone Group Laboratories, Jefferson City, Missouri, USA

References

Moon A.R. and Phillips M.R., 1984. An electron microscopy study of exsolved phases in natural black Australian sapphire. *Micron and Microscopica Acta*, **15**(3), 143–146, http://dx.doi.org/10.1016/0739-6260(84)90044-3.

Wüthrich A. and Weibel M., 1981. Optical theory of asterism. *Physics and Chemistry of Minerals*, **7**(1), 53–54.

Figure 12: This 8.65 ct black star sapphire is representative of material from the new find in Liberia. Photo by Orasa Weldon.

Figure 13: Hematite inclusions are seen here on the base of a black star sapphire cabochon. Photomicrograph by C. Williams; magnified 40×.

New Age Data for Blue Sapphires from Mogok, Myanmar

At the Gübelin Gem Lab, we recently had the opportunity to investigate the age of zircon inclusions in faceted blue sapphires from the Mogok area in Myanmar. To our knowledge, this is the first time that the formational ages of Mogok sapphires have been determined directly. This research not only demonstrates the power of *in-situ* age determination via laser ablation inductively coupled plasma mass spectrometry (LA-ICP-MS) as a tool for origin determination, but it also provides valuable insights into the formation of Burmese sapphires.

Following the methods described in Link (2015), radiometric U-Pb ages were determined quasi-non-destructively by LA-ICP-MS for two high-value blue sapphires weighing 26 and 11 ct (Figure 14) by analysing the zircon inclusions exposed at their girdles. The zircons measured 100–150 × 60–40 µm and were subhedral and stubby in appearance (Figure 15). Some of the zircons included in the larger sapphire were surrounded by radial tension cracks (Figure 15b). Routine laboratory examination indicated that both stones were unheated.

The concordant ages obtained from two zircons in each sample were 26.7 ± 4.2 million years (Ma) for the larger sapphire and 27.5 ± 2.8 Ma for the smaller stone (Figure 16). The crystal shape of the zircon inclusions does not allow a clear interpretation of whether they grew during or before their host sapphires. Nevertheless, a comparison of the determined ages with geochronologic data from the literature for rocks of the Mogok area indicate that the zircons are syngenetic. Therefore, the dates represent the formation ages of the sapphires.

Figure 14: These unheated sapphires (left, 26 ct, and right, 11 ct) from Mogok, Myanmar, contain zircon inclusions that were age dated using LA-ICP-MS. Photos by Janine Meyer.

Figure 15: The zircon inclusions in the 26 ct sapphire (a,b) are surrounded by tension cracks. The laser pits measure 25 µm (a) and 30 µm in diameter (b). Two zircon inclusions are exposed in the partially polished girdle of the 11 ct sapphire (c), and the diameter of the bottom one is about 60 µm. Photomicrographs by Klaus Schollenbruch in darkfield illumination (a,b) and by K. Link in reflected light (c).

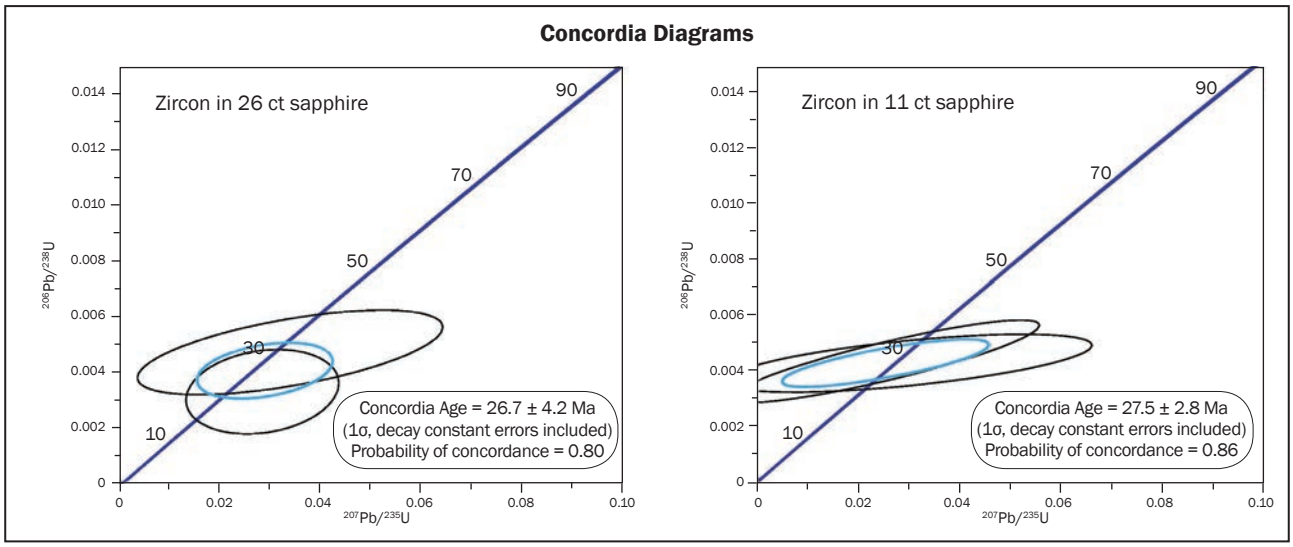

Figure 16: Concordia plots made with Isoplot software (Ludwig, 2003) are shown for the zircon inclusions in the 26 ct (left) and 11 ct (right) sapphires, which yield ages of 26.7 ± 4.2 Ma and 27.5 ± 2.8 Ma, respectively. The black ellipsoids each represent one measurement from a single zircon, and the blue ellipsoids give the resulting weighted mean concordant age and error from the two zircons within each sapphire.

The regional geology of Mogok is dominated by a complex lithological assemblage known as the Mogok Metamorphic Belt, which formed during the 60–50 Ma continental collision between the Indian plate with some micro-plates that at that time formed the southern margin of Eurasia (Searle et al., 2007). The ages of the protoliths (i.e. the original sedimentary and igneous rocks that were subsequently metamorphosed into marbles and gneisses) are suspected to be older than 170 Ma (Barley et al., 2003). During the India-Asia collision, the marbles and gneisses were multiply intruded by various igneous melts. At least one metamorphic episode post-dated the main continental collision, occurring at ~40 to 30 Ma. During this time, syeno-granitic melts began intruding the gneisses (Barley et al., 2003). Finally, at ~23 Ma, leucogranitic melts intruded the Mogok area (Searle et al., 2007). It has been suggested that the sapphires are closely related to these melts (Kan-Nyunt et al., 2013).

Considering the sapphire ages reported here and their error ranges, the formation of these sapphires is constrained to the time between the latest metamorphic event and the initial post-tectonic intrusions. The sapphires appear to be slightly younger than the marble-hosted rubies of Mogok, which formed at 31–32 Ma (see Zaw et al., 2014, and references therein)—although this apparent trend could also be an artefact of the error ranges of the age dates. It is debatable whether the two stones reported here represent the only crystallization age of blue sapphires in Mogok, or whether they indicate a (narrow?) time range of formation within their deposit(s). Significantly for origin determination, these zircon ages are completely different from those of the Pan-African-related gem corundum deposits such as those in Sri Lanka or Madagascar (~750–450 Ma; Giuliani et al., 2014, and references therein).

Klemens Link (klemens.Link@gubelingemlab.com)
Gübelin Gem Lab, Lucerne, Switzerland

References

Barley M.E., Pickard A.L., Zaw K., Rak P. and Doyle M.G., 2003. Jurassic to Miocene magmatism and metamorphism in the Mogok metamorphic belt and the India-Eurasia collision in Myanmar. *Tectonics*, **22**(3), 11 pages, http://dx.doi.org/10.1029/2002tc001398.

Giuliani G., Ohnenstetter D., Fallick A.E., Groat L. and Fagan A.J., 2014. Chapter 2: The geology and genesis of gem corundum deposits. In L.A. Groat, Ed., *The Geology of Gem Deposits*, 2nd edn., Mineralogical Association of Canada Short Course Series 44, Québec, Canada, 29–112.

Kan-Nyunt H.-P., Karampelas S., Link K., Thu K., Kiefert L. and Hardy P., 2013. Blue sapphires from the Baw Mar mine in Mogok. *Gems & Gemology*, **49**(4), 223–232, http://dx.doi.org/10.5741/gems.49.4.223.

Link K., 2015. Age determination of zircon inclusions in faceted sapphires. *Journal of Gemmology*,

34(8), 692–700, http://dx.doi.org/10.15506/jog.2015.34.8.692.

Ludwig K.R., 2003. Isoplot/Ex version 3.00: A geochronological toolkit for Microsoft Excel. Berkeley Geochronology Center, Berkeley, California, USA, www.bgc.org/isoplot_etc/isoplot.html.

Searle M.P., Noble S.R., Cottle J.M., Waters D.J., Mitchell A.H.G., Hlaing T. and Horstwood M.S.A., 2007. Tectonic evolution of the Mogok Metamorphic Belt, Burma (Myanmar) constrained by U-Th-Pb dating of metamorphic and magmatic rocks. *Tectonics*, **26**(3), article TC3014, 24 pages, http://dx.doi.org/10.1029/2006tc002083.

Zaw K., Sutherland L., Yui T.-F., Meffre S. and Thu K., 2014. Vanadium-rich ruby and sapphire within Mogok gemfield, Myanmar: Implications for gem color and genesis. *Mineralium Deposita*, **50**(1), 25–39, http://dx.doi.org/10.1007/s00126-014-0545-0.

Pink Spinel from Mozambique

In November 2015, rough stone dealer Farooq Hashmi was on a buying trip to East Africa when he encountered a new find of pink spinel that was reportedly discovered near the town of Namapa in Cabo Delgado Province, northern Mozambique. Hashmi saw approximately 50 kg of rough material, mostly as pieces weighing less than 3 g each. He loaned two crystals of ~1 g each (5.73 and 5.24 ct) and one faceted stone weighing 1.91 ct to this author for examination (Figure 17).

The samples exhibited a strong pink colour with a hint of purple. The crystals showed typical octahedral morphology with distinct triangular growth hillocks on the octahedral faces (Figure 18). Both crystals appeared slightly waterworn, indicating that the material originated from an eluvial or alluvial deposit not far from where it formed.

The faceted oval had RI = 1.709 and SG = 3.67, while the two crystals had SG values of 3.58 and 3.61, all of which are consistent with those expected for spinel. (Rough material tends to show a slightly lower SG due to surface tension when weighed in water.) The faceted stone exhibited a hazy appearance due to the presence

Figure 17: These rough and cut spinels are from a new find in Mozambique. The faceted gem weighs 1.91 ct and was cut by Marvin M. Wambua (Safigemscutters Ltd., Nairobi, Kenya). Photo by D. Bakker.

Figure 18: This 5.24 ct spinel crystal from Mozambique shows octahedral morphology with triangular growth hillocks, and only slight evidence of erosional transport. Photo by E. Boehm.

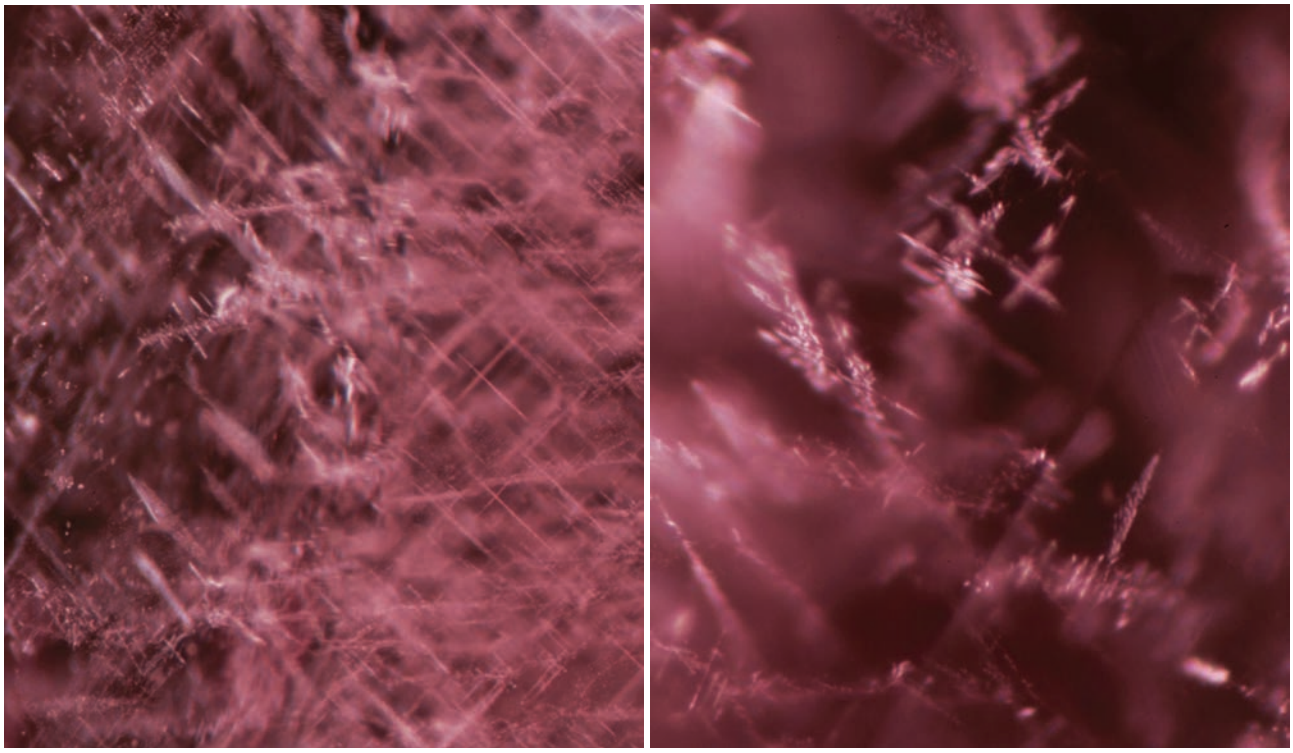

Figure 19: Inclusions in the 1.91 ct Mozambique spinel consisted of intersecting networks (left) and clusters (right) that resemble högbomite in pink spinel from Morogoro, Tanzania. Photomicrographs by E. Boehm; magnified 20× (left) and 40× (right).

Figure 20: Högbomite forms conspicuous parallel inclusions in this 3.34 ct pink spinel from Morogoro, Tanzania. Photomicrographs by E. Boehm; magnified 10× (left) and 40× (right).

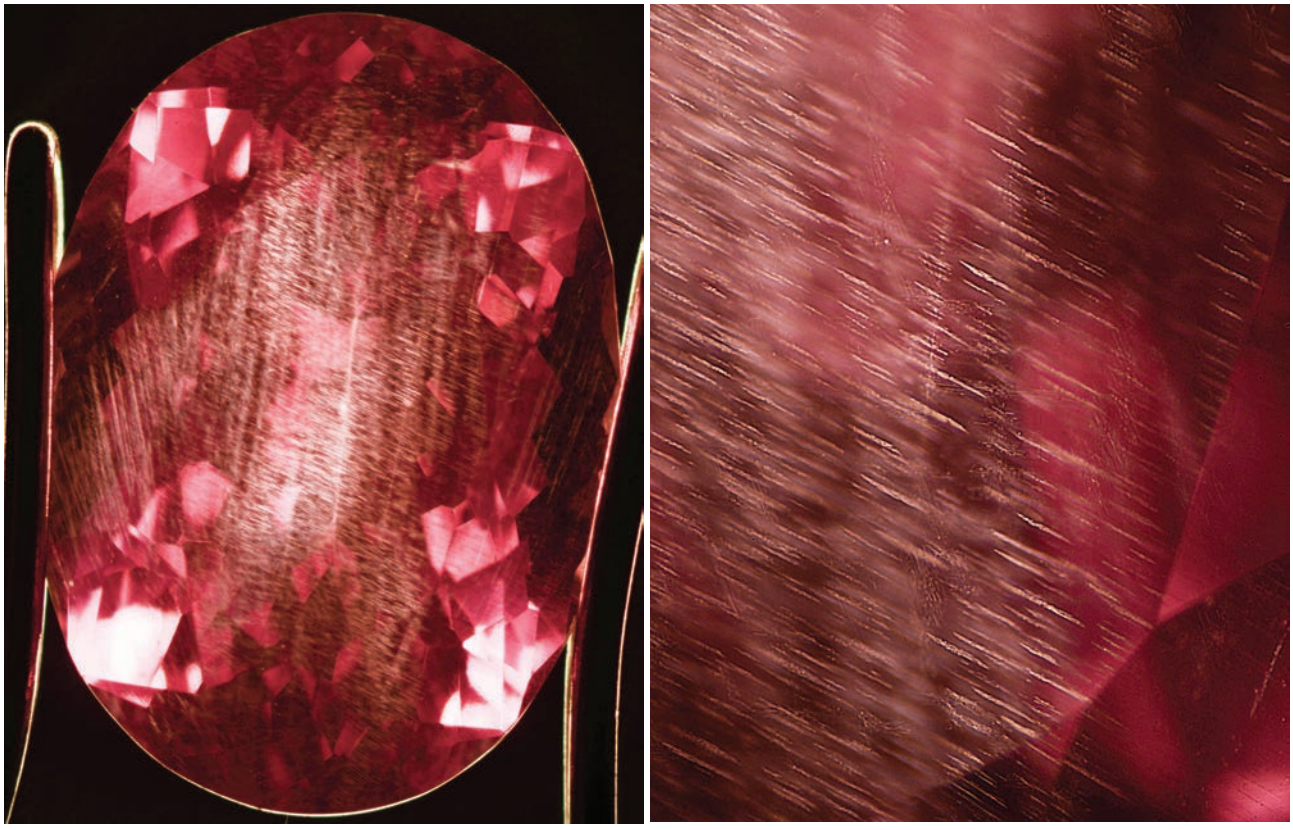

of inclusion networks (Figure 19) that resembled högbomite often seen in pink spinel from the Morogoro region of Tanzania (Figure 20; see also Schmetzer and Berger, 1990, 1992). Högbomite, $(Mg,Fe)_2(Al,Ti)_5O_{10}$, is an Al-rich mineral that typically replaces Fe-Ti-oxide inclusions such as ilmenite and rutile in spinel (Gübelin and Koivula, 2005). The author has also seen such inclusions in pink-to-red spinels from Mahenge, Tanzania. Interestingly, the Tanzanian spinel deposits are located directly north of Namapa and within the same Mozambique Belt.

The samples of spinel from Mozambique exhibited moderate red fluorescence when exposed to long-wave UV radiation, but were inert to short-wave UV. This same reaction is seen in pink spinel from Morogoro. However, pink-to-red stones from Mahenge tend to exhibit strong red fluorescence to long-wave UV and are inert to short-wave UV radiation.

Edward Boehm (edward@raresource.com)
RareSource, Chattanooga, Tennessee, USA

References

Gübelin E.J. and Koivula J.I., 2005. *Photoatlas of Inclusions in Gemstones*, Vol. 2. Opinio Publishers, Basel, Switzerland, 678–681.

Schmetzer K. and Berger A., 1990. Lamellar iron-free högbomite-24R from Tanzania. *Neues Jahrbuch für Mineralogie, Monatshefte*, **9**, 401–412.

Schmetzer K. and Berger A., 1992. Lamellar inclusions in spinels from Morogoro area, Tanzania. *Journal of Gemmology*, **23**(2), 93–94, http://dx.doi.org/10.15506/jog.1992.23.2.93.

Tantalite-(Mn) from Grangal, Nuristan, Afghanistan

Manganotantalite—renamed tantalite-(Mn) according to the conventions described by Burke (2008)—is an orthorhombic columbite-group mineral with the formula $MnTa_2O_6$ and a Mohs hardness of 6. Since 2011, one of the authors (DB) has occasionally obtained facetable 'manganotantalite' sourced from granitic pegmatites at Grangal and Watala in Kunar Province, Nuristan, Afghanistan. Although complete crystals are sometimes available, most of the production consists of broken fragments ranging from reddish brown to reddish black; the best is intense 'ruby' red in transmitted light. Most pieces contain only 10%–25% transparent areas that are cuttable; also, the tabular shape of the fragments limits the size of the faceted stones. Most recently, in January 2016, cutting of a parcel containing 29 pieces of rough totalling 86.4 g yielded 28 cut stones (~0.20–2.12 ct) with a total weight of 33.33 carats (7.7% yield). Most of them contained small inclusions visible with magnification. Due to the high specific gravity (see below), the stones had a relatively small size for their carat weight.

Two faceted samples of tantalite-(Mn) were characterized by one of the authors (JCZ): a round mixed cut weighing 1.10 ct (4.65 × 4.69 × 3.31 mm) and an oval mixed cut of 4.66 ct (8.82 × 6.98 × 4.10 mm). Both stones were transparent, and were very dark red with very high lustre (Figure 21). Pleochroism in dark red and dark reddish orange was observed using a calcite dichroscope. As expected for tantalite-(Mn), the RIs were above the limit of the refractometer, and the stones showed strong doubling of the pavilion facets when viewed face-up, consistent with the mineral's high birefringence (cf. RIs 2.19–2.34 and birefringence 0.15: Dedeyne and Quintens, 2007). Average hydrostatic SG values of 7.81 and 7.76 were obtained for the 1.10 and 4.66 ct samples, respectively. The gems were

Figure 21: These samples of tantalite-(Mn) from Afghanistan (4.66 and 1.10 ct) were studied for this report. Photo by Dirk van der Marel.

Figure 22: (a) Both of the tantalite-(Mn) gems contained partially healed fissures, such as those shown here (image width 3.6 mm). (b) The healed fissures are locally marked by larger irregular fluid inclusions that contain gas bubbles (image width 0.6 mm). (c) Crossing trails of partially healed fissures, containing minute two-phase inclusions, are shown in this view (image width 0.6 mm). Photomicrographs by J. C. Zwaan.

inert to long- and short-wave UV fluorescence. The prism spectroscope revealed transmission in the red region, extending only slightly into the orange. The stones were slightly and moderately included, respectively, both containing partially healed fissures (e.g. Figure 22a) that consisted of minute voids and also slightly larger irregular voids, most containing a fluid and a gas bubble (Figure 22b). Some minute voids also contained tiny doubly refractive mineral phases (too small to be identified). In places the partially healed fissures intersected one another, creating interesting patterns (Figure 22c).

UV-Vis spectra, obtained with a Thermo Scientific Evolution 600 spectrometer, showed a steep absorption edge at ~600 nm, with a gradual but rapid decrease in absorption toward 650–700 nm, confirming the observations with the spectroscope.

Raman spectra, collected with a Thermo Scientific DXR Raman microscope with 532 nm laser excitation, revealed a very strong main band at 885 cm^{-1}, and a series of supplementary bands at smaller wavenumbers. The spectra of these two samples appeared to show many more well-resolved peaks than reference spectra of tantalite-(Mn) from Afghanistan, Pakistan and China in the RRUFF database (Figure 23), as well as the spectra of tantalite-(Mn) from north-east Brazil, which contained supplementary bands at 621, 547, 526, 324, 282, 238, 202 and 121 cm^{-1} (Thomas et al., 2011).

EDXRF analyses were performed with an EDAX Orbis Micro-XRF analyser on the tables of

Figure 23: Raman spectra of the analysed samples (here, the 4.66 ct stone) show peaks that are more numerous and well resolved than reference spectra for tantalite-(Mn) from the RRUFF database.

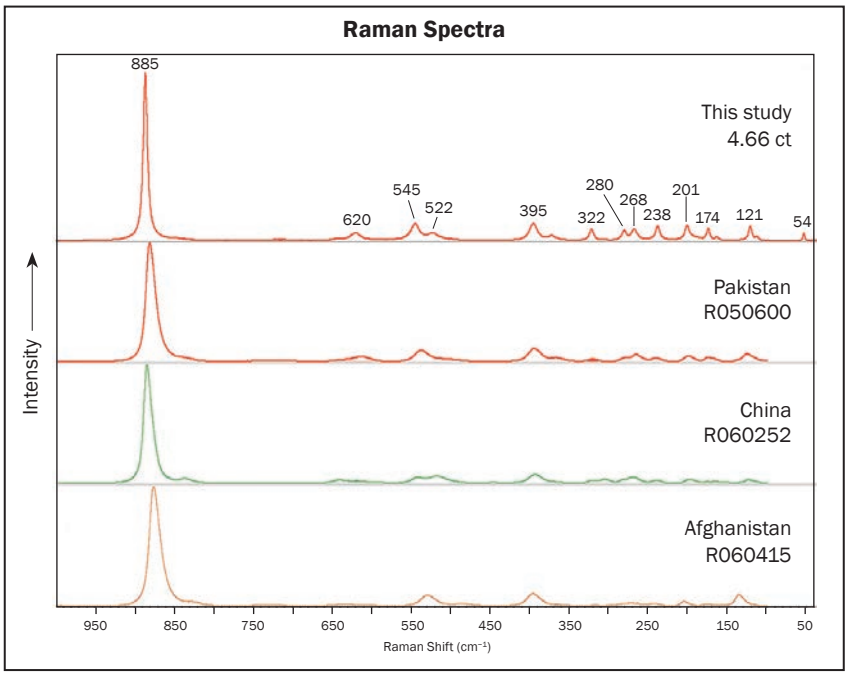

Table I: Chemical analyses and SG values of tantalite-(Mn) from Grangal, Afghanistan.

EDXRF analyses of two faceted stones

Oxides (wt.%)	**1.10 ct** (3 analyses)	**4.66 ct** (4 analyses)
FeO	0.30–0.35	0.70–1.55
MnO	12.5	12.1–12.9
Nb_2O_5	12.3–13.1	14.0–15.7
Ta_2O_5	74.1–74.9	70.8–72.4
SG	7.81	7.76

Representative SEM analyses of four crystal specimens

Oxides (wt.%)	**1**	**2-core**	**2-rim**	**3-core**	**3-rim**	**4**
FeO	0.33	3.58	0.54	2.37	2.02	3.83
MnO	13.81	11.88	13.23	13.07	13.40	13.81
Nb_2O_5	1.39	15.87	1.78	16.04	2.04	29.27
Ta_2O_5	84.47	68.67	84.45	68.52	82.54	53.09
Total	100.00	100.00	100.00	100.00	100.00	100.00
Ions per 6 oxygens						
Fe	0.023	0.231	0.038	0.153	0.142	0.299
Mn	0.989	0.777	0.946	0.854	0.953	0.835
Nb	0.053	0.554	0.068	0.559	0.077	0.944
Ta	1.942	1.442	1.939	1.438	1.885	1.030
TOTAL	3.007	3.005	2.990	3.003	3.057	3.038
Mn/(Mn+Fe)	0.977	0.771	0.961	0.700	0.870	0.785
Ta/(Ta+Nb)	0.973	0.722	0.966	0.720	0.961	0.522
X site	1.012	1.008	0.984	1.005	1.095	1.007
Y site	1.995	1.997	2.006	1.998	1.962	1.997
SG*	8.09	7.48	8.08	7.52	7.91	7.17

*SG values were measured from sample nos. 1 and 4, and were calculated from chemical analyses for nos. 2 and 3 due to the large amount of zoning in those samples. Sample nos. 1 and 4 had no significant chemical zoning in an analytical traverse from core to rim.

the two stones, using a spot size of 300 µm. The results of this semi-quantitative bulk technique (Table I, top) showed that the sample with greater Ta also had a higher SG value, consistent with known trends (Campbell and Parker, 1955).

Additional investigations of the composition and SG were undertaken by author AUF on four crystal specimens (Figure 24). Standard-based energy-dispersive spectroscopy analyses were performed with a Jeol JSM-6400 scanning electron microscope (SEM) using the Iridium Ultra software package by IXRF Systems Inc. The data showed that all specimens were Ta-dominant (Table I, bottom). Tantalum is the major controlling factor in the density of columbite-group minerals, and density (or SG) can be used to estimate Ta_2O_5 content (Campbell and Parker, 1955). The lowest SG of 7.17 was measured for sample no. 4, which corresponds to a calculated Ta_2O_5 content of ~55 wt.%. The slight discrepancy from the measured Ta_2O_5 content of 53 wt.% is probably due to sampling differences (i.e. the bulk sample was used for hydrostatic SG measurement, while only a small volume was analysed by SEM). The geochemically most evolved sample (no. 1) approached end-member tantalite-(Mn) composition, with Ta/(Ta+Nb) = 0.97, and had a measured SG value of 8.09 (corresponding to a calculated Ta_2O_5 content of 86.2 wt.%). Sample nos. 2 and 3 proved to be chemically zoned, with

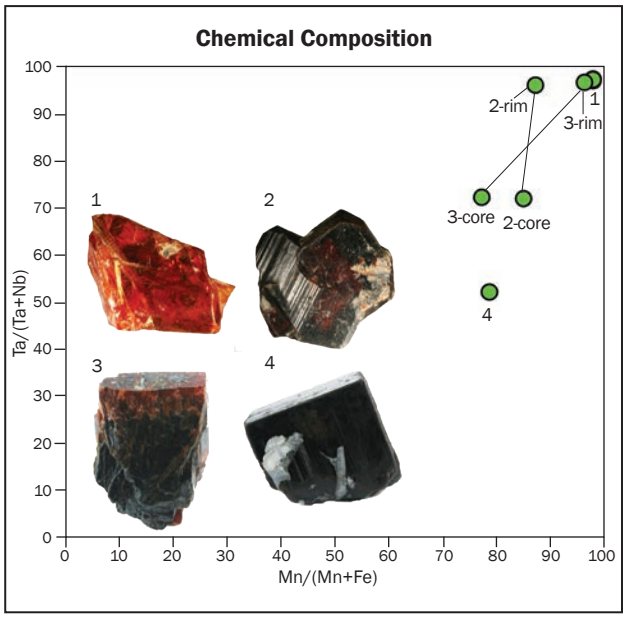

Figure 24: The chemical composition of four crystals of tantalite-(Mn) is summarized in this plot. Analyses of chemically zoned samples are joined by a line. The crystals measure 8, 20, 30 and 40 mm in maximum dimension (nos. 1–4, respectively), and their corresponding SG values are shown in Table I (bottom). Photos by A. Falster.

strong Ta enrichment in their rims compared to their cores (Table I and Figure 24).

The availability of this rare stone will remain limited, with author DB's supplier producing only ~150–200 g of rough per year, typically yielding only about 50–100 carats of faceted stones.

J. C. (Hanco) Zwaan (hanco.zwaan@naturalis.nl)
Netherlands Gemmological Laboratory
National Museum of Natural History 'Naturalis'
Leiden, The Netherlands

Alexander U. Falster and William 'Skip' B. Simmons
Maine Mineral and Gem Museum
Bethel, Maine, USA

Dudley Blauwet

References

Burke E.A.J., 2008. Tidying up mineral names: An IMA-CNMNC scheme for suffixes, hyphens and diacritical marks. *Mineralogical Record*, **39**(2), 131–135.

Campbell W.J. and Parker J.G., 1955. Relation of density to composition in the columbite-tantalite series. *U.S. Bureau of Mines Report of Investigations 5150*, 30 pp.

Dedeyne R. and Quintens I., 2007. *Tables of Gemstone Identification*. Glirico-Gent, Belgium, 307 pp.

Thomas R., Davidson P. and Beurlen H., 2011. Tantalite-(Mn) from the Borborema pegmatite province, northeastern Brazil: Conditions of formation and melt and fluid-inclusion constraints on experimental studies. *Mineralium Deposita*, **46**, 749–759, http://dx.doi.org/10.1007/s00126-011-0344-9.

PEARLS

A Coral Branch 'Pearl' from a Giant Clam

The Laboratoire Français de Gemmologie recently analysed an intriguing sample, submitted as a 'branch of coral' by Croissy Pearls. The client explained that the object was found in a giant clam (*Tridacna gigas*) by an Indonesian fisherman.

Corals are marine invertebrates that form colonies of polyps. Different species are commonly used for jewellery, such as *Corallium rubrum* (red coral from the Mediterranean Sea) or *Corallium elatius* (pink coral, also known as 'angel skin', from the waters around China and Japan). *Corallium spp.* have skeletons consisting of calcium carbonate, while the black corals (order Antipatharia) have skeletons composed of protein and chitin. Corals are often submitted to gemmological laboratories to test for imitations (e.g. glass and plastic) and treatments (e.g. bleaching, dyeing, waxing and plastic or resin impregnation). Some species are protected by the Convention on International Trade in Endangered Species of Wild Fauna and Flora (CITES), and cannot be imported or exported. These include *C. elatius*, *C. japonicum*, *C. konjoi* and *C. secundum* (from China only), as well as *Heliopora coerulea*, Scleractinia spp., Tubiporidae spp., Antipatharia spp., Milleporidae spp. and Stylasteridae spp. (see www.cites.org/eng/app/appendices.php).

The submitted object weighed 36.8 g and measured 65 × 38 × 29 mm (Figure 25). It had a

SSEF

SCHWEIZERISCHES GEMMOLOGISCHES INSTITUT
SWISS GEMMOLOGICAL INSTITUTE
INSTITUT SUISSE DE GEMMOLOGIE

ORIGIN DETERMINATION · TREATMENT DETECTION

DIAMOND GRADING · PEARL TESTING

EDUCATION · RESEARCH

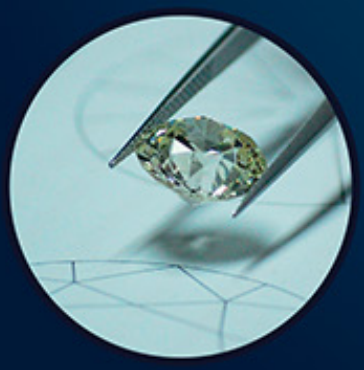

THE SCIENCE OF GEMSTONE TESTING

Aeschengraben 26, 4051 Basel, Switzerland Tel. +41 61 262 06 40 Fax + 41 61 262 06 41 admin@ssef.ch www.ssef.ch

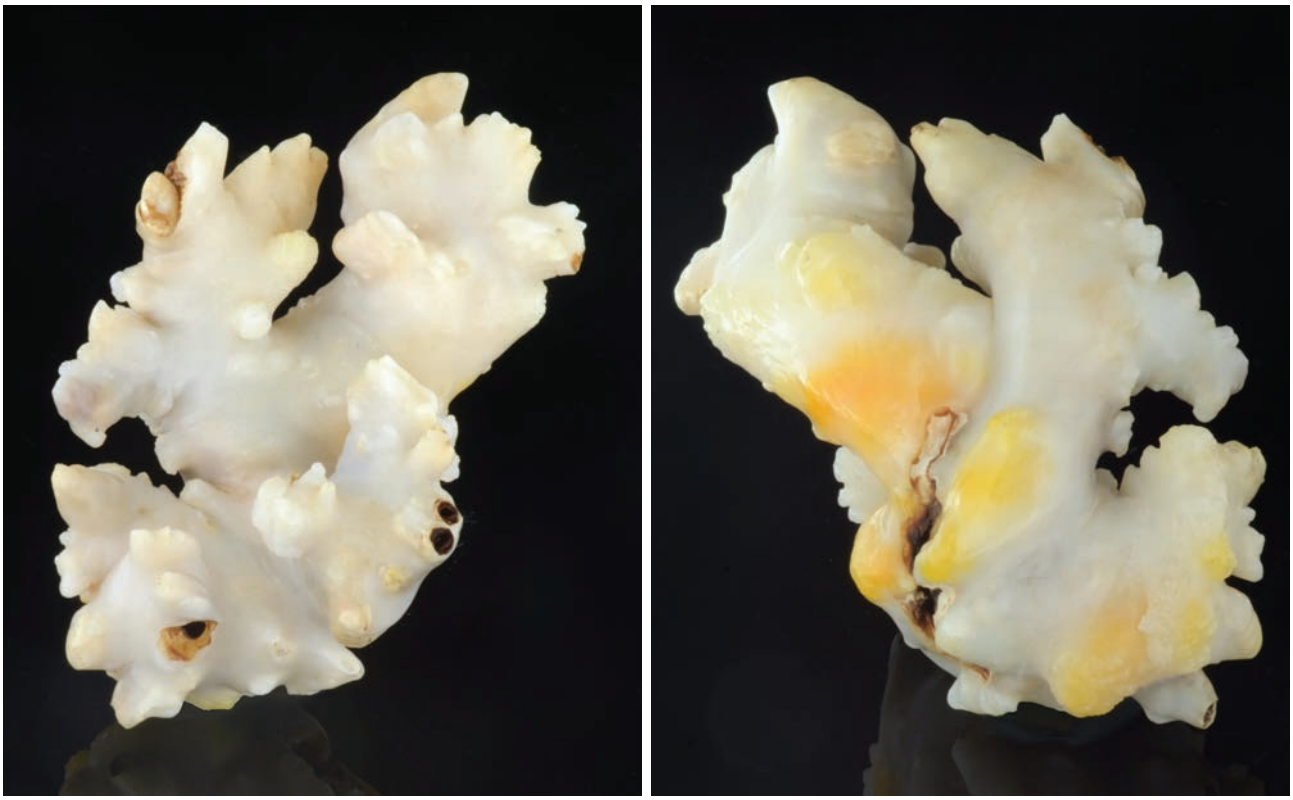

Figure 25: This irregularly shaped object (65 × 38 × 29 mm, shown in front and back views) is inferred to be a Tridacna gigas *'pearl' that formed when a branch of coral was covered by calcium carbonate. Photos by O. Segura.*

typical coral branch shape, but its porcelaneous white appearance (with some yellow areas) was not consistent with coral. Raman spectroscopy confirmed that the material consisted of a calcium carbonate phase; due to abundant luminescence, it was not possible to differentiate between calcite and aragonite. A few holes on the surface (e.g. Figure 26) provided a view into the interior of the object, which consisted of an open void. X-radiography likewise revealed a cavity inside the object (Figure 27). The shape of the hollow area showed a typical branching structure for coral.

These observations are consistent with *Tridacna* biomineralization of a branch of coral. Once inside the giant clam, the coral was covered by numerous layers of calcium carbonate produced

Figure 26: A hole on the surface of the object reveals multiple layers of calcium carbonate that were deposited on a pre-existing coral branch. The inside of the object now consists of a large void. Photomicrograph by O. Segura; magnified 30×.

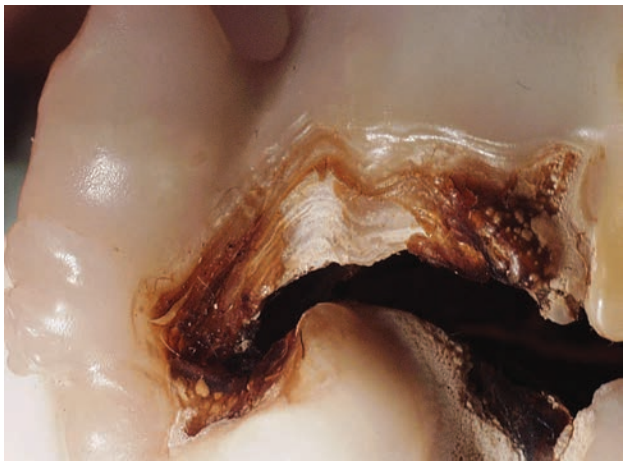

Figure 27: X-radiography of the biomineralized object (65 mm long) shows a dark-appearing void corresponding to a branch of coral that subsequently dissolved. Image by O. Segura.

by the mollusc. Subsequently, the coral branch was apparently dissolved, possibly through the action of enzymes produced by the host clam that entered through the holes in the object's surface, leaving an extraordinary envelope of calcium carbonate.

Technically we could call this object a natural baroque porcelaneous hollow pearl, and its rarity and probable origin make it a real treasure.

Olivier Segura (o.segura@bjop.fr),
Sophie Leblan and Laurent Croissy
Laboratoire Français de Gemmologie, Paris, France

TREATMENTS

Quartz Beads Treated with a Coloured Polymer to Imitate Tourmalinated Quartz

During the February 2016 Tucson gem shows, these authors acquired a strand of unusual beads (Figure 28). The vendor was unsure of their identity, but thought they consisted of quartz that was untreated. At first glance they appeared to be tourmalinated quartz, although the high concentration of greenish blue inclusions in some of the beads would be unusual for tourmaline needles in quartz. The dealer had several hanks of these beads in various sizes (8–12 mm in diameter), and one strand was purchased for testing.

The beads were approximately 10 mm in diameter and showed varying degrees of translucency. The deep greenish blue needle-like inclusions were concentrated in various amounts (Figure 29). Raman analysis with an Enwave 785 micro-Raman spectrometer confirmed the beads were quartz (463 cm^{-1} Raman peak), but the inclusions did not yield a useful signal, even where they reached the surface of the beads. During a prolonged reading, the Raman's 785 nm laser caused smoke to emanate from one such inclusion, suggesting the presence of a hydrocarbon. Using a PerkinElmer Spectrum100 Fourier-transform infrared spectrometer, a coloured polymer substance was confirmed in the inclusions, with bands at 4060, 3055 and 3037 cm^{-1}. Microscopic inspection revealed many of the needles were hollow, with their surfaces coated by the coloured polymer, while the polymer appeared to completely fill the finer tubes (e.g. Figure 30, left). Colour concentrations along fissures in a few of the beads (e.g. Figure

Figure 28 (left): These 'tourmalinated' quartz beads (10 mm in diameter) were studied for this report. Photo by C. Williams.

Figure 29 (below): The quartz beads contain varying amounts of deep greenish blue needle-like inclusions and colour concentrations. Photo by C. Williams.

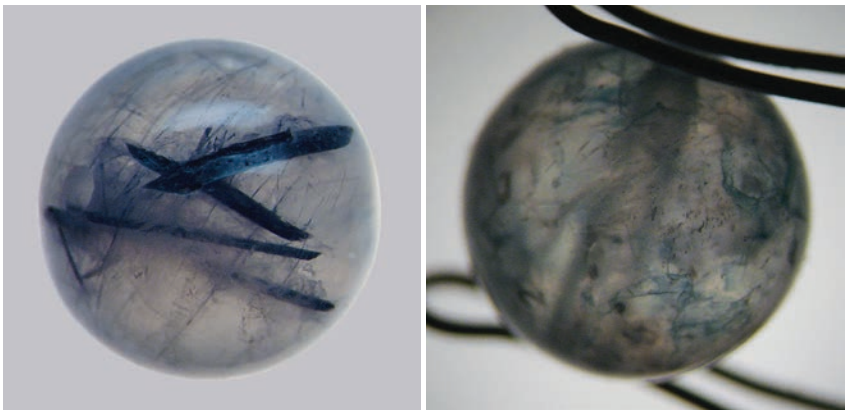

Figure 30: The surface-reaching inclusion in the bead on the left was found to consist of a hollow etch channel that contained coloured resin. In a few of the beads, the coloured polymer also penetrated surface-reaching fissures, as shown on the right. Photos by C. Williams; both beads are 10 mm in diameter.

30, right) also indicated the presence of an artificial dye. In places, air bubbles were visible within the filled fissures when viewed with higher magnification.

We concluded that the beads consisted of quartz with hollow etch channels and fissures that were filled with a deep greenish blue resinous dye.

Cara Williams FGA and Bear Williams FGA

First Circular & Call for Paper

Save your dates

GIT 2016

14 -15 November

"The Fullmoon of GEMUnity"

The 5th GIT International Gem and Jewelry Conference

with Pre - and Post - Conference Excursions

PATTAYA, THAILAND

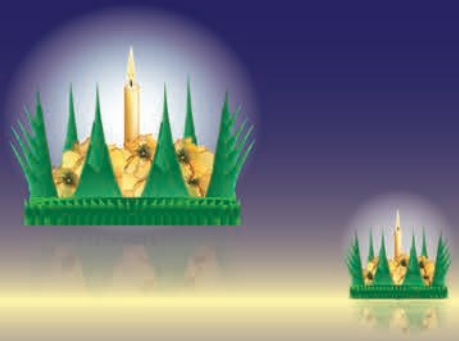

The Fullmoon of GEMUnity

November 14–15, 2016, Pattaya, Thailand

Conference Dates:

November 14-15, 2016: Technical session, oral & poster presentations
November 9-13, 2016: Pre-conference excursion to the legendary Mogok gem deposits, Myanmar
November 16-18, 2016: Post-conference excursion to Chanthaburi, the world's capital of colored stones & Trat, home of the renowned Siamese Ruby

Venue:

Pattaya, the world's premiere beach resort, Thailand
Special rates offered for accommodations
Further information announced on the GIT website

Important Dates

- Topics submission by May, 2016
- Extended abstract submission by August, 2016

Themes:

- Gem & precious metal deposits, exploration and responsible mining
- Bangkok rendezvous of the World's Ruby
- Innovation identification & characterization
- Treatment & synthetics update and disclosure
- Gem quality standards & gem optics and color science
- Jewelry trend & design
- Manufacturing & cutting edge technology
- Ethical, policy & good governance issues
- World gem & jewelry trading and ASEAN market

Registration Fees:

- Early bird USD 200, after Sep 30 USD 300
- Student USD 100, after Sep 30 USD 150
- On-Site USD 350
- *Pre-conference excursion to Mogok USD 1,800 or less (Air ticket to Mandalay and Visa for Myanmar excluded)
- *Post-conference excursion to Chanthaburi & Trat, Thailand USD 300

(*Limited seats available for excursion only on the first come first serve basis)

Highlights:

- Keynote addresses by top-notched speakers
- Creative forums by top designers, gemologists and business leaders
- CSR from the mine to the market
- Global gem and jewelry networking
- Adventurous excursions to gem fields and historical sites
- Intimate gem community rendezvous

Secretariat Office:

Tel: +66 2634 4999 ext. 453
Email: git2016@git.or.th
Website: www.git.or.th

สถาบันวิจัยและพัฒนาอัญมณีและเครื่องประดับแห่งชาติ (องค์การมหาชน)
The Gem and Jewelry Institute of Thailand (Public Organization)

Major- and Trace-element Composition of Paraíba-type Tourmaline from Brazil, Mozambique and Nigeria

Martin Okrusch, Andreas Ertl, Ulrich Schüssler, Ekkehart Tillmanns, Helene Brätz and Hermann Bank

Copper-bearing tourmalines are highly prized for their vivid coloration. We analysed the major and trace elements of some gem-quality Cu-bearing tourmalines (e.g. blue, greenish blue, yellowish green, green, violet and pink) from Brazil, Mozambique and Nigeria. Most of them contained significant amounts of Cu, Mn or a combination of both elements. There was no clear-cut correlation of the Cu and Mn contents with coloration. Blue colour was in most cases due to Cu^{2+}. Pink and violet coloration (due to Mn^{3+}) was shown by Mn-bearing tourmalines that contained no significant Fe. Green colour in the Nigerian tourmaline was most probably due to a combination of Mn, Cu and Fe. Some of the green samples from Brazil contained up to 0.6 wt.% V_2O_3. Among the trace elements, remarkable contents of Pb (up to 4,000 ppm) and Bi (up to 2,900 ppm) were detected rarely in samples from all three countries. Based on a comparison of unheated pink and violet samples with data for blue Paraíba-type tourmalines, CuO/MnO_{tot} is usually ≥0.5 for unheated blue samples. Hence, we suggest that blue Cu-bearing tourmalines with CuO/MnO_{tot} <0.5 may have been heat treated to reduce the contribution of the reddish component of Mn^{3+}.

The Journal of Gemmology, **35**(2), 2016, pp. 120–139, http://dx.doi.org/10.15506/JoG.2016.35.2.120

Introduction

"Tourmaline is unsurpassed by any other gemstone, even corundum, in the range of glorious colours that it displays, and it has risen high in the ranks of jewellery, thanks to the prodigal profusion in which nature has formed it…" (Smith and Phillips, 1972). With its diversity of coloration and moderate Mohs hardness of 7–7½, tourmaline is an excellent gem for pendants, earrings and brooches, and is also commonly used as a ring stone.

Tourmaline's extreme compositional variability is responsible for its multitude of colours. The generalized structural formula is $(X)(Y_3)(Z_6)[T_6O_{18}](BO_3)_3V_3W$, with the individual structural sites occupied (mainly) by the following cations (e.g. Henry et al., 2011, and references therein):

X = Ca, Na, K, □(vacancy)
Y = Li, Mg, Fe^{2+}, Mn^{2+}, Mn^{3+}, Al, Cr^{3+}, V^{3+}, Fe^{3+}, Zn, Cu
Z = Al, Fe^{3+}, V^{3+}, Cr^{3+}, Mg, Ti^{4+}
T = Si (with minor Al, B)
V = OH^-, O^{2-}
W = OH^-, F^-, Cl^-, O^{2-}

Substitutions at the Y site are more constrained by ionic radius than by valence. Consequently, the variety of cations in this site is larger than at the Z site, where substitutions are more constrained by valence than by size (e.g. Grice and Ercit, 1993). However, many additional crystallochemical constraints are related to interactions between different sites (e.g. the F and X sites; Henry and Dutrow, 1996).

According to the X-site occupancy, three primary tourmaline groups can be distinguished: a calcic group with dominant Ca^{2+}, an alkali group with dominant Na (+K) and an X-vacant group with dominant X-site vacancy. These three primary groups are subdivided based on the respective predominance of Li^{+}, Fe^{2+} or Mg^{2+} on the Y site (leading to, e.g., elbaite, schorl or dravite, respectively, in the alkali group). In addition, W-site occupancy leads to a further subdivision into the three general species hydroxyl-, fluor- and oxy-tourmaline. The combination of these classification aspects results in 32 tourmaline species that are recognized by the International Mineralogical Association (see Hawthorne and Dirlam, 2011; Henry et al., 2011; and for a recent update visit https://en.wikipedia.org/wiki/Tourmaline#Tourmaline_species_and_varieties).

Tourmaline is characterized by a variety of colours, and for gem applications it should not be too light or too dark, with the optimum colour being somewhere intermediate between these extremes. Therefore, gem-quality tourmaline should contain only very small amounts of Fe-rich end members, such as schorl, $NaFe^{2+}_{3}Al_{6}[Si_{6}O_{18}](BO_{3})_{3}(OH)_{3}(OH,F)$, which is an important constituent in most rock-forming tourmalines (e.g. Henry and Dutrow, 1996). Indeed, Epprecht (1953) realized that tourmalines with red, 'rose', green and yellowish green colours are virtually Mg,Fe-free elbaite, $NaLi_{1.5}Al_{1.5}Al_{6}[Si_{6}O_{18}](BO_{3})_{3}(OH)_{3}(OH,F)$, whereas tourmalines of the elbaite-schorl and dravite-schorl series typically range from light brown to brownish black and black with increasing Fe content. The same holds true for the uvite-feruvite series (Dunn et al., 1977). A colourless Mg,Fe-free elbaitic tourmaline revealed 0.33 apfu Mn (Epprecht, 1953; apfu = atoms per formula unit). Consistent with these results and those of other studies (e.g. Deer et al., 1986, and references therein), electron microprobe analyses of Dunn (1975) on zoned elbaite from Maine showed that

Figure 1: This 18 ct white gold ring contains a 3.47 ct heated Mozambique tourmaline that is surrounded by diamonds. Courtesy of collectorfinejewelry.com; ring manufactured by Ilka Bahn and photographed by Wimon Manorotkul.

Fe and Mn contents are highest in dark blue, lower in green and lowest in pink areas of the crystals. Further, the colour intensity of green elbaite was directly proportional to Fe content, and pink elbaite was virtually free of Fe (with the colour being due to small amounts of Mn that were not masked by Fe; Dunn, 1975). Several investigations of the colouring of elbaitic tourmalines (summarized in part by Deer et al., 1986) corroborate that the pink variety contains Mn combined with a low Fe content. This lack of Fe is more important than particularly high values of Mn. Investigations by Ertl et al. (2003) on a yellow-brown to pink Mn-rich tourmaline (~8.5 wt.% MnO_{tot}, ~0.15 wt.% FeO_{tot}) from Austria showed that Mn^{2+} was present in all regions of the crystal, but that Mn^{3+} was higher in the pink regions (where ~8% of the total Mn was Mn^{3+}) than in the yellow-brown areas. They argued, based on a gamma-irradiated crystal fragment, that the natural pink colour in this Mn-rich tourmaline is due to oxidation of the initial Mn^{2+} to Mn^{3+} by natural irradiation. Such a mechanism was initially proposed by Reinitz and Rossman (1988). Green and blue colours in Fe-bearing tourmaline have been attributed to both Fe^{2+}–Fe^{3+} (Mattson and Rossman, 1987) and Fe^{2+}–Ti^{4+} intervalence charge transfer (Mattson, as cited in Dietrich, 1985, p. 129), and yellow-green coloration may be produced by Mn^{2+}–Ti^{4+} (Rossman and Mattson, 1986). The coloration of Cu-bearing elbaite (e.g. Figure 1) is

Figure 2: Thirty-eight tourmaline samples were analysed from Brazil (BRA), Mozambique (MOZ) and Nigeria (NIG). For samples BRA11–BRA14, four samples were chosen at random from the group of stones shown. The red box on NIG2 shows the approximate area covered by the backscattered electron image in Figure 7. Photos by Klaus-Peter Kelber; scale bar in each image is 5 mm.

Figure 3: These gems show the bright coloration of Cu-bearing tourmaline from Brazil. The blue gems on the left weigh 1.87 and 1.49 ct, and the greenish blue to bluish green stones on the right weigh 2.80 ct (centre stone) and 2.51 carats (total weight of matched pair). Courtesy of Palagems.com; photos by Mia Dixon.

summarized in the following section. Many open questions still remain as to the relationships between colour and chemical composition of tourmaline, as they are not always directly correlated (Pezzotta and Laurs, 2011).

As a contribution to this problem, particularly regarding Cu-bearing tourmaline, we have analysed 38 gem-quality samples from Brazil, Mozambique and Nigeria (Figure 2) for major and minor elements using an electron microprobe. In addition, B, Li and several trace elements, including rare-earth elements (REE), were analysed by laser ablation inductively coupled plasma mass spectrometry (LA-ICP-MS) to obtain a comprehensive picture of the composition of these tourmalines. Analytical data on 15 additional, partly unpolished, crystals from Brazil (BRA20–BRA28) and Mozambique (MOZ19–MOZ24) were presented in an article that focused on the structural refinement of these tourmalines (Ertl et al., 2013); they generally show a strong negative correlation between X-site vacancy and Mn+Fe content. Ertl et al. (2013) concluded that the Mn content in such tourmaline depends on the geochemical availability of Mn and the formation temperature, as well as on stereochemical constraints. Because of a very weak correlation between MnO_{tot} and CuO, they argued that the Cu content in tourmaline is essentially dependent on the geochemical availability of Cu and on stereochemical constraints.

Provenance and Characteristics of the Samples

As the investigated tourmalines were purchased on the free market, only the general region of provenance was given. Therefore, the exact localities for the samples are unknown. Moreover, it cannot be excluded that some of the samples may have been initially purple-to-violet but were heat treated to achieve attractive blue coloration.

Brazil

In summer 1987, gem-quality tourmalines of radiant blue-to-green colour (e.g. Figure 3) were discovered in granitic pegmatites near the village of São José da Batalha near Salgadinho, Paraíba State, generating considerable interest of gemmologists and gem traders. Owing to their spectacular 'electric', 'neon' or 'swimming-pool' blue colours, these Paraíba tourmalines rapidly became popular on the gem market and eventually reached prices of US$25,000/carat (Pezzotta and Laurs, 2011) and higher. Their coloration is due to minor amounts of Cu (not previously recorded in tourmaline), partly in combination with Mn (Fritsch et al., 1990; Henn and Bank, 1990; Rossman et al., 1991; Abduriyim et al., 2006; Krzemnicki, 2006; Furuya and Furuya, 2007; Peretti et al., 2008; Shabaga et al., 2010; Beurlen et al., 2011). Interestingly, relatively Fe-rich Cu-Mn elbaite of greyish green colour from São José da Batalha may contain dendritic inclusions of native copper (Brandstätter and Niedermayer, 1993, 1994).

Polarized absorption spectra of dark blue Paraíba tourmaline display strong, pleochroic absorption bands with maxima at ~920 and ~700 nm due to Cu^{2+}, and at ~520 nm due to Mn^{3+}. Both of these cations occur in distorted octahedral coordination. In contrast, spectra of light blue Paraíba tourmaline show only the Cu^{2+} absorptions with no Mn^{3+} band (see Figure 6 in Henn and Bank, 1990). The vivid blue and yellowish green to

Figure 4: These unheated Cu-bearing tourmalines from Mozambique (1.29–2.24 ct) display a wide variety of colour, including green, 'lilac', bluish green, 'magenta', purple and blue. Courtesy of Palagems.com; photo by Mia Dixon.

blue-green colours are due primarily to Cu^{2+} (and varying amounts of Mn^{2+}), but may be influenced by absorption from Mn^{3+} toward violet-blue and violet hues. Heating of such tourmaline leads to a complete disappearance of the 520 nm Mn^{3+} band (e.g. Laurs et al., 2008; Pezzotta and Laurs, 2011).

Similar Cu-Mn-bearing, Paraíba-type tourmalines have been recorded in granitic pegmatites at other Brazilian localities, particularly Quintos de Baixo and Boqueirãozinho, both in the state of Rio Grande do Norte (Karfunkel and Wegner, 1996; Shigley et al., 2001; Milisenda, 2005; Milisenda et al., 2006).

Under the designation 'Brazil', we analysed 13 cut and five rough tourmalines. Most displayed greenish blue, blue or yellowish green colours, typical of Paraíba-type elbaite (Figure 2). Two samples, BRA3 and BRA5, were purple and violet, respectively.

Mozambique

Gem-quality tourmaline, beryl, spodumene and garnet are found in numerous Nb-Ta-Bi-bearing granitic pegmatites, of about 550 million years old, that occur in the crystalline basement of the Alto Ligonha plateau in northern Mozambique (e.g. Hutchinson and Claus, 1956; Simmons et al., 2012). A new occurrence of Cu-bearing elbaite was detected in the mid-2000s in the eastern Alto Ligonha pegmatite province, some 150 km southwest of the city of Nampula (Abduriyim et al., 2006; Krzemnicki, 2006; Milisenda et al., 2006; Laurs et al., 2008; Peretti et al., 2008). The stones are mined from placer deposits, but are presumably derived from pegmatites (Milisenda et al., 2006).

The Cu-bearing tourmalines display a broad spectrum of colours (i.e. violet, pink, purple, blue, greenish blue, yellowish green and green; e.g. Figure 4). Zoned crystals may consist of two (e.g. green–violet) or three (e.g. green–violet–blue) different colours. In blue, bluish green and green specimens, considerable Mn and Cu contents have been revealed by electron microprobe analysis. Heating of purple-to-violet samples to 600°C led to a reduction of the Mn^{3+} absorption bands at 395 and 520 nm, and an increase of the broad Cu^{2+} maxima at 690 and 905 nm. As a result, the colour may be changed to a vivid 'turquoise' blue (Figure 5), typical of Paraíba-type tourmaline (Milisenda and Henn, 2001; Milisenda et al., 2006).

We investigated 15 cut and three rough stones from Mozambique that displayed a large variety of colours (i.e. purple to reddish purple or purplish pink, brownish pink, orangey pink, blue, bluish green, greenish blue, green, yellowish green and yellow brown; Figure 2).

Nigeria

In 2001, green, blue, and blue-violet to amethyst-coloured tourmalines containing Mn^{3+} and Cu^{2+} were discovered at the Edoukou mine near Ilorin in Oyo State (Milisenda, 2001b; Milisenda and Henn, 2001; Smith et al., 2001; Zang et al., 2001; Abduriyim et al., 2006; Krzemnicki, 2006; Furuya

Figure 5: The light greenish blue gems in this 12-piece suite of Mozambique Cu-bearing tourmaline (30.66 carats total weight) have been heated, while the others are unheated. Courtesy of Palagems.com; photo by Mia Dixon.

Figure 6: Weighing up to 4.73 ct, these Cu-bearing tourmalines are from Nigeria. Courtesy of Ekkehard Schneider; photo by Jeff Scovil.

and Furuya, 2007; Peretti et al., 2008). Some of the stones are colour zoned. Upon heating the violet crystals, the ~520 nm absorption band of Mn^{3+} is reduced and the ~700 and ~920 nm absorption bands typical of Cu^{2+} become obvious. Although the resulting colour is blue (e.g. Figure 6), the particularly vivid 'neon blue' typical of Paraíba-type tourmalines has been only rarely encountered. We analysed one blue faceted stone and one rough colour-zoned tourmaline from Nigeria (NIG1 and NIG2, respectively; see Figure 2).

Analytical Techniques

The tourmalines from Brazil (18 samples; Table I), Mozambique (18; Table II) and Nigeria (2; Tables III and IV) were analysed for major, minor and trace elements, including REE, at the Division of Geodynamics and Geomaterial Research, Würzburg University, Germany. Electron microprobe analysis (EMPA) of the faceted stones was carried out on the table facet (which is generally oriented nearly parallel to the optic axis; Smith and Phillips, 1972) while, for laser ablation inductively coupled plasma mass spectrometry (LA-ICP-MS), a pavilion facet on the back of the stone was selected in the majority of cases. On the crystal fragments, a randomly selected surface was polished for analysis.

EMPA was carried out on a Cameca SX50 microprobe with three wavelength-dispersive spectrometers. Analytical conditions were 15 kV accelerating voltage and 15 nA beam current. As F was analysed together with other elements, the beam diameter was 10 µm for all measurements. Counting times were 20 s for most elements, and 30 s for Fe and Mn. Standards consisted of well-characterised natural and synthetic silicate and oxide minerals or pure elements supplied by Cameca. *K*α radiation was used for the analysis of F, Na, Al, Si, Cl, K, Ca, Ti, V, Mn and Fe, and *L*α for the analysis of Ba. Special care was taken to account for overlapping peaks, especially V (*K*α) with Ti (*K*β). The matrix correction of the EMPA data was done by Cameca's PAP software. Using these analytical conditions, the detection limit was about 0.05 wt.%. The analytical precision was below 1% relative for all major elements except Na (2%), and up to 10% relative for F and the minor elements. In general, 10 or more individual EMPA point analyses were carried out on each sample. From these, average compositions for the tourmalines were calculated. On the colour-zoned sample from Nigeria, a traverse of 82 points were measured, a selection of which are given in Table III.

For all samples, B, Li, REE and some minor-to-trace elements (Mg, Cr, Ni, Cu, Zn, Pb and Bi) were analysed by LA-ICP-MS. The measurements were undertaken using a New Wave Research (Merchantek) 266 nm Nd:YAG laser ablation unit, connected to an Agilent 7500i ICP-MS quadrupole instrument at 1,250 W plasma power. Argon was used as carrier gas (1.28 L/min) as well as plasma gas (14.9 L/min) and auxiliary gas (0.9 L/min). Data acquisition was performed in time-resolved mode with measurements on the maximum peak and 25 ms integration time for all chosen isotopes, except for 10 ms for B and Si. The background was measured for 15 s and the acquisition time also was 15 s. Three spots with a crater size of 40 µm, a repetition rate of 10 Hz and a laser energy of 0.51–0.74 mJ (energy density 43–52 J/cm^2) were ablated on each sample. Data analysis was performed via Glitter software (version 3.0, Macquarie Research Ltd., 2000), using Si as an internal standard (values known from EMPA). Results of the LA-ICP-MS analyses are the mean values of three ablated spots. On the colour-zoned sample from Nigeria, a traverse of six points were measured, and these data are given in Table IV.

Table I: Chemical analyses of tourmaline from Brazil.[a]

Sample no.	BRA1	BRA2	BRA3	BRA4	BRA5	BRA6	BRA7	BRA8	BRA9
Weight (ct)	0.95	0.81	1.10	0.82	0.56	0.38	0.24	0.51	0.34
Max. size (mm)	8.5	7.6	10.8	9.2	7.4	5.2	5.7	5.9	4.5
Colour	Blue	Violetish blue	Purple	Blue	Violet	Yellow-green	Bluish green	Greenish blue	Yellowish green
Oxides (wt.%)									
SiO_2	37.30	36.28	36.94	37.19	36.35	37.01	36.16	36.94	37.47
TiO_2	0.01	bdl	0.01	0.01	0.01	0.07	0.05	0.01	0.01
B_2O_3*	10.80	10.51	10.70	10.77	10.53	10.72	10.47	10.70	10.85
B_2O_3**	9.44	9.39	9.24	9.31	9.98	9.21	9.60	10.67	9.16
Al_2O_3	39.06	40.93	40.15	39.78	42.06	38.99	39.01	40.64	41.27
V_2O_3	0.01	bdl	0.03	0.01	bdl	0.48	0.13	0.01	0.01
MgO	0.01	bdl	0.02	0.01	bdl	0.46	0.13	0.01	0.01
CaO	0.24	0.30	0.11	0.54	0.30	0.25	0.28	0.50	0.53
MnO_{tot}	2.90	1.38	1.91	2.30	0.35	3.66	1.98	2.72	0.55
FeO_{tot}	3.21	0.01	0.06	bdl	0.01	0.28	0.03	bdl	2.43
CuO**	bdl	0.42	0.52	1.07	1.69	1.74	0.89	1.39	bdl
ZnO**	0.07	0.27	1.45	bdl	bdl	1.72	bdl	0.08	0.09
PbO**	bdl	bdl	bdl	0.01	bdl	bdl	0.01	bdl	0.02
BiO**	bdl	bdl	0.01	0.14	0.05	0.03	0.10	0.08	bdl
Li_2O*	1.17	1.12	1.22	1.51	0.83	0.62	1.37	1.00	1.24
Li_2O**	1.47	1.53	1.70	1.87	2.03	1.39	1.76	2.04	1.73
Na_2O	2.67	2.10	2.30	2.31	1.92	2.62	2.48	2.29	2.08
F	1.97	1.39	1.35	2.09	1.14	2.09	1.91	2.02	1.66
H_2O*	2.78	2.84	2.90	2.75	2.90	2.73	2.70	2.74	2.87
-O=F	–0.83	–0.58	–0.57	–0.88	–0.48	–0.88	–0.81	–0.85	–0.70
Sum (EMPA data)	**101.38**	**96.95**	**99.11**	**99.60**	**97.67**	**102.59**	**96.89**	**100.28**	**100.40**
Ions per 31 (O+OH+F)									
Si	6.000	6.000	6.000	6.000	6.000	6.000	6.000	6.000	6.000
B	3.000	3.000	3.000	3.000	3.000	3.000	3.000	3.000	3.000
Al	7.406	7.978	7.684	7.563	8.181	7.451	7.630	7.781	7.788
Mg	0.002	0.000	0.005	0.001	0.000	0.112	0.032	0.002	0.002
Ti^{4+}	0.001	0.000	0.001	0.001	0.001	0.009	0.006	0.001	0.002
V^{3+}	0.002	0.000	0.003	0.001	0.000	0.062	0.018	0.001	0.001
Mn^{2+}	0.395	0.193	0.263	0.315	0.049	0.502	0.278	0.374	0.075
Fe^{2+}	0.432	0.001	0.008	0.000	0.001	0.038	0.004	0.000	0.326
Cu^{2+}	0.000	0.052	0.064	0.131	0.211	0.213	0.112	0.171	0.000
Zn	0.009	0.033	0.174	0.000	0.000	0.206	0.000	0.010	0.010
Li	0.754	0.742	0.797	0.976	0.552	0.404	0.912	0.653	0.795
Sum Y,Z	**9.000**	**9.000**	**8.999**	**8.988**	**8.995**	**8.998**	**8.990**	**8.992**	**8.999**
Ca	0.042	0.052	0.019	0.094	0.053	0.044	0.049	0.087	0.090
Pb	0.000	0.000	0.000	0.000	0.000	0.000	0.000	0.000	0.001
Bi	0.000	0.000	0.001	0.060	0.025	0.001	0.005	0.004	0.000
Na	0.833	0.674	0.723	0.722	0.614	0.823	0.797	0.723	0.647
Vacancy	0.125	0.273	0.258	0.173	0.328	0.131	0.144	0.183	0.262
Sum X	**1.000**	**1.000**	**1.000**	**1.000**	**1.000**	**1.000**	**1.000**	**1.000**	**1.000**
F	1.027	0.743	0.718	1.093	0.608	1.086	1.026	1.054	0.863
OH	0.000	0.128	0.141	0.000	0.196	0.000	0.000	0.000	0.068
O	0.000	0.129	0.141	0.000	0.196	0.000	0.000	0.000	0.069
Sum W	**1.027**	**1.000**	**1.000**	**1.093**	**1.000**	**1.086**	**1.026**	**1.054**	**1.000**
Trace elements (ppm)									
Mg	10.20	3.57	139	0.69	0.32	841	6.13	1.38	84.2
Ni	bdl	bdl	bdl	bdl	bdl	bdl	bdl	bdl	bdl
Cu	2.73	3354	4148	8571	13532	13917	7110	11111	1.84
Zn	601	2179	11670	12.6	17.5	13820	18.9	643	692
La	0.30	bdl	bdl	0.39	4.46	0.18	0.24	1.06	0.79
Ce	0.46	bdl	bdl	0.26	2.72	0.09	0.12	0.56	1.52
Pr	0.04	bdl	bdl	0.03	0.10	bdl	bdl	0.06	0.14
Nd	bdl	bdl	bdl	bdl	bdl	bdl	bdl	bdl	0.40
Sm	bdl	bdl	bdl	bdl	bdl	bdl	bdl	bdl	bdl
Pb	20.2	1.90	6.44	64.5	21.9	26.3	52.2	36.6	168
Bi	0.51	14.2	103	1265	480	252	972	788	bdl
Σ REE	0.80	bdl	bdl	0.67	7.28	0.27	0.37	1.68	2.85

[a] Notes: The V site is completely occupied by OH in all samples. The values B_2O_3*, Li_2O* and H_2O* were calculated (these values were used for the formula calculation; for details, see text). Data for B_2O_3**, CuO**, ZnO**, PbO**, BiO** and Li_2O** are from LA-ICP-MS. Standards used for EMPA measurements were andradite [$Ca_3Fe_2(SiO_4)_3$] for Si and Ca, Al_2O_3 for Al, Fe_2O_3 for Fe, MgO for Mg, albite [$NaAlSi_3O_8$] for Na, $MnTiO_3$ for Mn and Ti, vanadinite [$Pb_5Cl(VO_4)_3$] for V, PbS for Pb, ZnS for Zn, pure elements for Cu and Bi, and LiF for F. Below detection limit in all samples were K, Ba and Cl (EMPA), and Cr, Eu, Gd, Tb, Dy, Ho, Er, Tm, Yb and Lu (LA-ICP-MS). For LA-ICP-MS analyses, tourmalines supplied from

BRA10	BRA11	BRA12	BRA13	BRA14	BRA15	BRA16	BRA17	BRA18
8.91	0.03	0.03	0.03	0.03	0.19	0.27	0.38	0.11
13.3	1.7	1.7	1.7	1.7	4.7	5.0	5.3	4.0
Brownish green	Greenish blue	Greenish blue	Greenish blue	Greenish blue	Greenish blue	Greenish blue	Greenish blue	Greenish blue
36.86	37.31	36.54	36.14	38.73	37.93	37.60	37.81	37.40
0.10	0.01	0.02	0.02	0.02	0.01	0.01	bdl	bdl
10.68	10.81	10.59	10.47	11.22	10.99	10.89	10.95	10.83
10.34	9.84	9.71	9.78	9.47	10.64	10.03	10.98	9.97
38.75	41.13	40.45	40.09	41.42	41.43	41.41	42.18	41.80
0.62	bdl	0.01	bdl	0.01	0.02	bdl	bdl	bdl
0.62	bdl	bdl	bdl	bdl	0.01	bdl	0.01	bdl
0.35	0.74	0.76	0.73	0.66	0.69	0.77	0.78	0.60
1.79	0.44	0.49	1.08	2.23	0.40	0.74	0.68	0.29
0.53	0.03	0.04	0.02	0.02	0.02	bdl	0.01	bdl
0.97	1.38	1.06	1.05	1.03	1.22	0.99	1.22	1.03
0.85	0.03	0.02	bdl	0.01	0.04	bdl	bdl	0.02
0.01	0.01	0.01	0.01	bdl	0.01	0.01	0.01	0.43
0.15	0.12	0.09	0.05	0.03	0.07	0.05	0.05	0.06
1.18	1.48	1.45	1.30	1.63	1.66	1.54	1.36	1.40
1.95	1.83	1.94	1.51	1.55	2.17	2.00	2.38	2.04
2.44	2.17	2.11	2.06	2.48	2.07	2.06	2.08	2.00
1.83	1.81	1.69	1.63	1.84	1.86	1.70	1.44	1.89
2.78	2.82	2.79	2.77	2.94	2.86	2.88	2.96	2.81
–0.77	–0.76	–0.71	–0.68	–0.77	–0.78	–0.71	–0.61	–0.80
99.74	**99.50**	**97.38**	**96.71**	**103.48**	**100.48**	**99.91**	**100.93**	**99.77**
6.000	6.000	6.000	6.000	6.000	6.000	6.000	6.000	6.000
3.000	3.000	3.000	3.000	3.000	3.000	3.000	3.000	3.000
7.434	7.796	7.827	7.843	7.562	7.725	7.787	7.888	7.904
0.150	0.000	0.000	0.000	0.000	0.001	0.000	0.002	0.000
0.012	0.001	0.002	0.002	0.002	0.001	0.001	0.000	0.000
0.080	0.000	0.001	0.000	0.001	0.003	0.000	0.000	0.000
0.246	0.059	0.068	0.152	0.292	0.054	0.100	0.091	0.039
0.072	0.004	0.005	0.003	0.002	0.002	0.000	0.001	0.000
0.119	0.168	0.131	0.132	0.120	0.145	0.119	0.146	0.125
0.102	0.004	0.002	0.000	0.001	0.005	0.000	0.000	0.003
0.769	0.958	0.956	0.865	1.016	1.058	0.988	0.868	0.905
8.986	**8.989**	**8.992**	**8.996**	**8.998**	**8.994**	**8.995**	**8.995**	**8.976**
0.061	0.127	0.133	0.130	0.109	0.117	0.131	0.132	0.103
0.000	0.000	0.000	0.000	0.000	0.000	0.000	0.000	0.019
0.008	0.005	0.004	0.002	0.001	0.003	0.003	0.003	0.003
0.771	0.677	0.673	0.663	0.744	0.633	0.636	0.641	0.621
0.154	0.185	0.186	0.203	0.144	0.244	0.229	0.222	0.252
1.000	**1.000**	**1.000**	**1.000**	**1.000**	**1.000**	**1.000**	**1.000**	**1.000**
0.963	0.940	0.900	0.874	0.927	0.954	0.879	0.742	0.979
0.019	0.030	0.050	0.063	0.037	0.023	0.061	0.129	0.011
0.018	0.030	0.050	0.063	0.036	0.023	0.060	0.129	0.010
1.000	**1.000**	**1.000**	**1.000**	**1.000**	**1.000**	**1.000**	**1.000**	**1.000**
3637	6.13	9.21	2.66	2.68	12.4	1.92	3.42	26.5
bdl	bdl	bdl	bdl	bdl	bdl	bdl	bdl	3.62
7742	11032	8439	8380	8220	9723	7878	9721	8254
6850	264	138	24.5	84.1	326	11.6	<12	194
0.20	0.51	2.50	1.52	3.62	0.31	3.12	0.64	0.23
0.40	0.52	3.46	1.52	3.54	0.39	3.28	0.44	0.21
bdl	0.03	0.32	0.09	0.19	0.06	0.26	0.08	bdl
bdl	bdl	1.02	0.20	0.35	0.17	0.53	bdl	bdl
bdl	bdl	0.44	bdl	0.19	bdl	bdl	bdl	bdl
65.9	67.4	47.0	47.3	38.4	46.8	55.0	51.5	4002
1433	1105	828	420	249	608	495	495	532
0.60	1.07	7.91	3.33	7.88	0.92	7.19	1.17	0.43

Harvard University (dravite, schorl, elbaite; Dyar et al., 2001) were measured as monitors to check for accuracy; the relative standard deviation for B varied from 3–8%, and for Li 5–17% relative. External calibration was performed via NIST glass standard SRM 610 (nominal 500 ppm) with the values from Pearce et al. (1997); the reproducibility for NIST glass SRM 612 (nominal 50 ppm) was 5–11% relative. Abbreviation: bdl = below detection limit.

Table II: Chemical analyses of tourmaline from Mozambique.[a]

Sample no.	M0Z1	M0Z2	M0Z3	M0Z4	M0Z5	M0Z6	M0Z7	M0Z8	M0Z9
Weight (ct)	6.95	2.78	3.95	2.58	1.59	2.36	2.31	1.41	1.54
Max. size (mm)	17.5	9.7	10.7	11.1	8.7	9.1	9.3	8.8	8.0
Colour	Reddish purple	Brownish pink	Yellowish green	Purple	Blue	Orangey pink	Yellowish green	Reddish purple	Blue
Oxides (wt.%)									
SiO_2	37.07	36.73	36.00	37.06	37.17	37.52	37.46	37.10	36.53
TiO_2	0.03	0.05	0.05	bdl	0.01	0.01	0.01	0.01	0.04
B_2O_3*	10.74	10.64	10.43	10.73	10.77	10.87	10.85	10.75	10.58
B_2O_3**	9.19	8.69	8.52	9.26	9.14	8.96	8.79	8.94	9.51
Al_2O_3	41.44	40.88	40.22	41.94	41.99	43.48	42.45	42.56	40.77
V_2O_3	bdl	bdl	bdl	bdl	bdl	0.01	bdl	bdl	0.01
MgO	bdl	bdl	bdl	0.01	bdl	bdl	0.01	bdl	0.01
CaO	0.10	0.09	0.08	0.08	0.31	0.18	0.89	0.11	0.30
MnO_{tot}	3.03	3.46	4.06	2.69	2.34	1.38	0.32	1.25	3.06
FeO_{tot}	bdl	bdl	bdl	0.01	bdl	0.01	0.01	bdl	bdl
CuO**	0.09	0.17	0.16	0.16	0.35	0.06	0.16	0.13	0.40
ZnO**	bdl	bdl	bdl	bdl	bdl	bdl	bdl	bdl	bdl
PbO**	bdl	bdl	bdl	bdl	bdl	bdl	0.02	bdl	0.01
BiO**	bdl	bdl	bdl	bdl	0.04	0.01	0.24	0.01	0.03
Li_2O*	1.02	0.95	0.74	0.93	0.99	0.94	1.40	1.07	0.94
Li_2O**	1.47	1.44	1.31	1.74	1.45	1.74	2.05	1.65	1.77
Na_2O	2.24	2.28	2.28	2.18	2.08	2.04	1.80	2.07	2.22
F	1.10	1.46	1.31	1.22	1.59	1.32	1.58	1.24	1.72
H_2O*	2.97	2.86	2.83	2.83	2.87	2.96	2.89	2.94	2.78
–O=F	–0.46	–0.61	–0.55	–0.51	–0.67	–0.56	–0.66	–0.52	–0.72
Sum (EMPA data)	**99.38**	**98.96**	**97.62**	**99.32**	**99.85**	**100.23**	**99.41**	**98.72**	**98.66**
Ions per 31 (O+OH+F)									
Si	6.000	6.000	6.000	6.000	6.000	6.000	6.000	6.000	6.000
B	3.000	3.000	3.000	3.000	3.000	3.000	3.000	3.000	3.000
Al	7.905	7.869	7.900	8.003	7.987	8.195	8.012	8.113	7.892
Mg	0.001	0.001	0.001	0.001	0.000	0.001	0.002	0.001	0.001
Ti^{4+}	0.003	0.006	0.006	0.000	0.002	0.002	0.001	0.002	0.005
V^{3+}	0.000	0.000	0.001	0.000	0.001	0.001	0.001	0.000	0.001
Mn^{2+}	0.415	0.478	0.573	0.369	0.320	0.187	0.043	0.171	0.426
Fe^{2+}	0.000	0.000	0.000	0.001	0.000	0.001	0.001	0.001	0.000
Cu^{2+}	0.011	0.021	0.020	0.020	0.042	0.007	0.020	0.016	0.050
Zn	0.000	0.000	0.000	0.000	0.000	0.000	0.000	0.000	0.000
Li	0.664	0.624	0.498	0.606	0.645	0.606	0.899	0.696	0.623
Sum Y,Z	**9.000**	**9.000**	**9.000**	**9.000**	**8.997**	**9.000**	**8.978**	**8.999**	**8.997**
Ca	0.017	0.016	0.014	0.013	0.053	0.031	0.152	0.018	0.052
Pb	0.000	0.000	0.000	0.000	0.000	0.000	0.001	0.000	0.000
Bi	0.000	0.000	0.000	0.000	0.001	0.000	0.010	0.001	0.001
Na	0.703	0.722	0.737	0.685	0.651	0.633	0.560	0.649	0.707
Vacancy	0.280	0.262	0.248	0.301	0.293	0.336	0.266	0.332	0.238
Sum X	**1.000**	**1.000**	**1.000**	**1.000**	**1.000**	**1.000**	**1.000**	**1.000**	**1.000**
F	0.580	0.773	0.706	0.642	0.831	0.685	0.817	0.652	0.908
OH	0.210	0.114	0.147	0.179	0.085	0.158	0.091	0.174	0.046
O	0.210	0.113	0.147	0.179	0.084	0.157	0.092	0.174	0.046
Sum W	**1.000**	**1.000**	**1.000**	**1.000**	**1.000**	**1.000**	**1.000**	**1.000**	**1.000**
Trace elements (ppm)									
Mg	0.33	0.35	bdl	bdl	0.54	bdl	0.25	0.19	0.64
Ni	bdl	bdl	bdl	bdl	bdl	bdl	bdl	bdl	bdl
Cu	742	1342	1262	1303	2782	447	1314	1049	3224
Zn	bdl	7.89	14.0	bdl	bdl	4.48	bdl	bdl	19.3
La	bdl	bdl	bdl	bdl	bdl	0.06	bdl	bdl	bdl
Ce	bdl	bdl	bdl	bdl	bdl	0.05	bdl	bdl	bdl
Pr	bdl	bdl	bdl	bdl	bdl	bdl	bdl	bdl	bdl
Nd	bdl	bdl	bdl	bdl	bdl	bdl	bdl	bdl	bdl
Sm	bdl	bdl	bdl	bdl	bdl	bdl	bdl	bdl	bdl
Pb	7.71	8.10	7.28	8.50	39.0	10.7	141	9.11	50.5
Bi	35.3	32.5	28.1	40.6	342	48.8	2324	57.8	253
Σ REE	bdl	bdl	bdl	bdl	bdl	0.11	bdl	bdl	bdl

[a] See notes in Table I. Abbreviation: bdl = below detection limit.

MOZ10	MOZ11	MOZ12	MOZ13	MOZ14	MOZ15	MOZ16	MOZ17	MOZ18
1.23	1.41	1.27	1.13	0.32	1.49	1.53	8.19	7.69
8.0	9.1	8.1	8.0	5.0	8.5	9.4	15.5	12.4
Purplish pink	Orangey pink	Purple	Green	Bluish green	Greenish blue	Yellowish green	Yellow-brown	Bluish grey
37.10	37.49	37.50	35.91	35.62	37.59	36.40	37.24	38.25
bdl	0.01	0.01	0.10	0.07	0.03	0.04	0.01	0.01
10.75	10.86	10.86	10.40	10.32	10.89	10.54	10.79	11.08
9.21	9.25	9.61	9.11	9.19	10.51	9.44	8.89	10.10
42.67	43.56	42.26	39.30	38.91	41.21	40.38	42.19	43.77
0.01	bdl	bdl	bdl	0.02	0.01	0.01	bdl	bdl
bdl	bdl	bdl	bdl	0.02	0.01	0.01	bdl	bdl
0.10	0.20	0.07	0.28	0.37	0.71	0.30	0.11	0.38
1.70	0.60	2.27	4.75	4.37	0.86	3.45	2.67	0.10
bdl	bdl	bdl	bdl	0.01	bdl	bdl	bdl	0.01
0.13	0.04	0.16	0.51	0.42	1.22	0.38	0.08	0.16
bdl	bdl	bdl	bdl	bdl	0.03	bdl	0.01	bdl
bdl	bdl	bdl	bdl	0.01	0.01	bdl	0.01	0.01
0.01	bdl	bdl	0.02	0.04	0.07	0.04	0.03	0.30
0.95	1.08	1.09	0.76	0.85	1.51	0.93	0.94	1.35
1.45	1.88	1.72	1.63	1.50	2.22	1.67	1.81	2.34
2.03	1.99	2.25	2.43	2.39	2.07	2.30	2.21	1.93
1.23	1.10	1.15	1.74	1.71	1.80	1.62	1.32	1.35
2.94	3.01	3.00	2.72	2.70	2.85	2.79	2.94	3.02
–0.52	–0.46	–0.48	–0.73	–0.72	–0.76	–0.68	–0.56	–0.57
99.11	**99.49**	**100.15**	**98.18**	**97.09**	**100.12**	**98.49**	**100.00**	**101.14**
6.000	6.000	6.000	6.000	6.000	6.000	6.000	6.000	6.000
3.000	3.000	3.000	3.000	3.000	3.000	3.000	3.000	3.000
8.133	8.216	7.967	7.739	7.727	7.752	7.845	8.011	8.090
0.001	0.001	0.000	0.000	0.004	0.002	0.002	0.000	0.000
0.000	0.001	0.001	0.013	0.009	0.004	0.005	0.002	0.001
0.001	0.000	0.001	0.000	0.002	0.001	0.001	0.000	0.000
0.233	0.081	0.308	0.672	0.624	0.117	0.481	0.364	0.013
0.000	0.000	0.000	0.000	0.001	0.001	0.000	0.000	0.001
0.016	0.005	0.019	0.064	0.053	0.148	0.047	0.010	0.019
0.000	0.000	0.000	0.000	0.000	0.004	0.000	0.001	0.000
0.615	0.695	0.703	0.509	0.576	0.966	0.615	0.609	0.850
8.999	**9.000**	**9.000**	**8.998**	**8.996**	**8.994**	**8.997**	**8.997**	**8.974**
0.018	0.035	0.013	0.050	0.067	0.122	0.052	0.018	0.063
0.000	0.000	0.000	0.000	0.000	0.000	0.000	0.000	0.000
0.001	0.000	0.000	0.001	0.002	0.003	0.002	0.002	0.013
0.635	0.618	0.697	0.788	0.779	0.641	0.734	0.690	0.586
0.346	0.346	0.290	0.160	0.150	0.231	0.210	0.289	0.324
1.000	**1.000**	**1.000**	**1.000**	**1.000**	**1.000**	**1.000**	**1.000**	**1.000**
0.647	0.570	0.599	0.933	0.929	0.932	0.862	0.692	0.688
0.176	0.215	0.201	0.034	0.036	0.034	0.069	0.154	0.156
0.177	0.215	0.200	0.033	0.035	0.034	0.069	0.154	0.156
1.000	**1.000**	**1.000**	**1.000**	**1.000**	**1.000**	**1.000**	**1.000**	**1.000**
bdl	bdl	bdl	0.28	0.68	2.67	bdl	133	1.01
bdl	bdl	bdl	bdl	bdl	bdl	bdl	0.74	bdl
1071	353	1242	4074	3338	9780	3032	628	1273
bdl	bdl	bdl	23.7	11.6	269	bdl	81	bdl
bdl	bdl	bdl	bdl	bdl	0.39	bdl	3.28	bdl
bdl	bdl	bdl	bdl	bdl	0.35	bdl	5.24	bdl
bdl	bdl	bdl	bdl	bdl	0.04	bdl	0.59	bdl
bdl	bdl	bdl	bdl	bdl	bdl	bdl	1.42	bdl
bdl	bdl	bdl	bdl	bdl	bdl	bdl	0.41	bdl
10.2	7.25	9.31	31.9	53.1	54.6	39.2	60.3	54.9
59.9	39.7	43.8	193	356	675	346	305	2900
bdl	bdl	bdl	bdl	bdl	0.78	bdl	10.94	bdl

Table III: Chemical analyses of tourmaline from Nigeria, measured by EMPA.[a]

Sample no.	NIG1	NIG2								
Weight (ct)	8.20	2.41								
Max. size (mm)	17.1	10.5								
Colour	Greenish blue	Violet		Blue						
Point	–	V1	V2	B1	B2	B3	B4	B5	B6	B7
Oxides (wt.%)										
SiO_2	37.77	37.19	37.07	36.87	36.61	36.97	36.83	36.80	36.99	36.85
TiO_2	bdl	bdl	bdl	bdl	bdl	bdl	bdl	0.06	0.07	bdl
B_2O_3*	10.94	10.78	10.74	10.68	10.61	10.71	10.67	10.66	10.72	10.68
Al_2O_3	41.24	40.69	40.90	40.20	40.16	40.32	39.55	39.11	39.22	40.28
MgO	bdl	bdl	bdl	bdl	bdl	bdl	bdl	bdl	bdl	bdl
CaO	0.79	0.09	0.08	0.47	0.43	0.12	0.12	0.13	0.15	0.28
MnO_{tot}	0.98	1.15	1.23	0.55	0.38	0.91	1.63	1.57	1.59	1.00
FeO_{tot}	0.01	bdl	bdl	bdl	bdl	0.06	0.39	0.55	0.49	bdl
CuO	0.27	0.54	0.51	1.61	1.85	0.92	0.90	0.81	0.86	1.32
ZnO	0.01	bdl	bdl	bdl	bdl	bdl	bdl	0.06	0.07	bdl
PbO	0.09	bdl	bdl	bdl	bdl	bdl	bdl	bdl	bdl	bdl
BiO	0.05	bdl	bdl	0.19	0.44	0.41	0.30	0.35	0.26	0.15
Li_2O*	1.73	1.61	1.48	1.54	1.43	1.57	1.53	1.62	1.66	1.47
Na_2O	2.01	1.94	2.04	1.95	1.94	2.00	2.09	2.13	2.11	1.97
F	1.64	0.76	0.60	0.99	1.26	0.86	1.05	1.13	1.00	0.87
H_2O*	2.75	3.06	3.09	2.98	2.89	3.02	2.96	2.94	2.99	3.01
–O=F	–0.69	–0.32	–0.25	–0.42	–0.53	–0.36	–0.44	–0.48	–0.42	–0.36
Sum (EMPA data)	**99.58**	**97.48**	**97.48**	**97.61**	**97.46**	**97.50**	**97.58**	**97.43**	**97.74**	**97.50**
Ions per 31 (O+OH+F)										
Si	6.000	6.000	6.000	6.000	6.000	6.000	6.000	6.000	6.000	6.000
B	3.000	3.000	3.000	3.000	3.000	3.000	3.000	3.000	3.000	3.000
Al	7.721	7.736	7.804	7.710	7.757	7.712	7.595	7.516	7.500	7.729
Mg	0.000	0.000	0.000	0.000	0.000	0.000	0.000	0.000	0.000	0.000
Ti^{4+}	0.000	0.000	0.000	0.000	0.000	0.000	0.000	0.007	0.008	0.000
Mn^{2+}	0.415	0.157	0.168	0.076	0.053	0.125	0.225	0.216	0.218	0.138
Fe^{2+}	0.000	0.000	0.000	0.000	0.000	0.008	0.053	0.075	0.066	0.000
Cu^{2+}	0.011	0.066	0.062	0.197	0.229	0.112	0.111	0.100	0.106	0.162
Zn	0.000	0.000	0.000	0.000	0.000	0.000	0.000	0.007	0.008	0.000
Li	0.664	1.041	0.965	1.008	0.942	1.025	1.003	1.064	1.083	0.964
Sum Y,Z	**8.992**	**9.000**	**9.000**	**8.992**	**8.981**	**8.982**	**8.987**	**8.985**	**8.989**	**8.994**
Ca	0.134	0.015	0.014	0.082	0.075	0.020	0.021	0.023	0.026	0.048
Pb	0.004	0.000	0.000	0.000	0.000	0.000	0.000	0.000	0.000	0.000
Bi	0.002	0.000	0.000	0.008	0.019	0.018	0.013	0.015	0.011	0.006
Na	0.618	0.607	0.639	0.615	0.618	0.630	0.662	0.674	0.663	0.621
Vacancy	0.243	0.378	0.347	0.295	0.288	0.332	0.304	0.288	0.300	0.325
Sum X	**1.000**	**1.000**	**1.000**	**1.000**	**1.000**	**1.000**	**1.000**	**1.000**	**1.000**	**1.000**
F	0.848	0.405	0.322	0.530	0.674	0.463	0.563	0.609	0.535	0.465
OH	0.076	0.298	0.339	0.235	0.163	0.268	0.219	0.195	0.233	0.267
O	0.076	0.297	0.339	0.235	0.163	0.269	0.218	0.196	0.232	0.268
Sum W	**1.000**	**1.000**	**1.000**	**1.000**	**1.000**	**1.000**	**1.000**	**1.000**	**1.000**	**1.000**

[a] See notes in Table I regarding the EMPA analyses. V is below detection limit in all measurements. For sample NIG2, representative analyses are given for various zones from the violet core to the dark yellowish green rim. Abbreviation: bdl = below detection limit.

Table IV: Trace elements in tourmaline from Nigeria, measured by LA-ICP-MS.[a]

Sample No.	NIG1	NIG2A	NIG2B	NIG2C	NIG2D	NIG2E	NIG2F
Colour	Greenish blue	Violet	Violet	Violet	Blue	Blue	Yellowish green
Trace elements (ppm)							
Li	9881	7083	9304	8885	8964	9697	7995
B	28623	30472	31371	28634	28505	30723	29772
Mg	0.27	bdl	bdl	0.30	2.18	232	455
Cu	2120	3668	3040	2929	5023	5053	4321
Zn	48.5	bdl	bdl	bdl	49.9	420	1048
La	bdl	bdl	bdl	bdl	bdl	0.87	0.85
Ce	bdl	bdl	bdl	bdl	bdl	1.37	1.65
Pr	bdl	bdl	bdl	bdl	bdl	0.08	0.13
Nd	bdl	bdl	bdl	bdl	bdl	bdl	0.25
Sm	bdl	bdl	bdl	bdl	bdl	bdl	0.33
Pb	859	21.1	15.2	15.5	75.7	24.2	69.3
Bi	431	125	84.1	78.6	2905	2011	2415
Σ REE	bdl	bdl	bdl	bdl	bdl	2.3	3.2

[a] See notes in Table I regarding the LA-ICP-MS analyses. Ni is below detection limit in all samples. Abbreviation: bdl = below detection limit.

NIG2						
2.41						
10.5						
Yellowish green						
G1	G2	G3	G4	G5	G6	G7
36.60	36.48	36.49	36.77	36.69	36.60	36.40
0.12	0.10	0.09	0.06	0.09	0.09	0.07
10.60	10.57	10.57	10.65	10.63	10.60	10.54
39.32	38.89	38.61	39.29	38.86	38.88	38.56
bdl	bdl	bdl	bdl	bdl	bdl	0.06
0.33	0.30	0.33	0.25	0.24	0.31	0.27
2.05	2.40	2.44	2.21	2.26	2.20	2.55
0.69	0.64	0.76	0.64	0.64	0.69	0.66
0.93	0.87	0.81	0.48	0.71	0.84	0.78
0.09	0.06	0.06	0.11	0.05	bdl	bdl
bdl	bdl	bdl	bdl	bdl	0.09	bdl
0.29	0.36	0.29	0.32	0.22	0.29	0.32
1.33	1.36	1.42	1.46	1.51	1.45	1.40
2.10	2.13	2.21	2.13	2.15	2.15	2.26
1.16	1.16	1.01	0.91	1.24	1.01	1.46
2.91	2.90	2.94	2.99	2.90	2.95	2.82
−0.49	−0.49	−0.43	−0.38	−0.52	−0.42	−0.62
98.01	**97.72**	**97.61**	**97.87**	**97.66**	**97.71**	**97.53**
6.000	6.000	6.000	6.000	6.000	6.000	6.000
3.000	3.000	3.000	3.000	3.000	3.000	3.000
7.596	7.538	7.483	7.556	7.490	7.513	7.491
0.000	0.000	0.000	0.000	0.000	0.000	0.014
0.014	0.013	0.011	0.007	0.012	0.011	0.008
0.285	0.334	0.339	0.306	0.313	0.306	0.356
0.094	0.088	0.105	0.087	0.087	0.094	0.092
0.115	0.108	0.101	0.059	0.087	0.103	0.097
0.010	0.007	0.008	0.013	0.006	0.000	0.000
0.874	0.896	0.940	0.958	0.995	0.956	0.928
8.987	**8.984**	**8.987**	**8.986**	**8.990**	**8.984**	**8.986**
0.058	0.052	0.057	0.043	0.042	0.055	0.048
0.000	0.000	0.000	0.000	0.000	0.004	0.000
0.013	0.016	0.013	0.014	0.010	0.013	0.014
0.668	0.680	0.704	0.674	0.681	0.683	0.724
0.261	0.252	0.226	0.269	0.267	0.246	0.214
1.000	**1.000**	**1.000**	**1.000**	**1.000**	**1.000**	**1.000**
0.625	0.627	0.550	0.489	0.669	0.545	0.788
0.187	0.186	0.225	0.256	0.165	0.228	0.106
0.188	0.187	0.225	0.255	0.166	0.227	0.106
1.000	**1.000**	**1.000**	**1.000**	**1.000**	**1.000**	**1.000**

The formula units of tourmaline were calculated by normalising to 31 (O+OH+F) and 15 cations in the tetrahedral and octahedral sites (T+Z+Y). OH and O were calculated by using the empirical formulae OH = 3+(1–F)/2 and O = 31–(F+OH) of Grice and Ercit (1993). Li_2O was calculated based on the assumptions that (1) Si = 6 apfu, (2) Al on the tetrahedral position is negligible (Ertl et al., 2013) and (3) the Y position is completely filled with 3 apfu. Because there is no indication of tetrahedrally coordinated B, the B_2O_3 content was calculated with the assumption that the B site is completely filled with 3 apfu. The Z position will be almost completely occupied by $^{[6]}$Al and perhaps additional small amounts of Ti (Ertl et al., 2012), while the Y position is occupied by the remaining amounts of $^{[6]}$Al, V, Mg, Mn, Fe, Cu, Zn and Li. Calcium, Pb, Bi, Na, K and vacancies are on the X site.

Results

Average chemical analyses and corresponding formulae for each sample are presented in Tables I, II and III/IV for Brazil, Mozambique and Nigeria, respectively. Except for the colour-zoned crystal NIG2, no individual point analyses are presented, although chemical variations within the individual samples may be considerable.

All of the samples show homogeneous coloration except for NIG2, which has a violet core, a blue intermediate zone and a dark yellowish green rim (Figure 2). A backscattered electron (BSE) image of this tourmaline (produced using the electron microprobe) revealed that the core is homogeneous in composition and has a sharp boundary with the adjacent blue zone (Figure 7). The visually more diffuse boundary between that zone and the yellowish green rim is due to the presence of domains of variable composition, as revealed by darker and lighter areas, with the latter corresponding to higher average atomic number. Darker-appearing domains in the BSE image are predominant in the blue zone, whereas the yellowish green rim has darker and lighter domains that are present in similar proportions.

X-site Composition

With average Na_2O values between 1.8 and 2.7 wt.%, Na is by far the most important cation in the X site of the tourmaline samples analysed, whereas K is always below the detection limit of EMPA. CaO never exceeds 1 wt.%. Thus, based on their X-site occupancy, all of the tourmalines belong to the alkali group (Henry et al., 2011; Figure 8a) with 0.56–0.83 apfu Na, up to 0.15 apfu Ca and up to 0.38 apfu vacancies. Within the alkali group, all samples plot in the elbaite field, and most of them are close to the elbaite end member (Figure 8b).

Lithium

Li contents were measured by LA-ICP-MS (Li_2O** in Tables I and II), but calculation of the tourmaline formulas using these values consistently resulted in excessive occupancy of the Y position (=Li+Al+Mn+Cu[+Mg+Fe]), that is, exceeding the

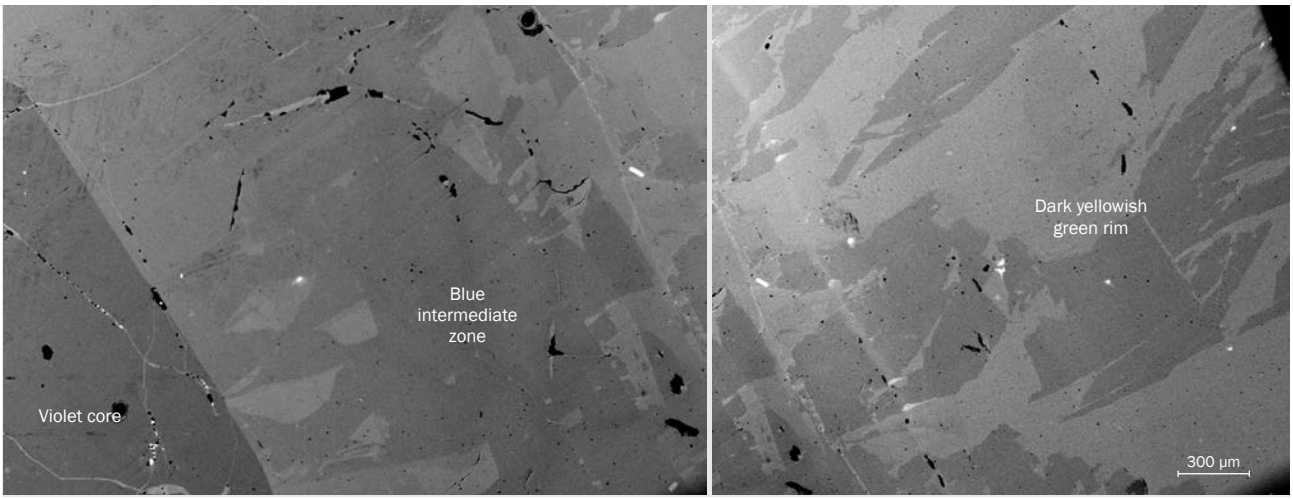

Figure 7: BSE imaging of the zoned tourmaline NIG2 shows a sharp boundary between the compositionally homogeneous violet core and the blue intermediate zone, the latter gradually merging with the dark yellowish green rim. The outer zones are formed by darker- and lighter-appearing domains of different composition. The crystallographic orientation of the section is perpendicular to the c-axis.

maximum possible site occupancy of 3 cations. This discrepancy may be due to problems with the non-routine Li standardization of the LA-ICP-MS analyses. Consequently, the Li contents theoretically calculated for the tourmaline formula at Y = 3 are used in the following considerations and are given as Li_2O* in Tables I–III.

The calculated Li_2O contents fall within a range of 0.62–1.73 wt.% (or 0.40–1.08 apfu). The Li/(Li+^{Y}Al) ratios are in the range of 0.20–0.39 (average of 0.32) for the Brazilian samples and 0.21–0.36 (lower average of 0.25) for those from Mozambique. The unzoned Nigerian tourmaline NIG1 yielded a Li/(Li+^{Y}Al) ratio of 0.39, while the zoned sample provided a range of 0.25–0.42. In general, tourmaline with a relatively low Li/(Li+^{Y}Al) ratio of <0.5 and/or a high amount of vacancies at the X site may have a considerable content of the rossmanite end member □$(LiAl_2)Al_6(BO_3)_3[Si_6O_{18}](OH)_4$. However, there is only a very indistinct negative correlation between the Li/(Li+^{Y}Al) ratio and X-site vacancies in our samples, which is expected for the substitution $^{X}□^{Y}(1.5Li+1.5Al) = {}^{X}Na^{Y}(Li+2Al)$.

Boron

As stated above, the B_2O_3 contents for our tourmalines are calculated for a boron position that is completely filled with 3.0 apfu B (see B_2O_3* in Tables I–III). The B_2O_3 contents determined by LA-ICP-MS vary between 8.52 and 10.98 wt.% (see B_2O_3** in Tables I–II), leading to <3.0 apfu B, with BRA17 as the only exception. We assume that the variability of our B_2O_3** data and a tendency toward an unfilled B position are, at least partly, due to the relatively high analytical uncertainty of the LA-ICP-MS method (which is more suited for trace than for major elements).

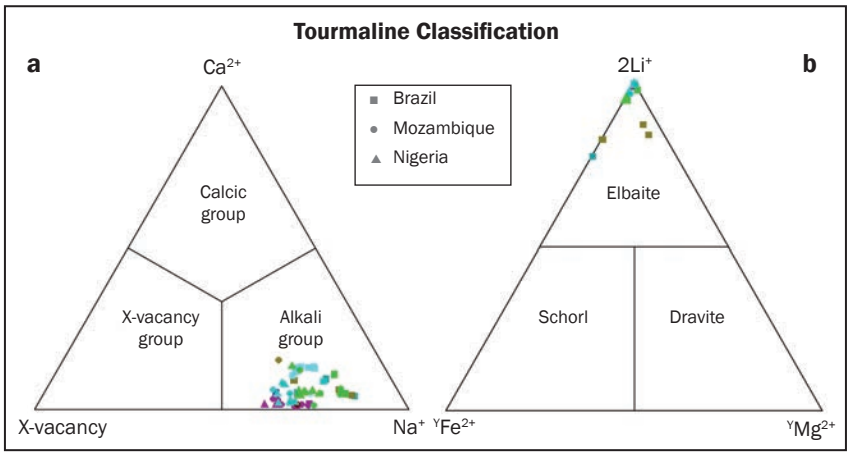

Figure 8: (a) The ternary plot of Ca^{2+}–Na^{+}–X-site vacancy is used to classify the principal groups of tourmaline based on X-site occupancy (Henry et al., 2011). All of the samples belong to the alkali group. (b) The ternary diagram $2Li^{+}$–Mg^{2+}–Fe^{2+} for Y-site occupancy of alkali-group tourmalines indicates that all of the analysed samples are elbaite. The colour of the symbols broadly correlates with the colour of the tourmaline.

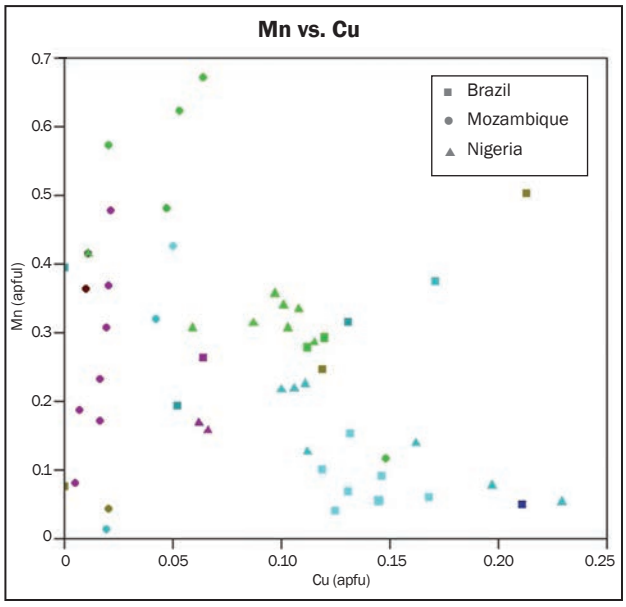

Figure 9: In this plot of Mn vs.Cu, there is no systematic correlation between the contents of these elements and coloration of the tourmalines.

W-site Composition

Fluorine is an important minor constituent in all samples, with average values of 1.1–2.1 wt.% F (0.61–1.09 apfu) for the Brazilian and 1.1–1.8 wt.% F (0.58–0.93 apfu) for the Mozambique tourmalines, while the unzoned Nigerian sample NIG1 contains 1.6 wt.% F and the zoned crystal NIG2 has 0.6–1.5 wt.% F. However, even optically unzoned tourmalines revealed a considerable F variation within individual samples (e.g. 0.6–2.0 wt.% in BRA5 and 1.3–2.3 wt.% in MOZ14). All of the data plot in the field of the 'fluor-' tourmaline subgroup in the ternary diagram F^{-}–OH^{-}–O^{2-} for the W-site occupancy (Henry et al., 2011) and, consequently, are assigned to fluor-elbaite. The Brazilian tourmalines are typically richer in F than those from Mozambique. Five of the former reach the theoretical maximum value of F = 1 apfu for W-site occupancy (Cl was below the EMPA detection limit), and thus approach the theoretical fluor-elbaite end member $Na(Li_{1.5}Al_{1.5})Al_6(BO_3)_3[Si_6O_{18}](OH)_3F$. In the zoned Nigerian tourmaline NIG2, the F contents range between 0.32 and 0.85 apfu.

Other Minor and Trace Elements

Manganese is by far the most important minor element in the tourmalines and, consequently, the main substitution on the Y site is $2Mn^{2+} = Li^{+} + Al^{3+}$. The content of MnO_{tot} (in wt.%) ranges from 0.1 in MOZ18 to 4.8 in MOZ13, and from 0.3 in BRA18 to 3.7 in BRA6; we noted a tendency for lower Mn contents in the tourmalines from Brazil than in those from Mozambique (Figure 9; Tables I and II). In the zoned crystal NIG2, the MnO_{tot} content is 1.1–1.2 wt.% in the violet core, 0.4–1.6 wt.% in the blue intermediate zone, and increases to 2.1–2.5 wt.% in the dark yellowish green rim (Table III).

Copper also is an important minor element in the samples. Contents of >6,000 ppm Cu were recorded in most of those from Brazil, with a maximum value of 13,917 ppm in yellow-green tourmaline BRA6 (Figure 9; Table I). In contrast, two of the Brazilian samples—BRA1 and BRA9—display exceptionally low Cu contents of only 2–3 ppm and thus do not conform to the definition of Paraíba-type tourmalines. The Mozambique tourmalines show a rather wide variation between 353 and 4,074 ppm Cu, with an exceptionally high value of 9,780 ppm Cu for greenish blue sample MOZ15 (Figure 9; Table II). In the zoned crystal NIG2, the Cu contents are 2,929–3,668 ppm in the violet core, sharply increase to 5,023–5,053 ppm in the blue intermediate zone and decrease to 4,321 ppm in the dark yellowish green rim (Figure 9 and Table IV). Within this sample, Cu shows a roughly negative correlation with Mn and a somewhat positive correlation with Ca (Figure 10).

With rare exception, Fe, Mg and Ti are at or below the detection limit of EMPA (Tables I–III). Only two of the Paraíba-type samples from Brazil revealed slightly higher Fe contents (i.e. BRA6 = 0.3 and BRA10 = 0.5 wt.% FeO_{tot}), corresponding to Y-site occupancies of 0.04 and 0.07 apfu Fe^{2+} (Table I; Figures 8b and 11). Hence these tourmalines contain very little of the schorl end member. In the zoned crystal NIG2, the Fe content increases significantly from the core (below detection limit) to the rim (0.8 wt.% FeO_{tot}; Table III).

In most of the tourmalines, Mg contents are at the ppm level, although with a few significant exceptions. The Brazilian samples exhibit a strong variation between 0.3 and 84 ppm Mg, with distinctly higher contents of 139, 841 and 3,637 ppm in samples BRA3, BRA6 and BRA10, corresponding to 0.02–0.60 wt.% MgO (Table I; Figure 8b). Lower Mg contents were recorded in the Mozambique tourmalines, in which Mg is below the detection limit in seven samples and, for the remaining 11 pieces, only three yielded >1 ppm (i.e. up to 2.7 ppm and an exceptional value of 133 ppm in

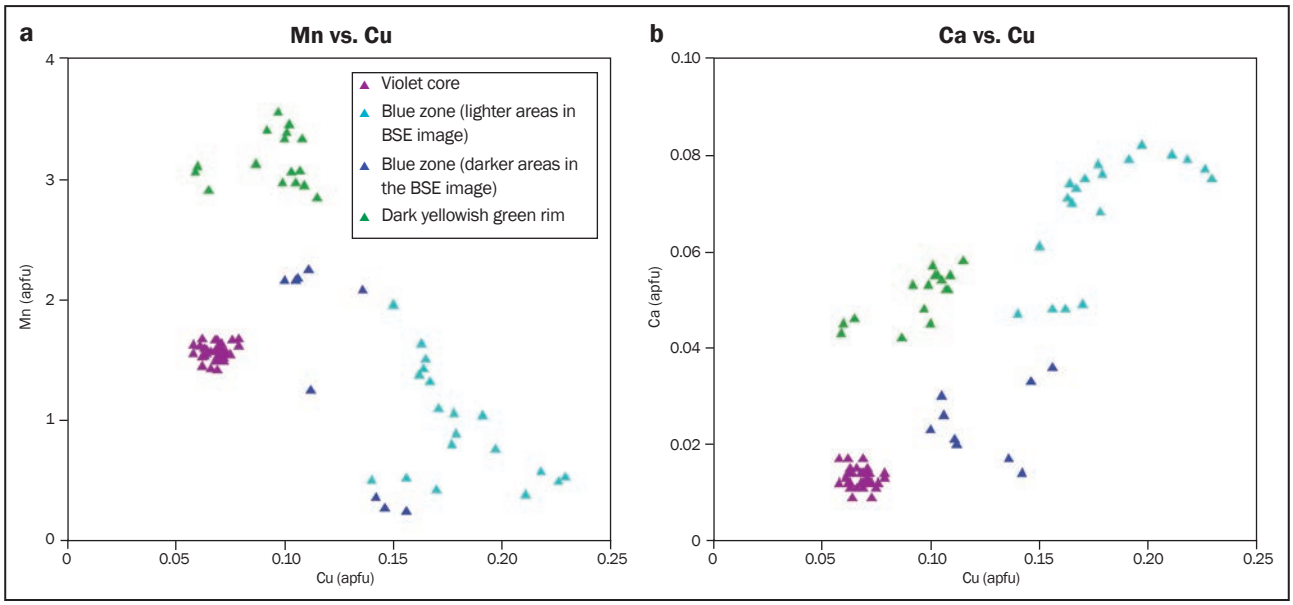

Figure 10: The composition of the zoned tourmaline NIG2 (selected analyses shown in Tables III and IV) is shown in these diagrams of (a) Mn vs. Cu and (b) Ca vs. Cu. The violet core displays a homogeneous composition, whereas the yellowish green rim covers a somewhat broader field of higher Mn and Ca contents. Together with the blue intermediate zone, this field forms a rough compositional trend with a negative correlation of Mn vs. Cu and a positive correlation of Ca vs. Cu.

MOZ17; see Table II). In the zoned crystal NIG2, Mg slightly increases from values below the detection limit in the violet core to 2.2 → 232 → 455 ppm toward the dark yellowish green rim (Table IV).

Among other minor elements frequently present in tourmaline, Cr is below the detection limit, and V is near the detection limit of the EMPA in all samples except BRA6 (0.48 wt.% V_2O_3) and BRA10 (0.62 wt.% V_2O_3). Those tourmalines also contain significant contents of Mg (0.46 and 0.62 wt.% MgO, respectively) and Cu (1.74 and 0.97 wt.% CuO). Such relatively high amounts of Cu, together with V_2O_3 contents up to ~0.6 wt.%, are quite unusual in tourmaline.

Figure 11: The ternary diagram of Al–$Al_{50}Fe_{50}$–$Al_{50}Mg_{50}$ is used to correlate tourmaline composition to host-rock type. As expected, all of the analysed samples plot in the field corresponding to granitic pegmatites. Modified after Henry and Guidotti (1985) and van Hinsberg et al. (2011).

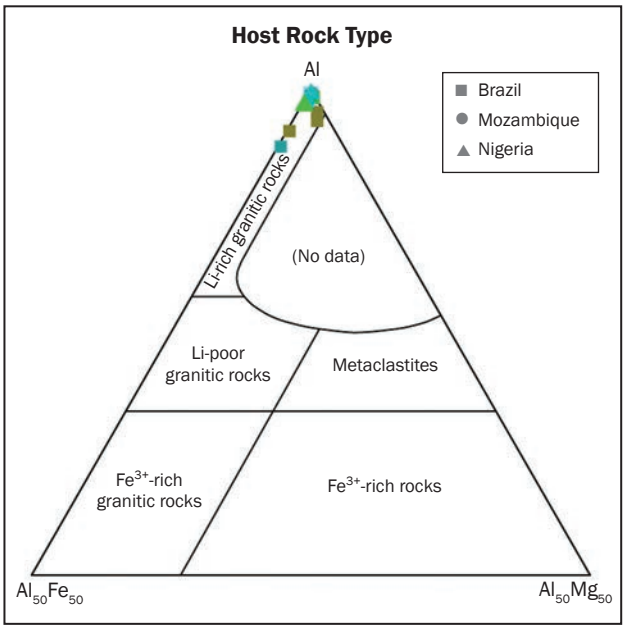

Nickel is below the detection limit of the LA-ICP-MS, except for MOZ17 with 0.74 ppm and BRA18 with 3.6 ppm. For most of the Mozambique tourmalines, Zn values are at the detection limit, although four samples have Zn contents between 4.5 and 24 ppm and MOZ15 and MOZ17 contain 269 and 81 ppm Zn, respectively. In contrast, almost all the Brazilian tourmalines show Zn contents above the detection limit, between 12 and 25 ppm in five samples and from 80 ppm up to 13,820 ppm in 12 samples. Zinc contents in the Nigerian tourmalines are 49 ppm in NIG1 and in NIG2 Zn ranges from below the detection limit in the violet core, up to ~50 → 420 → 1,048 ppm towards the dark yellowish green rim (Table IV).

Lead contents typically range between values close to the detection limit and ~170 ppm. Exceptionally high Pb values were recorded in NIG1 (859 ppm) and BRA18 (4,002 ppm). Bismuth is present in values up to ~2,900 ppm. Whereas Bi is between 84 and 125 ppm in the violet core of

NIG2, values of 2,905 → 2,011 → 2,415 ppm were recorded from the blue zone to the dark yellowish green rim (Table IV).

Rare-earth elements are generally below or near the detection limit in the Mozambique samples, except for MOZ15 and MOZ17 that contain some light REE, with REE totals of 0.8 and 11 ppm, respectively. In the Brazilian tourmalines, trace amounts of the light REE were almost always recorded, particularly La, Ce and Pr. REE totals are between 0.3 and 7.9 ppm except for BRA2 and BRA3, with REE generally below the detection limit. In sample NIG1, all REE are below the detection limit, as well as in the core of NIG2. Near the rim, minor contents of the light REE were measured, with REE totals of 2.3 and 3.2 ppm.

Discussion

Colour and Trace-Element Contents

The contents of Cu measured in the studied tourmalines are similar to those published in the literature. For instance, Abduriyim et al. (2006) analysed 198 stones of various shades of blue and green from Brazil, Mozambique and Nigeria, and obtained Cu ranges of 3,200–20,000, 1,300–25,600 and 3,800–25,500 ppm, respectively.

Although Mn and Cu are important colouring elements in tourmaline, there is no obvious correlation between the contents of these elements and coloration in the investigated samples (Tables I–IV and Figure 9). Even within optically unzoned crystals, considerable variations in MnO_{tot} and Cu were recorded (e.g. 1.6–3.0 wt.% MnO_{tot} in MOZ5 and 10,900–15,300 ppm Cu in BRA5). Nevertheless, certain trends may be observed in the Mn vs. Cu diagram (Figure 9): Most of the green and blue tourmalines from Brazil belong to the high-Cu group (>7,000 ppm Cu), except for one purple and one violetish blue sample (4,148 and 3,354 ppm Cu, respectively). Moreover, one yellowish green and one blue Brazilian tourmaline yielded <3 ppm Cu; the coloration of these non-Paraíba-type stones is mainly due to varying amounts of Fe^{2+} and Fe^{3+}; the green colour can be due to both Fe^{2+} and Fe^{3+} (Mattson and Rossman, 1987) and the blue colour is due to Fe^{2+} (Rossmann, 2016). In the authors' opinion, intervalence charge transfer involving Mn^{2+}–Ti^{4+} (Rossman and Mattson, 1986) probably has only a minor influence (if any) on the greenish coloration of most of the investigated tourmalines, because their Ti contents are very small (usually close to the EMPA detection limit, although some samples have up to ~0.1 wt.% TiO_2).

For the tourmalines from Mozambique, two distinct groups can be distinguished: one group of six blue-to-green samples displays higher Cu contents (>2,500 ppm), whereas the other group with pink-to-violet samples displays lower Cu contents (<1,500 ppm). However, two greenish tourmalines belong to the second group as well, thus blurring the distinction (Figure 9). Colour zonation in NIG2 is matched by variations in Mn and Cu contents (Figure 10a).

The green colour of the three vanadium-bearing Paraíba-type tourmalines (BRA6, BRA7 and BRA10) from Brazil is apparently due to both Cu^{2+} and V^{3+}. Sample BRA7, with the lowest V_2O_3 content (0.13 wt.%), has a greenish blue colour mainly caused by Cu^{2+} (0.89 wt.% CuO; bluish component) with only a minor effect of V^{3+} (greenish component; see also Schmetzer et al., 2007). The tourmalines BRA6 and BRA10 may owe their 'olive' green colour mainly to V^{3+} (0.48 and 0.62 wt.% V_2O_3), whereas Cr is below the detection limit. Spectroscopic features of an Austrian tourmaline with a similar colour and V_2O_3 content strongly testify to V^{3+} (Ertl et al., 2008). Gem tourmalines containing simultaneously significant amounts of V and Cu are quite rare.

It is widely known that Cu- and Mn-bearing, initially purple-to-violet tourmaline may be heat treated to produce the famous Paraíba blue coloration (e.g. Milisenda et al., 2006; Laurs et al., 2008). According to our data, CuO/MnO_{tot} ratios of such heated tourmalines should commonly be low (<0.5), due to low CuO/MnO_{tot} ratios in the original purple-to-violet tourmalines. For example, these values vary between 0.03 and 0.39 (average 0.13) in our purple and violet tourmalines (MOZ1, 2, 4, 6, 8, 10–12 and BRA3). Ratios of CuO/MnO_{tot} within this range (0.04–0.27) also were reported by Laurs et al. (2008) for pink, purple and violet tourmalines from Mozambique. In contrast, CuO/MnO_{tot} ratios in blue to bluish green Cu- and Mn-bearing tourmaline from Brazil usually are higher, ranging between 0.6 and 4.2 (i.e. BRA11–18 and BRA21–25 in Ertl et al., 2013). These samples are assumed to be untreated, and showed an average CuO/MnO_{tot} value of 2.25. Hence, there are indications that blue Cu-bearing tourmaline with CuO/MnO_{tot} <0.5 has been heat treated to

reduce the originally reddish component of Mn^{3+}. This appears to be the case for greenish blue sample NIG1, with a CuO/MnO_{tot} ratio of 0.40. However, more samples should be analysed to test this criterion.

For greenish Cu- and Fe-bearing tourmalines, the cause of colour is more complex. For instance, the blue and yellowish green colours displayed by sample NIG2 are presumably caused by different proportions of the domains richer and poorer in Cu (0.48–1.85 wt.% CuO; Figures 7 and 10) and Fe (up to 0.76 wt.% FeO_{tot}), whereas the Ti contents are generally very low (up to 0.12 wt.%). The Mn contents are distinctly higher in the yellowish green rim (2.05–2.55 wt.% MnO_{tot}) than in the violet core (1.15–1.23 wt.% MnO_{tot}), whereas they are highly variable in the transitional blue zone (0.38–1.63 wt.% MnO_{tot}). This means that the patchy appearance observed in the BSE image of the outer portion of this sample (Figure 7) is mainly due to variations in the Mn, Cu and Fe contents.

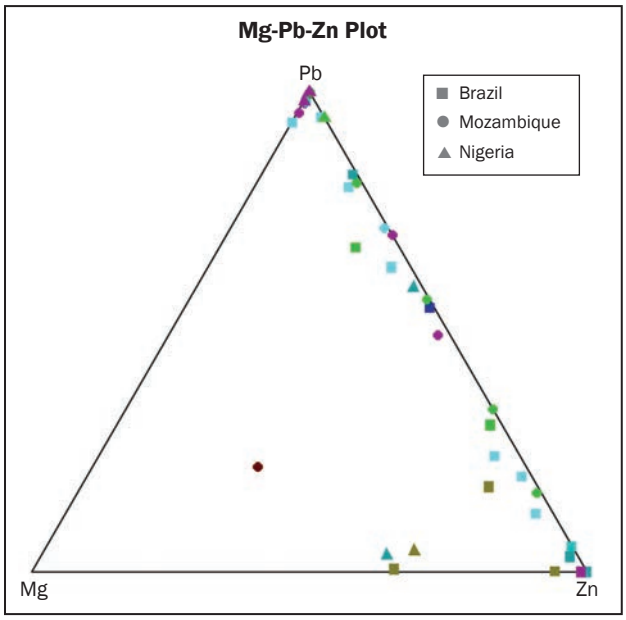

Figure 12: The ternary diagram Pb-Zn-Mg used by Abduriyim et al. (2006) for provenance discrimination does not reveal any systematic differences between the Paraíba-type tourmalines from Brazil, Mozambique and Nigeria that were analysed for this study.

Source Rock and Provenance Criteria

In the ternary diagram Al-Mg-Fe_{tot} for discriminating the host rock of various tourmalines (Figure 11), all of the investigated samples plot at, or near, the Al apex, within the field of Li-rich granitoids or their pegmatites and aplites (Henry and Guidotti, 1985). This is consistent with the known or inferred geological origin of these tourmalines as originating from granitic pegmatites and/or related placer deposits.

As seen in the Mn vs. Cu variation diagram (Figure 9), tourmalines from Brazil and Mozambique display similar ranges of Mn, with maximum values of 3.66 and 4.75 wt.% MnO_{tot}, respectively, but in general show significant differences in their Cu contents. Whereas nearly all samples from Mozambique contained <4,100 ppm Cu, 14 Brazilian stones yielded >7,000 ppm Cu. Notable exceptions are samples BRA2 and BRA3 with intermediate Cu contents, BRA1 and BRA9 with <3 ppm Cu, as well as MOZ15 with nearly 9,800 ppm Cu. However, due to their large variability, contents of Mn, Cu and other elements are not sufficient for a reliable discrimination between the localities.

Based on a ternary plot of Pb-Zn-Mg, Abduriyim et al. (2006) revealed tendencies to distinguish between different provenances of Paraíba-type tourmalines, with Brazilian ones being typically Mg-Zn dominant, Mozambique samples showing Pb dominance and Nigerian tourmalines being Pb-Zn dominant. However, almost all of our samples are poor in Mg and plot unsystematically along the Pb-Zn side of the triangle (Figure 12). The zoned tourmaline from Nigeria NIG2 is lacking Mg and Zn in the inner part, so analyses from the violet and the blue zones therefore plot close to the Zn apex, whereas one analysis from the outer portion of the blue zone and from the green zone have somewhat elevated Zn and Mg contents and plot along the Zn-Mg side.

Milisenda et al. (2006) used a CuO/CaO vs. Pb diagram for the first step of discriminating Cu-bearing tourmalines from Brazil, Mozambique and Nigeria. They defined a Brazilian field by CuO/CaO ratios up to 10 and Pb contents up to 100 ppm. Our tourmalines from Brazil in general plot into this field. The Mozambique tourmalines analysed by Milisenda et al. (2006) defined two fields in the diagram, a first one overlapping the Brazilian field and a second one with CuO/CaO ratios below 1 and Pb contents up to 1,200 ppm. Our Mozambique samples plot into the first field and, therefore, are not distinct from the Brazilian ones. Tourmaline compositions of Milisenda et al. (2006) from Nigeria matched either the first or second field mentioned above (corresponding to type I

Figure 13: This 18 ct white gold and diamond pendant features a 6.98 ct green Cu-bearing tourmaline from Mozambique. Courtesy of collectorfinejewelry.com; photo by Mia Dixon.

and type II, respectively). All analyses of our zoned tourmaline NIG2 display CuO/CaO ratios between 2 and 8 at Pb contents clearly below 100 ppm, thus belonging to Nigeria type I of Milisenda et al. (2006). In contrast, sample NIG1 clearly fits with type 2. For further discriminations, a CuO+MnO versus Pb/Be diagram was used by Milisenda et al. (2006), but this diagram also does not allow for unambiguous provenance assignment of our samples. A third diagram used by Milisenda et al. (2006) involved the Pb/Be ratio, but Be was not analysed in our study. It should be noted that for origin determination the isotope ratios of boron and lithium, $\delta^{11}B$ and $\delta^{7}Li$, are more suitable than trace-element content (e.g. Shabaga et al., 2010; Marschall and Jiang, 2011).

From plate-tectonic considerations, a spatial and temporal connection between the tourmaline-bearing pegmatites in northeast Brazil and Nigeria seems possible (Milisenda, 2001a; Milisenda and Henn, 2001), although precise results from radiometric dating are still needed to prove this possibility.

Conclusions

Paraíba-type tourmaline is prized for its vibrant coloration (e.g. Figure 13), and is currently known from pegmatite provinces in Paraíba and Rio Grande del Norte States, Brazil, from Alto Ligonha, Mozambique and from Oyo State, Nigeria. Chemical analysis by EMPA and LA-ICP-MS of 38 samples from these three countries revealed that they are virtually Mg-free and Fe-poor elbaite (close to the end-member composition). In all samples, F occupied >0.5 apfu in the W site, thus conforming to the fluor-elbaite species. Significant, though highly variable amounts of Cu^{2+} ± Mn^{2+} ± Mn^{3+} are the main chromophores in most of the variably coloured tourmalines, consistent with results previously published in the literature. Our blue-to-green samples from Brazil contain up to 13,920 ppm Cu and 3.7 wt.% MnO_{tot}, and from Mozambique the maximum contents are 9,780 ppm Cu and 4.8 wt.% MnO_{tot}, whereas a zoned crystal from Nigeria yielded up to 5,050 ppm Cu and 2.6 wt.% MnO_{tot}. Some of the green Cu-bearing tourmalines from Brazil may partially owe their colour to V (with up to 0.6 V_2O_3) in rare combination with Cu. Green coloration in the Nigerian tourmalines is probably caused by a combination of Mn, Cu and Fe. We suggest that CuO/MnO_{tot} <0.5 is indicative of heat treatment in blue Cu-bearing tourmaline to reduce the contribution of the reddish component of Mn^{3+}.

References

Abduriyim A., Kitawaki H., Furuya M. and Schwarz D., 2006. "Paraíba"-type copper-bearing tourmaline from Brazil, Nigeria, and Mozambique: Chemical fingerprinting by LA-ICP-MS. *Gems & Gemology*, **42**(1), 4–21, http://dx.doi.org/10.5741/gems.42.1.4.

Beurlen H., Moura O.J.M., Soares D.R., Da Silva M.R.R. and Rhede D., 2011. Geochemical and geological controls on the genesis of gem-quality "Paraíba tourmaline" in granitic pegmatites from northeastern Brazil. *Canadian Mineralogist*, **49**(1), 277–300, http://dx.doi.org/10.3749/canmin.49.1.277.

Brandstätter F. and Niedermayr G., 1993. Einschlüsse von gediegen Kupfer in Cu-Elbait von São José da Batalha in Paraíba, Brasilien. *Zeitschrift der Deutschen Gemmologischen Gesellschaft*, **42**(1), 37–41.

Brandstätter F. and Niedermayr G., 1994. Copper and tenorite inclusions in cuprian-elbaite tourmaline from Paraíba, Brazil. *Gems & Gemology*, **30**(3), 178–183, http://dx.doi.org/10.5741/gems.30.3.178.

Deer W.A., Howie R.A. and Zussman J., 1986. *Rock-Forming Minerals, Vol. 1B: Disilicates and Ring Silicates*, 2nd edn. Geological Society of London, 630 pp.

Dietrich R.V., 1985. *The Tourmaline Group*. Springer, New York, New York, USA, 302 pp.

Dunn P.J., 1975. On gem elbaite from Newry, Maine. *Journal of Gemmology*, **14**(8), 357–368.

Dunn P.J., Appleman D., Nelen J.A. and Norberg J., 1977. Uvite, a new (old) common member of the tourmaline group and its implications for collectors. *Mineralogical Record*, **8**(2), 100–108.

Dyar M.D., Wiedenbeck M., Robertson D., Cross L.R., Delaney J.S., Ferguson K., Francis C.A., Grew E.S., Guidotti C.V., Hervig R.L., Hughes J.M., Husler J., Leeman W., McGuire A.V., Rhede D., Rothe H., Paul R.L., Richards I. and Yates M., 2001. Reference minerals for the microanalysis of light elements. *Geostandards and Geoanalytical Research*, **25**(2–3), 441–463, http://dx.doi.org/10.1111/j.1751-908x.2001.tb00616.x.

Epprecht W., 1953. Die Gitterkonstanten der Turmaline. *Schweizerische Mineralogische und Petrographische Mitteilungen*, **33**(2), 481–505.

Ertl A., Hughes J.M., Prowatke S., Rossman G.R., London D. and Fritz E.A., 2003. Mn-rich tourmaline from Austria: Structure, chemistry, optical spectra, and relations to synthetic solid solutions. *American Mineralogist*, **88**(8–9), 1369–1376, http://dx.doi.org/10.2138/am-2003-8-921.

Ertl A., Rossman G.R., Hughes J.M., Ma C. and Brandstätter F., 2008. V^{3+}-bearing, Mg-rich, strongly disordered olenite from a graphite deposit near Amstall, Lower Austria: A structural, chemical and spectroscopic investigation. *Neues Jahrbuch für Mineralogie, Abhandlungen*, **184**(3), 243–253, http://dx.doi.org/10.1127/0077-7757/2008/0100.

Ertl A., Kolitsch U., Dyar M.D., Hughes J.M., Rossman G.R., Pieczka A., Henry D.J., Pezzotta F., Prowatke S., Lengauer C.L., Korner W., Brandstätter F., Francis C.A., Prem M. and Tillmanns E., 2012. Limitations of Fe^{2+} and Mn^{2+} site occupancy in tourmaline: Evidence from Fe^{2+}- and Mn^{2+}-rich tourmaline. *American Mineralogist*, **97**(8–9), 1402–1416, http://dx.doi.org/10.2138/am.2012.4028.

Ertl A., Giester G., Schüssler U., Brätz H., Okrusch M., Tillmanns E. and Bank H., 2013. Cu- and Mn-bearing tourmalines from Brazil and Mozambique: Crystal structures, chemistry and correlations. *Mineralogy and Petrology*, **107**(2), 265–279, http://dx.doi.org/10.1007/s00710-012-0234-6.

Fritsch E., Shigley J.E., Rossman G.R., Mercer M.E., Muhlmeister S.M. and Moon M., 1990. Gem-quality cuprian-elbaite tourmalines from São José da Batalha, Paraíba, Brazil. *Gems & Gemology*, **26**(3), 189–205, http://dx.doi.org/10.5741/gems.26.3.189.

Furuya M. and Furuya M., 2007. *The World of Gemstones—Paraiba Tourmaline: Electric Blue Brilliance Burnt into Our Minds*. Japan Germany Gemmological Laboratory, Kofu, Japan, 24 pp.

Grice I.B. and Ercit S.T., 1993. Ordering of Fe and Mg in the tourmaline crystal structure: The correct formula. *Neues Jahrbuch für Mineralogie, Abhandlungen*, **165**(3), 245–266.

Hawthorne F.C. and Dirlam D.M., 2011. Tourmaline the indicator mineral: From atomic arrangement to Viking navigation. *Elements*, **7**(5), 307–312, http://dx.doi.org/10.2113/gselements.7.5.307.

Henn U. and Bank H., 1990. On the colour and pleochroism of Cu-bearing blue and green tourmalines from Paraiba, Brazil. *Neues Jahrbuch für Mineralogie, Monatshefte*, **1990**(6), 280–288.

Henry D.J. and Guidotti C.V., 1985. Tourmaline as a petrogenetic indicator mineral: An example from the staurolite-grade metapelites of NW Maine. *American Mineralogist*, **70**(1–2), 1–15.

Henry D.J. and Dutrow B.L., 1996. Metamorphic tourmaline and its petrologic applications. *Reviews in Mineralogy and Geochemistry*, **33**(1), 503–557.

Henry D.J., Novák M., Hawthorne F.C., Ertl A., Dutrow B.L., Uher P. and Pezzotta F., 2011. Nomenclature of the tourmaline-supergroup minerals. *American Mineralogist*, **96**(5–6), 895–913, http://dx.doi.org/10.2138/am.2011.3636.

Hutchinson R.W. and Claus R.J., 1956. Pegmatite deposits, Alto Ligonha, Portuguese East Africa. *Economic Geology*, **51**(8), 757–780, http://dx.doi.org/10.2113/gsecongeo.51.8.757.

Karfunkel J. and Wegner R.R., 1996. Paraiba tourmalines: Distribution, mode of occurrence, and geologic environment. *Canadian Gemmologist*, **17**(4), 99–106.

Krzemnicki M., 2006. Paraíba tourmalines from Brazil, Nigeria & Mozambique. *Midlands Focus*, **9**, 6–11.

Laurs B.M., Zwaan J.C., Breeding C.M., Simmons W.B., Beaton D., Rijsdijk K.F., Befi R. and Falster A.U., 2008. Copper-bearing (Paraíba-type) tourmaline from Mozambique. *Gems & Gemology*, **44**(1), 4–30, http://dx.doi.org/10.5741/gems.44.1.4.

Marschall H.R. and Jiang S.-Y., 2011. Tourmaline isotopes: No element left behind. *Elements*, **7**(5), 313–319, http://dx.doi.org/10.2113/gselements.7.5.313.

Mattson S.M. and Rossman G.R., 1987. Fe^{2+}-Fe^{3+} interactions in tourmaline. *Physics and Chemistry of Minerals*, **14**(2), 163–171, http://dx.doi.org/10.1007/bf00308220.

Milisenda C.C., 2001a. Edelsteinvorkommen und Plattentektonik. *Gemmologie: Zeitschrift der Deutschen Gemmologischen Gesellschaft*, **50**(2), 75–88.

Milisenda C.C., 2001b. Gemmologie Aktuell: Cuprian tourmalines from Nigeria. *Gemmologie: Zeitschrift der Deutschen Gemmologischen Gesellschaft*, **50**(3), 121–122.

Milisenda C.C., 2005. "Paraiba-Turmaline" aus Quintos de Baixo, Rio Grande do Norte, Brasilien. *Gemmologie: Zeitschrift der Deutschen Gemmologischen Gesellschaft*, **54**(2–3), 73–84.

Milisenda C.C. and Henn U., 2001. Kupferhaltige Turmaline aus Nigeria. *Gemmologie: Zeitschrift der Deutschen Gemmologischen Gesellschaft*, **50**(4), 217–223.

Milisenda C.C., Horikawa Y., Emori K., Miranda R., Bank F.H. and Henn U., 2006. Neues Vorkommen kupferführender Turmaline in Mosambik. *Gemmologie: Zeitschrift der Deutschen Gemmologischen Gesellschaft*, **55**(1–2), 5–24.

Pearce N.J.G., Perkins W.T., Westgate J.A., Gorton M.P., Jackson S.E., Neal C.R. and Chenery S.P., 1997. A compilation of new and published major and trace element data for NIST SRM 610 and NIST SRM 612 glass reference materials. *Geostandards and Geoanalytical Research*, **21**(1), 115–144, http://dx.doi.org/10.1111/j.1751-908x.1997.tb00538.x.

Peretti A., Bieri W.P., Reusser E., Hametner K. and Günther D., 2008. Chemical variations of multicolored "Paraíba"-type tourmalines from Brazil and Mozambique: Implications for origin and authenticity determination. *Contributions to Gemology*, **9**, 1–77.

Pezzotta F. and Laurs B.M., 2011. Tourmaline: The kaleidoscopic gemstone. *Elements*, **7**(5), 333–338, http://dx.doi.org/10.2113/gselements.7.5.333.

Reinitz I.M. and Rossman G.R., 1988. The role of natural radiation in tourmaline coloration. *American Mineralogist*, **73**(7–8), 822–825.

Rossman G.R., 2016. Spectroscopic studies of minerals. Visible spectra. Metal ions in crystals. Two blue tourmalines. Elbaite from Salinas, Minas Gerais, Brazil. http://minerals.gps.caltech.edu/mineralogy/Current_Projects/Spectra (accessed 26 May 2016).

Rossman G.R. and Mattson S.M., 1986. Yellow, Mn-rich elbaite with Mn-Ti intervalence charge transfer. *American Mineralogist*, **71**(3–4), 599–602.

Rossman G.R., Fritsch E. and Shigley J.E., 1991. Origin of color in cuprian elbaite from São Jose de [sic] Batalha, Paraíba, Brazil. *American Mineralogist*, **76**(9–10), 1479–1484.

Schmetzer K., Bernhardt H.-J., Dunaigre C. and Krzemnicki M.S., 2007. Vanadium-bearing gem-quality tourmalines from Madagascar. *Journal of Gemmology*, **30**(7-8), 413–433, http://dx.doi.org/10.15506/jog.2007.30.7.413.

Shabaga B.M., Fayek M. and Hawthorne F.C., 2010. Boron and lithium isotopic compositions as provenance indicators of Cu-bearing tourmalines. *Mineralogical Magazine*, **74**(2), 241–255, http://dx.doi.org/10.1180/minmag.2010.074.2.241.

Shigley J.E., Cook B.C., Laurs B.M. and Bernardes M.O., 2001. An update on "Paraíba" tourmaline from Brazil. *Gems & Gemology*, **37**(4), 260–276, http://dx.doi.org/10.5741/gems.37.4.260.

Simmons W.B., Pezzotta F., Shigley J.E. and Beurlen H., 2012. Granitic pegmatites as sources of colored gemstones. *Elements*, **8**(4), 281–287, http://dx.doi.org/10.2113/gselements.8.4.281.

Smith G.F.H. and Phillips F.C., 1972. *Gemstones*, 14th edn. Chapman and Hall, London, 580 pp.

Smith C.P., Bosshart G. and Schwarz D., 2001. Gem News International: Nigeria as a source of copper-manganese-bearing tourmaline. *Gems & Gemology*, **37**(3), 239–240.

van Hinsberg V.J., Henry D.J. and Dutrow B.L., 2011. Tourmaline as a petrologic forensic mineral: A unique recorder of its geologic past. *Elements*, **7**(5), 327–332, http://dx.doi.org/10.2113/gselements.7.5.327.

Zang J.W., Fonseca-Zang W.A.D., Fliß F., Höfer H.E. and Lahaye Y., 2001. Cu-haltige Elbaite aus Nigeria. *Berichte der Deutschen Mineralogischen Gesellschaft, Beihefte zum European Journal of Mineralogy*, **13**(1), 202.

The Authors

Dr Martin Okrusch[1], Dr Andreas Ertl[2,3], Dr Ulrich Schüssler[1], Dr Ekkehart Tillmanns[3], Dr Helene Brätz[1,4] and Dr Hermann Bank[5]

[1] Lehrstuhl für Geodynamik und Geomaterialforschung, Institut für Geographie und Geologie, Universität Würzburg, Am Hubland, D-97074 Würzburg, Germany.
Email: okrusch@uni-wuerzburg.de

[2] Mineralogisch-Petrographische Abt., Naturhistorisches Museum, Burgring 7, A-1010 Wien, Austria

[3] Institut für Mineralogie und Kristallographie, Geozentrum, Universität Wien, Althanstrasse 14, A-1090 Wien, Austria

[4] Geozentrum Nordbayern, Universität Erlangen, Schlossgarten 5a, D-91054 Erlangen, Germany

[5] Gebrüder Bank, Dietzenstrasse 1, D-55743 Idar-Oberstein, Germany

Acknowledgements

We thank Peter Späthe for carefully polishing the rough tourmaline samples and Nikola Koglin for help with the diagrams. This work was funded by Austrian Science Fund (FWF) project no. P 26903-N19. We sincerely thank three anonymous reviewers of the manuscript for their constructive reviews and helpful comments.

Identification of Colourless HPHT-grown Synthetic Diamonds from Shandong, China

Zhonghua Song, Taijin Lu, Shi Tang, Jie Ke, Jun Su, Bo Gao, Ning Hu, Jun Zhang, Jun Zhou, Lijun Bi and Dufu Wang

Colourless HPHT-grown synthetic diamonds are becoming more common in the marketplace. The authors recently studied 20 samples weighing 0.06–0.67 ct from a producer located in Jinan, Shandong, China. The 10 crystals showed a combination of cubic and octahedral forms, sometimes with small faces corresponding to {110} and {113}, and the 10 round brilliant cuts had colour grades up to D–E and clarity grades up to VS1. Some of the samples were attracted to a magnet due to their metallic inclusions. They showed very weak anomalous birefringence with low-order interference colours between crossed polarizers. UV-Vis spectra recorded a weak absorption at 270 nm, and infrared spectra indicated that all samples contained variable traces of boron, suggesting that they are mixed type Ib and IIb. DiamondView imaging revealed distinct cuboctahedral growth sectors and produced strong greenish blue phosphorescence. These synthetic diamonds can be reliably identified using a combination of FTIR, UV-Vis, microscopy and luminescence imaging techniques.

The Journal of Gemmology, **35**(2), 2016, pp. 140–147, http://dx.doi.org/10.15506/JoG.2016.35.2.140

Introduction

Since 2014, remarkable progress has been made in the production of colourless high-pressure, high-temperature (HPHT)-grown synthetic diamonds. Companies such as AOTC Group (The Netherlands) and New Diamond Technology (NDT; Russia) have succeeded in growing colourless to near-colourless material for use in jewellery (e.g. D'Haenens-Johansson et al., 2014, 2015). AOTC mainly uses BARS or toroid presses, and NDT employs cubic press technology. In the first half of 2015, several HPHT synthetic diamond companies in China also began producing high-quality colourless synthetic diamonds in large volume, mainly as melee-sized material (Lan et al., 2015). In late 2015, the present authors had the opportunity to study samples produced by Jinan Zhongwu New Materials Co. Ltd. (Jinan, Shandong), and in March 2016 representatives from the National Gemstone Testing Center (NGTC) in Beijing visited the facility to learn about the equipment, growth techniques, production, etc. Recently, Wang and Moses (2016) reported initial observations of 50 colourless gem-quality crystals obtained from the same company.

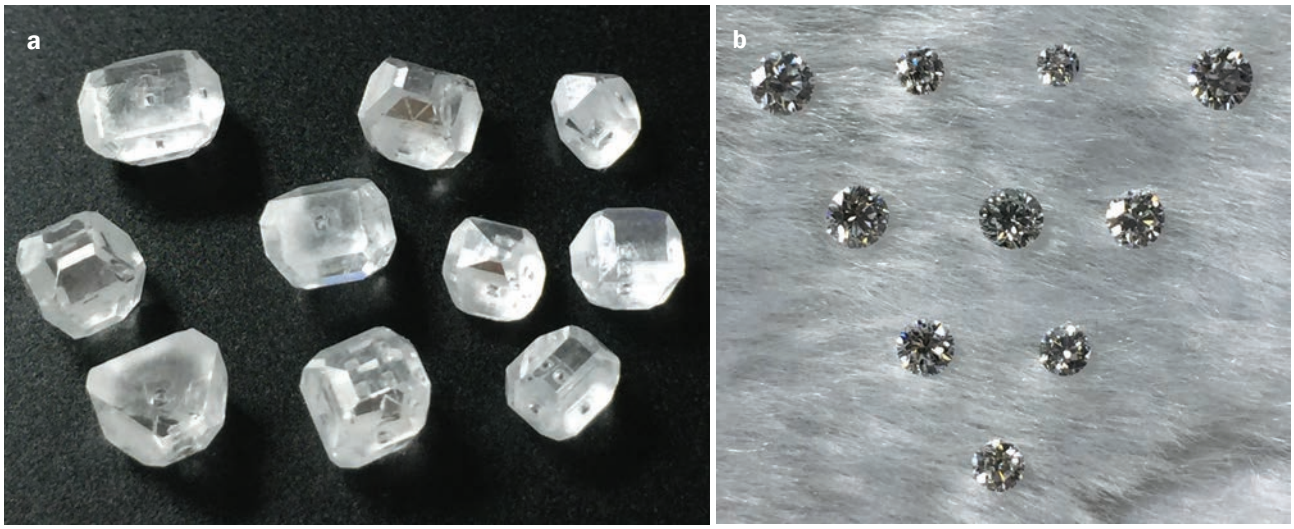

Figure 1: Studied for this report were (a) 10 colourless crystals (0.26–0.67 ct) and (b) 10 colourless faceted HPHT-grown synthetic diamonds (0.06–0.19 ct) from Jinan Zhongwu New Materials in Shangdong, China. Photos by Z. Song.

Jinan Zhongwu New Materials employs domestically made cubic HPHT presses, and there are about 70 of these apparatuses now being used by the company to grow synthetic diamonds. Their synthesis techniques came from a project titled 'Large-sized Synthetic Diamonds Technology Introduction' that was launched in 2011, jointly undertaken by Jinan Zhongwu New Materials and a prominent academic research institution abroad. By combining foreign technology and China's equipment advantages, the company has successfully grown large synthetic diamonds (crystals up to 10 ct). In addition to yellow and blue material, they have produced commercial quantities of colourless synthetic diamonds.

As part of a project to study the characteristics of synthetic diamonds from different producers over time, and to provide updated information to the market and to gem laboratories, the authors characterized a selection of rough and cut colourless HPHT-grown synthetic diamonds from Jinan Zhongwu New Materials for this report.

Materials and Methods

The 10 crystals weighed 0.26–0.67 ct and the 10 faceted synthetics (all round brilliant cuts) were 0.06–0.19 ct (Figure 1). Characterization took place at the NGTC laboratory in Beijing, and all the faceted samples were tested with the methods described below. (The crystals were subjected only to microscopic examination and photoluminescence spectroscopy.) A gemmological microscope was used to observe their inclusions and anomalous birefringence. Fluorescence and phosphorescence were observed with both long-wave (365 nm) and short-wave (253 nm) UV radiation and a DiamondView instrument. Phosphorescence spectra were collected with an Ocean Optics QE Pro spectrometer equipped with an Avantes AvaLight-DH-S deuterium-halogen light source, using the methods described by Eaton-Magaña et al. (2008). Fourier-transform infrared (FTIR) spectroscopy was performed using a Thermo Nicolet 6700 spectrometer in the range of 6000–400 cm^{-1} (128 scans at a resolution of 2 cm^{-1}). A Renishaw InVia Raman microspectrometer was used to collect photoluminescence (PL) spectra of the samples with four laser excitations (325, 473, 532 and 785 nm) at liquid-nitrogen temperature. A Gem-3000 ultraviolet-visible (UV-Vis) spectrometer was used to obtain absorption spectra at room temperature. Chemical analyses were performed with a Thermo Scientific ARL QUANT'X energy-dispersive X-ray fluorescence (EDXRF) spectrometer, with 20 kV voltage, 1.98 mA current and a Pd thin filter for 100 seconds.

About 50 colourless crystals ranging up to 3.50 ct also were examined with a loupe at the factory.

Results

Basic Properties

The crystals showed typical cuboctahedral morphology with well-developed {100} and {111} forms and weakly developed faces corresponding

to {110} and {113}. In some samples, the {110} form was more developed than {113}, while others showed the opposite. All samples contained distinct metallic inclusions, and some could be attracted to a strong magnet.

The details of the weight, colour and clarity grades of the faceted samples are reported in Table I. One sample was colour graded as D and the remaining nine were E colour. Clarity grades ranged from VS_1 to I_2, with most samples containing a few rod-like inclusions (Figure 2a). Some of these inclusions displayed colourful iridescence in reflected light (Figure 2b). Samples with lower clarity grades contained numerous irregular-shaped dark metallic inclusions (Figure 2c). A small square-shaped cloud was present in one of the synthetics (Figure 2d). Those with VS clarity grades were not attracted to the magnet, while the lower grades usually had obvious metallic inclusions and were easily attracted. Sample BST008 was even attracted to magnetized tweezers as a result of the large quantity of metallic inclusions.

Viewed with the microscope between crossed polarizers, all the colourless HPHT synthetic diamonds showed only weak or very weak anomalous birefringence, with low-order interference colours (mostly grey or brown), indicating low levels of strain (Figure 3a). Moreover, weak anomalous birefringence was seen around pinpoint inclusions where the synthetic diamond lattice was possibly distorted. By comparison, noticeable anomalous birefringence is a common optical feature in natural and CVD synthetic diamonds. Normally, the birefringence of natural diamond appears as mottled, banded or cross-hatched ('tatami') patterns (see Figure 3b and Howell, 2012), while CVD synthetic diamond shows linear or grid-like patterns (see Figure 3c and Pinto and Jones, 2009).

Fluorescence and Phosphorescence

The luminescence characteristics of the polished samples are reported in Table I. When exposed to long-wave UV radiation, all samples displayed weak yellow fluorescence and no phosphorescence. The response to short-wave UV radiation, however, was medium-to-strong yellow-green fluorescence with green phosphorescence. Obvious bluish green phosphorescence was seen with the unaided eye after the synthetic diamonds were illuminated with the Avantes AvaLight-DH-S deuterium-halogen light source.

Further observations of the samples' fluorescence and phosphorescence characteristics were conducted using the DiamondView, in which all samples fluoresced greyish blue (Figure 4) and phosphoresced strong greenish blue. The cuboctahedral growth sector could be seen in all samples through the pavilion, but was only visible through the table when the table facet was cut parallel or nearly parallel to the [100] direction.

Phosphorescence spectra showed a band centred at approximately 500 nm (e.g. Figure 5). The 575 nm band reported by D'Haenens-Johansson et al. (2015) in the HPHT-grown synthetic diamonds from NDT was not detected in our samples.

Table I: Properties of faceted HPHT-grown synthetic diamonds from Shandong, China.

Sample no.	Weight (ct)	Colour	Clarity	Magnetic?	EDXRF (Fe?)	Long-wave UV		Short-wave UV	
						Fluorescence	Phosphorescence	Fluorescence	Phosphorescence
BST006	0.19	E	SI_1	No	No	Weak yellow	None	Strong yellow-green	Weak green
BST007	0.08	E	I_1	Yes	Yes	Weak yellow	None	Strong yellow-green	Strong green
BST008	0.06	E	I_2	Yes	Yes	Weak yellow	None	Medium yellow-green	Strong green
BST009	0.19	E	VS_2	No	Weak	Weak yellow	None	Strong yellow-green	Strong green
BST010	0.19	E	VS_1	No	No	Weak yellow	None	Strong yellow-green	Strong green
BST011	0.19	E	SI_2	Yes	Yes	Weak yellow	None	Strong yellow-green	Strong green
BST012	0.14	E	SI_1	Yes	Yes	Weak yellow	None	Medium yellow-green	Medium green
BST013	0.14	E	VS_2	No	No	Weak yellow	None	Medium yellow-green	Medium green
BST014	0.10	D	SI_1	No	No	Weak yellow	None	Strong yellow-green	Strong green
BST015	0.10	E	SI_2	Yes	Yes	Weak yellow	None	Strong yellow-green	Strong green

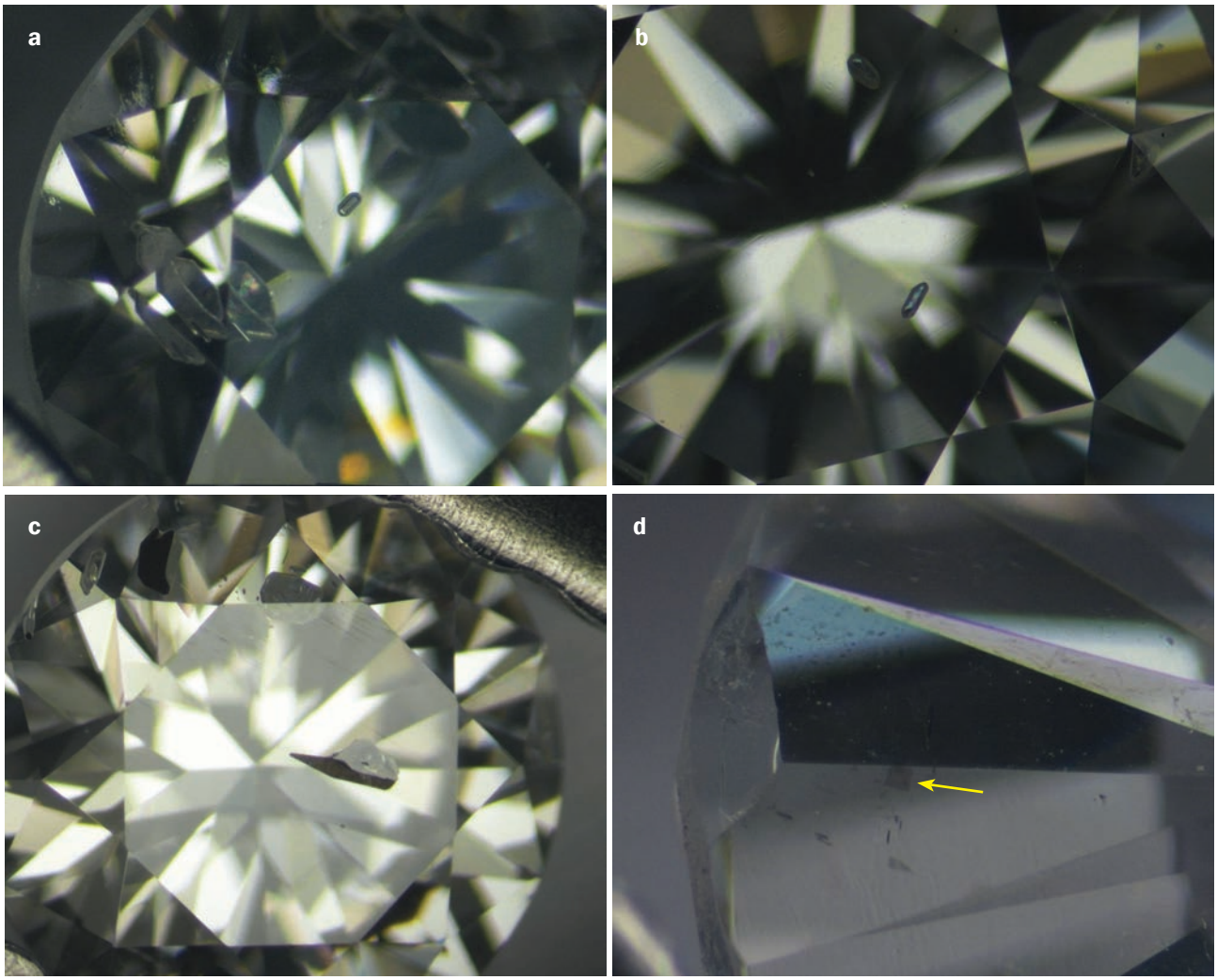

Figure 2: The Shandong HPHT synthetic diamonds commonly contained metallic inclusions, including (a) stubby rod-like shapes (magnified 30×), (b) those showing iridescence in reflected light (magnified 25×) and (c) irregular shapes (magnified 15×). (d) One sample also contained a square-shaped cloud, possibly consisting of metallic particles (see arrow; magnified 45×). Photomicrographs by Z. Song.

Figure 3: Weak birefringence is shown by the Shandong HPHT synthetic diamonds (a; magnified 25×), in contrast to typical patterns displayed by natural diamonds (b; magnified 15×) and CVD synthetic diamonds (c; magnified 15×). Photomicrographs by Z. Song.

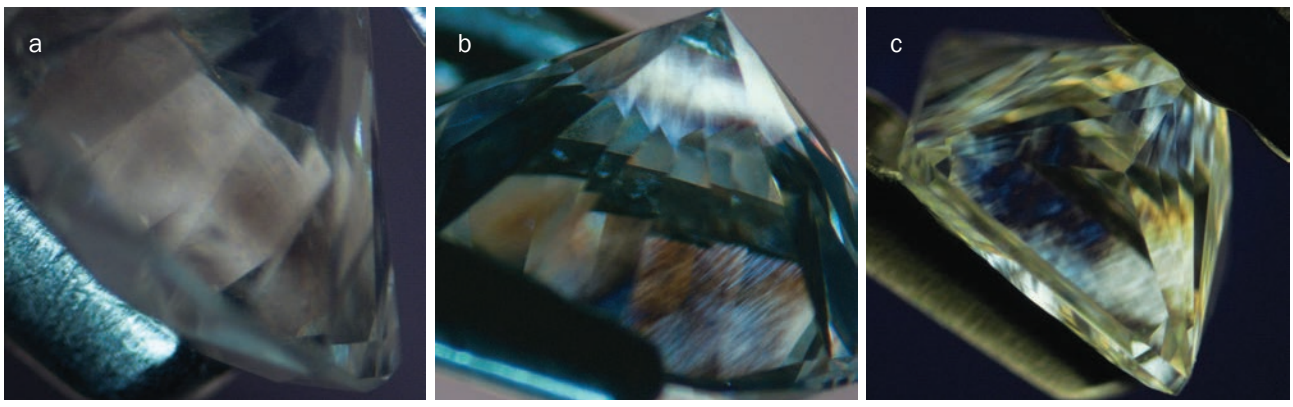

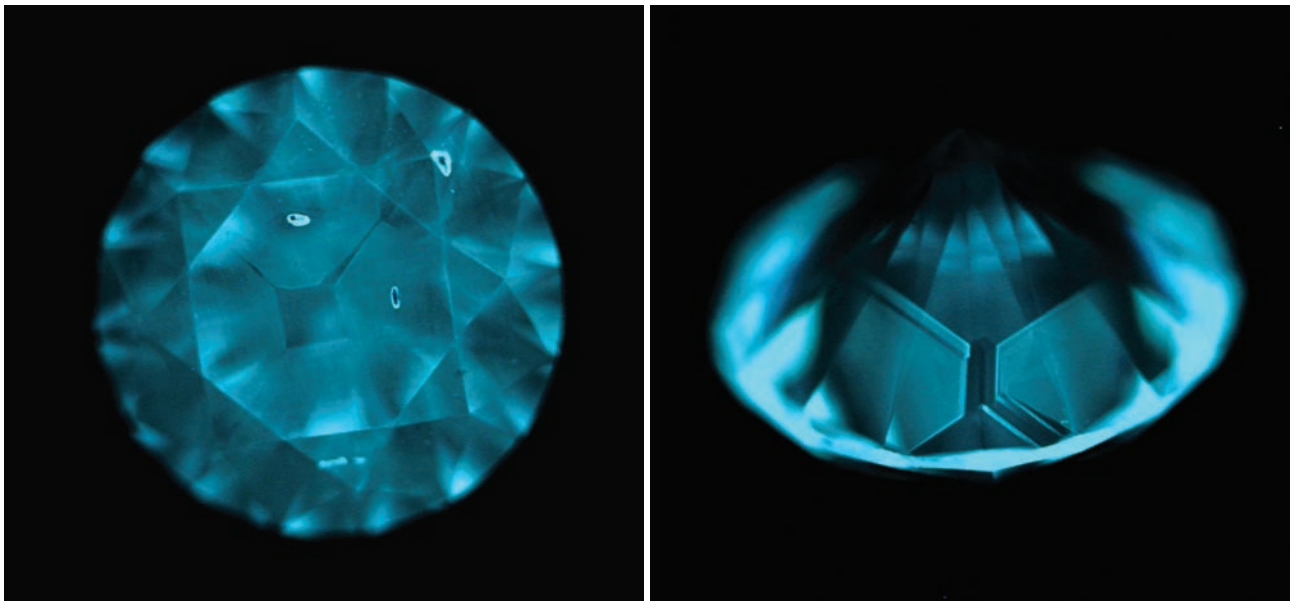

Figure 4: In the DiamondView, the Shandong HPHT synthetic diamonds showed greyish blue fluorescence (here, seen in two views of sample BST012, 0.14 ct). The cuboctahedral growth sector is also evident. Photos by Z. Song.

FTIR Spectra

All samples examined for this article proved to be mixed type Ib and IIb with variable boron content (Figure 6). Boron often concentrates in the {111} growth sector and has absorption features located at 4090, 2800 and 1290 cm^{-1} in FTIR spectra (King et al., 1998). A weak line at 1332 cm^{-1} and bands at 1075 and 960 cm^{-1} also were observed in all samples. The latter two absorptions were stronger (relative to the 1332 cm^{-1} band) than similar bands at 1046 and 950 cm^{-1} shown by Lawson et al. (1998), who assigned the 1332 cm^{-1} band to N^+. We did not detect any isolated nitrogen-related absorption peaks at 1344 and 1130 cm^{-1}. The cause of the 1332 cm^{-1} line is uncertain, although it has been observed in boron-doped synthetic diamonds and in those grown using a Ni-containing solvent/catalyst (Collins et al., 1990; Lawson and Kanda, 1993; Lawson et al., 1998). More samples from Jinan Zhongwu New Materials should be tested to further clarify the existence of the 1075 and 960 cm^{-1} bands.

UV-Vis Spectra

The UV-Vis spectra of the samples (Figure 7) displayed a weak 270 nm absorption associated with isolated nitrogen (Dyer et al., 1965), as well as a weak broad band centred at 350 nm. There was also weak general absorption due to boron in the near-infrared region, but absorption due to boron and nitrogen in the visible region was extremely low, resulting in the samples having a colourless (D–E) grade.

Photoluminescence Spectra

No emissions related to defect impurities (such as N, Ni and Si) were detected in any of the 10 faceted samples when excited with the 325, 473 and 532 nm lasers, but four of them showed a weak Ni-related doublet at 883.2/884.9 nm with the 785 nm laser (Figure 8). In addition, weak 737

Figure 5: These representative phosphorescence spectra of the Shandong HPHT synthetic diamonds show a band centred at approximately 500 nm.

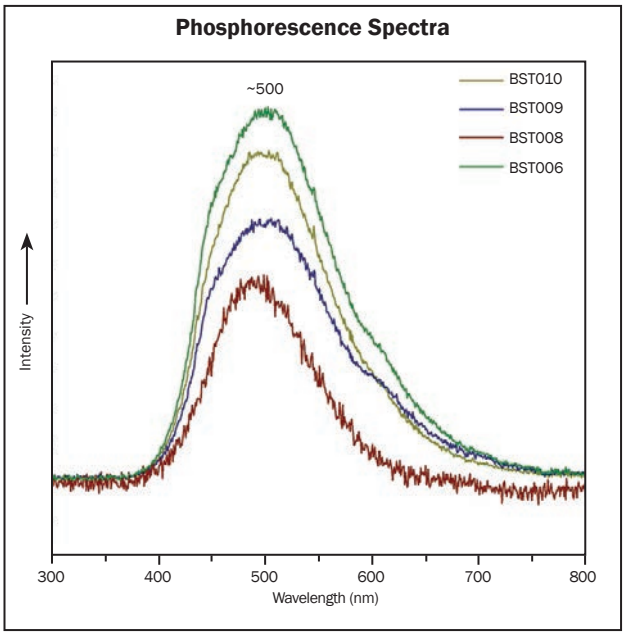

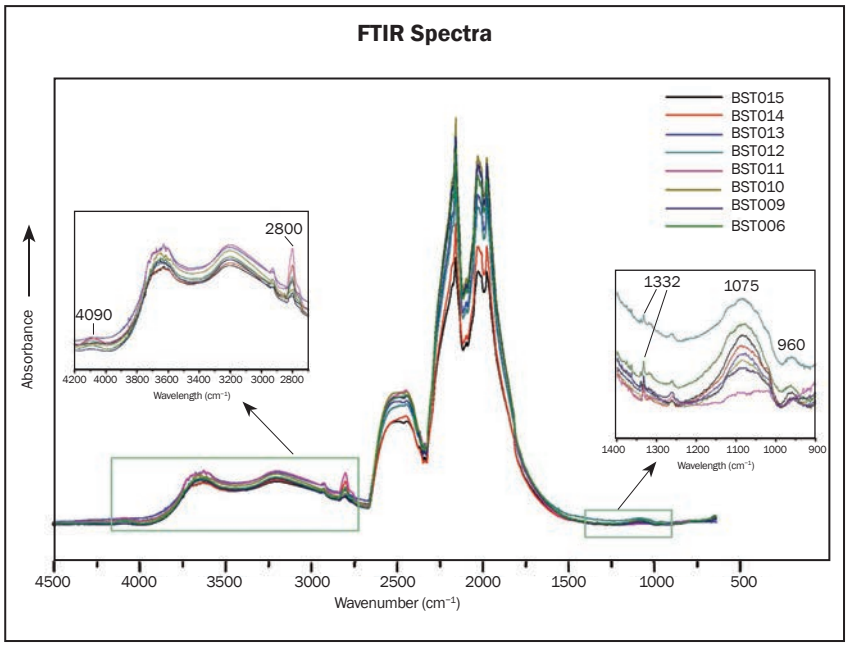

Figure 6: These representative FTIR absorption spectra of the HPHT synthetic diamonds show that they are mixed type Ib and IIb with variable boron content.

and 637 nm emissions were recorded in some of the crystals and a 692/693 nm doublet was detected in all of them with the 532 nm laser. The assignment of the 692/693 nm emission has yet to be determined, and it is not clear why it was present only in the rough samples.

EDXRF Analysis

The only element detected by EDXRF spectroscopy in the samples was Fe (with no Co or Ni). Samples BST007–008, 011–012 and 015 showed considerable amounts of Fe, while only traces were found in BST009, and Fe was not detectable in BST006, 010, 013 or 014. The presence of Fe in these samples is consistent with their inclusion abundance and, as shown in Table I, magnetic behaviour. These results suggest that Fe was likely the dominant solvent/catalyst used during the growth process.

Figure 7: UV-Vis spectra of the Shandong HPHT synthetic diamonds display a weak 270 nm absorption feature.

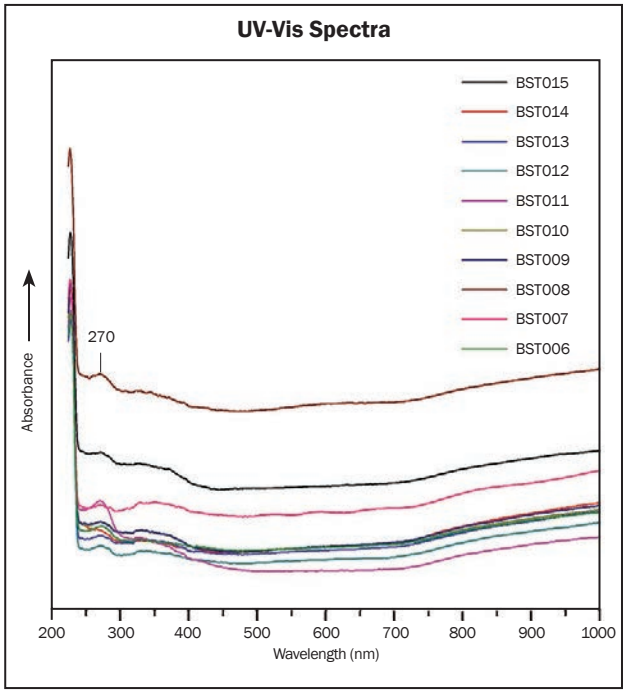

Figure 8: The Shandong HPHT synthetic diamonds generally had featureless PL spectra. Only a few samples showed Ni-related peaks at 883.2 and 884.9 nm that were excited by the 785 nm laser.

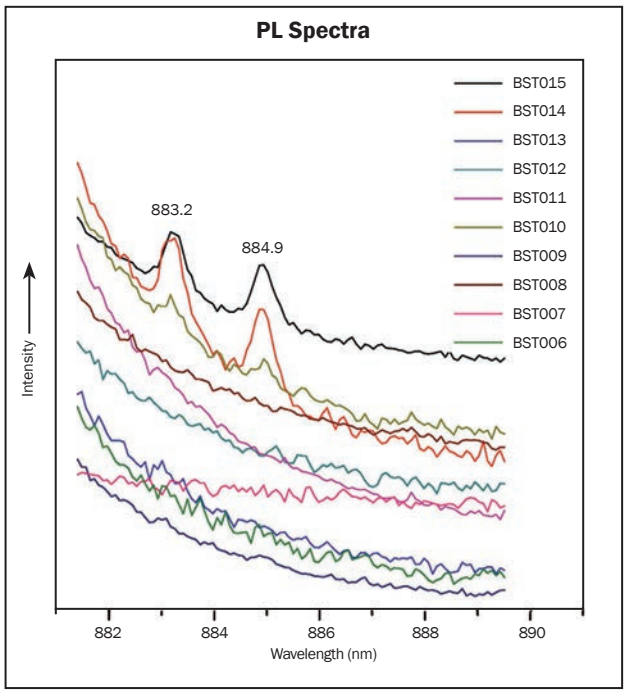

Discussion

With the continued development of synthesis techniques, the characteristics of HPHT- (and CVD-) grown synthetic diamonds are increasingly similar to those of natural diamonds. However, it remains possible to conclusively identify them through a combination of gemmological and spectroscopic observations.

Magnification revealed the common presence of metallic inclusions in our samples, which have not been observed in natural diamonds or in CVD synthetics. The more metallic inclusions present (and thus higher Fe content, as confirmed by EDXRF spectroscopy), the stronger a sample's magnetism.

The cuboctahedral growth sector was distinctly visible in the DiamondView when the samples were thoroughly observed from different directions. Typically this growth sector was more obvious through the pavilion than the table. Moreover, all the samples displayed strong greenish blue phosphorescence in the DiamondView, a characteristic rarely seen in natural diamonds.

Compared to synthetic diamonds from other producers that the authors have tested previously, the 270 nm absorption in the UV-Vis spectra of our samples was generally weaker, as a result of the higher colour grades of these samples. It is known that the 270 nm absorption relates to isolated nitrogen (Dyer et al., 1965), which causes yellow coloration in diamond.

The presence of boron in all samples was indicated by the strong 2800 cm^{-1} and weak 4090 cm^{-1} absorptions in the FTIR spectra. To grow colourless synthetic diamonds, the amount of impurities such as N and B that enter the diamond lattice must be controlled to some extent. To do so, a 'nitrogen getter' is introduced to form compounds with N, thus reducing the amount of this element available to enter the crystallizing synthetic diamond. Also, by controlling the content of B, the resulting weak absorption in the red and near-infrared regions (producing blue coloration) will neutralize the yellow colour caused by isolated nitrogen, thus causing the diamond to appear colourless overall.

Although Raman PL spectroscopy is a useful method for studying the trace impurities in diamond, it was difficult to detect useful emissions in our faceted synthetic diamond samples, regardless of the laser excitation wavelength, even with full power and 10 accumulations. Only a weak 883/885 nm doublet related to Ni was found in a few samples. This may be due to the use of catalysts or growth conditions that are different from other producers. According to D'Haenens-Johansson et al. (2014), synthetic diamonds from AOTC grown with toroid presses also showed few (or weak) PL features, and one exceptionally pure sample did not have any PL-detectable optical centres.

Conclusions

As with CVD lab-grown diamonds, HPHT synthetics can be identified using a combination of gemmological and spectroscopic techniques, as reported here for colourless samples from Shandong, China. Important identification features include metallic inclusions, green to greenish blue phosphoresce after exposure to short-wave (and especially ultra-short-wave) UV radiation and cuboctahedral growth zoning observable with the DiamondView (particularly from the pavilion side), as well as a weak 270 nm absorption and a 2800 cm^{-1} band, consistent with a mixed type Ib and IIb affinity.

References

Collins A.T., Kanda H. and Burns R.C., 1990. The segregation of nickel-related optical centres in the octahedral growth sectors of synthetic diamond. *Philosophical Magazine Part B*, **61**(5), 797–810, http://dx.doi.org/10.1080/13642819008207562.

D'Haenens-Johansson U.F.S., Moe K.S., Johnson P., Wong S.Y., Lu R. and Wang W., 2014. Near-colorless HPHT synthetic diamonds from AOTC Group. *Gems & Gemology*, **50**(1), 2–14, http://dx.doi.org/10.5741/gems.50.1.30.

D'Haenens-Johansson U.F.S., Katrusha A., Moe K.S., Johnson P. and Wang W., 2015. Large colorless HPHT-grown synthetic gem diamonds from New Diamond Technology, Russia. *Gems & Gemology*, **51**(3), 260–279, http://dx.doi.org/10.5741/gems.51.3.260.

Dyer H.B., Raal F.A., Preez L.D. and Loubser J.H.N., 1965. Optical absorption features associated with paramagnetic nitrogen in diamond. *Philosophical Magazine*, **11**(112), 763–774, http://dx.doi.org/10.1080/14786436508230081.

Eaton-Magaña S., Post J.E., Heaney P.J., Freitas J., Klein P., Walters R. and Butler J.E., 2008. Using phosphorescence as a fingerprint for the Hope and other blue diamonds. *Geology*, **36**(1), 83–86, http://dx.doi.org/10.1130/g24170a.1.

Howell D., 2012. Strain-induced birefringence in natural diamond: A review. *European Journal of Mineralogy*, **24**(4), 575–585, http://dx.doi.org/10.1127/0935-1221/2012/0024-2205.

King J.M., Moses T.M., Shigley J.E., Welbourn C.M., Lawson S.C. and Cooper M., 1998. Characterizing natural-color type IIb blue diamonds. *Gems & Gemology*, **34**(4), 246–268, http://dx.doi.org/10.5741/gems.34.4.246.

Lan Y., Liang R., Lu T., Zhang T., Song Z., Ma H. and Ma Y., 2015. Identification characteristic [sic] of near-colourless melee-sized HPHT synthetic diamond in Chinese jewelry market. *Journal of Gems & Gemmology*, **17**(5), 12–17.

Lawson S.C. and Kanda H., 1993. Nickel in diamond: An annealing study. *Diamond and Related Materials*, **2**(2–4), 130–135, http://dx.doi.org/10.1016/0925-9635(93)90043-2.

Lawson S.C., Fisher D., Hunt D.C. and Newton M.E., 1998. On the existence of positively charged single-substitutional nitrogen in diamond. *Journal of Physics: Condensed Matter*, **10**(27), 6171–6180, http://dx.doi.org/10.1088/0953-8984/10/27/016.

Pinto H. and Jones R., 2009. Theory of the birefringence due to dislocations in single crystal CVD diamond. *Journal of Physics: Condensed Matter*, **21**(36), article 364220, http://dx.doi.org/10.1088/0953-8984/21/36/364220.

Wang W. and Moses T., 2016. Gem News International: Large colorless HPHT synthetic gem diamonds from China. *Gems & Gemology*, **52**(1), 101–102.

The Authors

Zhonghua Song, Shi Tang, Jie Ke, Jun Su, Bo Gao, Ning Hu, Jun Zhang and Jun Zhou
National Gemstone Testing Center, National Gems & Jewelry Technology Administrative Center, North 3rd Ring East Road, Beijing 100013, China

Dr Taijin Lu and Lijun Bi
National Gems & Jewelry Technology Administrative Center, North 3rd Ring East Road, Beijing 100013, China. Email: lutj@ngtc.gov.cn

Dr Dufu Wang
Jinan Zhongwu New Materials Co. Ltd., 2000 Shunhua Road, Gaoxin District, Jinan 250101, Shandong Province, China

Acknowledgements

The authors are grateful to Dr Tian Liangguang from the Shandong Quality and Technical Examination Assess Center (Weihai), and to Cheng Youfa from the National Gold and Diamond Testing Center of China (Jinan), for providing useful discussion and assistance.

Gem-quality Sekaninaite from the Czech Republic

Radek Hanus, Ivana Kusá and Jana Kasíková

Sekaninaite—the Fe-rich end member of the cordierite-sekaninaite series—was recently found for the first time in gem quality at the type locality of Dolní Bory in the Czech Republic. The mineral is known from several granitic pegmatites in the Hatě area as conical pseudo-hexagonal crystals up to 1 m long that are embedded in feldspar and commonly altered (pinitized). Small unaltered areas of the crystals may show an attractive blue-violet colour and vitreous lustre. Several dozen stones have been faceted that range up to ~11 ct; they have an average weight of ~1 ct. This rare gem-quality sekaninaite can be distinguished from cordierite in some cases by using RI and SG data, although overlap in these measurements may require that additional methods such as X-ray diffraction or quantitative chemical analysis be used to distinguish between the two minerals.

The Journal of Gemmology, **35**(2), 2016, pp. 148–154, http://dx.doi.org/10.15506/JoG.2016.35.2.148

Introduction

Blue-violet cordierite is an attractive gem material that is available at affordable prices. Cordierite is an end member of the cordierite-sekaninaite series, and the latter mineral is significantly rarer. During the past two years, the type locality of sekaninaite, Dolní Bory in the Czech Republic, has yielded several gem-quality specimens (e.g. Figure 1) as a result of activities by mineral collectors. These gems possess a greyish blue to bluish violet colour with very strong pleochroism, as is commonly seen in cordierite.

To the authors' knowledge, sekaninaite was previously unknown as a gemstone and has not yet been set into jewellery. This article reports on the new production of gem-quality sekaninaite, describes its properties and compares them to cordierite.

Background

The chemical formula of the cordierite-sekaninaite series is $(Mg,Fe^{2+})_2Al_3(AlSi_5O_{18})$–$(Fe^{2+}Mg)_2Al_3(AlSi_5O_{18})$; both minerals are complex cyclosilicates of Mg, Fe and Al crystallizing in the orthorhombic system. There is also a high-temperature hexagonal dimorph of cordierite called indialite, $Mg_2Al_3(AlSi_5O_{18})$, which is isostructural with beryl (Fleischer and Jambor, 1977; Geiger and Voigtländer, 2000; Yakubovich et al., 2004). Sekaninaite from Dolní Bory was approved as a new mineral by the International Mineralogical Association in 1968, and described by J. Staněk and J. Miškovský in 1975; it was named in honour of the Czech mineralogist Dr Josef Sekanina (1901–1986). Another significant occurrence of sekaninaite is Winklarn village in eastern Bavaria, Germany, where it forms within

Figure 1: These rough (~0.5–2 g) and cut (0.22–0.30 ct) samples of sekaninaite are from the Czech Republic. Photo by R. Hanus.

Figure 2: Gem-quality sekaninaite is known only from Dolní Bory in the South Moravian Region, Czech Republic.

pegmatitic veins that are hosted by serpentinite, and is associated with andalusite, chlorite, feldspar and muscovite (Keck et al., 2010). Other localities for sekaninaite include Italy, Russia and the USA (Grapes et al., 2011; Korchak et al., 2011).

Until now, cordierite was the only mineral of the cordierite-sekaninaite series known in gem quality. Named after the French geologist and mineralogist Pierre Cordier, cordierite is also known as *iolite*, and rarely in old literature as *dichroite*. Both names are derived from Greek words—*iolite* for violet, and *dichroite* for a two-coloured stone (although it actually displays trichroism). The authors are also aware of colourless cordierite, although very rare, from Sri Lanka, Tanzania and Madagascar; in addition, Tanzania hosts a bicoloured variety. Chatoyancy may be rarely displayed by cabochons cut from cordierite.

Cordierite is generally not subjected to any treatments. Heat treatment is not viable due to cordierite's low thermal stability. However, one of the authors (RH) has rarely encountered cordierite treated with a surface coating; those stones, which were purchased in Chanthaburi, Thailand, lost much of their attractive blue-violet colour during the recutting/repolishing process.

Location and Geology

The gem-quality sekaninaite was found in the Hatě area, approximately 8 km north of Velké Meziříčí town and 1.5 km west of Dolní Bory village, in the Vysočina area of the South Moravian Region, Czech Republic (Figure 2). The mining area is located in woodland between the Oslava River and Dolní Bory village, south of Babačka Creek. Approximately 20 pegmatites are known in this area of the Moldanubian complex on the northern periphery of the Borsky granulite massif (Staněk, 1991; 2009); however sekaninaite was recovered from only a few veins of the former MKZ feldspar mine (MKZ = Moravské keramické závody or Moravian ceramic plants). The sekaninaite is typically enclosed in orthoclase (and albite), the main resource of the mining operations. The orthoclase was manually sorted and used for the ceramic industry (Duda, 1986). Small-scale pit mining for orthoclase began in 1887, and underground mining commenced after World War II; the final operations ceased in 1972. Since that time, many collectors have visited the deposit and the surrounding area to collect mineral specimens, including crystals of smoky quartz, mica, schorl, secondary uranium minerals and others of aesthetic value (Staněk, 1952a,b; 1991).

The veins from this locality are classified as peraluminous granite pegmatites, of an orthoclase type with weak albitization and secondary rare-element mineralization (Staněk, 2009). The majority of the thicker veins are highly differentiated with a symmetrical-zoned structure from the margins inward: (1) medium- to coarse-grained pegmatite, (2) coarse-grained graphic pegmatite, (3) blocky K-feldspar and quartz and (4) a quartz core. Some areas of

Figure 3: Sekaninaite from the Czech Republic often occurs as conical pseudo-hexagonal crystals (left, 5 cm tall) that commonly break apart into tabular pieces (right, 4 cm diameter). Both specimens are strongly pinitized. Photo by R. Hanus.

the outer edge of the blocky zone underwent metasomatic replacement that is associated with less common minerals. The contacts with the surrounding host rocks are predominantly sharp, and a contact aureole of granitic hornfels is locally present (Staněk, 1952b; 2009). In total, more than 81 mineral species are known from this famous Czech locality (see, e.g., www.mindat.org/loc-787.html), including andalusite, quartz, dumortierite, corundum (sapphire), garnet (almandine-spessartine), albite, 'oyamalite' (REE-P rich variety of zircon), monazite, apatite, augelite, zwieselite, triplite, triphylite, sarcopside, wolframite, ilmenite, löllingite, pyrite, rutile, hematite, marcasite, arsenopyrite, chalcopyrite, sphalerite, dolomite, siderite and less frequently symplesite, autunite, torbernite, cookeite, diaspore, anatase, halotrichite and gypsum (Jaroš, 1936; Němec, 1981; Duda, 1986; Staněk, 1991).

Sekaninaite is fairly abundant in some veins of the Hatě locality. It forms complex parallel twins, often having a conical pseudo-hexagonal form (Figure 3), and can reach 1 m in length. All of the sekaninaite from the Hatě locality has been variably altered (pinitized), which causes the prisms to disintegrate along 1–5 mm-thick layers oriented perpendicular to the c-axis. These parting planes are coated by a film of pale green chlorite/chloritoid that partially replaces the sekaninaite, often with acicular crystals of dark green Fe-amphibole (ferrogedrite). Microscopic assemblages of paragonite and hercynite are also products of the pinitization of sekaninaite (Staněk, 2009).

Based on fluid inclusion studies, the temperature of sekaninaite formation at Dolní Bory is estimated at 530°C; at lower temperatures, Fe-rich chlorite and muscovite are more stable (Staněk, 2009).

Materials and Methods

Seventy-eight faceted sekaninaite samples were studied for this report. They ranged from 0.11 to 11.05 ct (average 1.06 ct). The majority were faceted as octagonal and round brilliant cuts. Approximately 1 kg of rough sekaninaite was also available for testing.

The following tests were done on 50 faceted and 20 rough samples: pleochroism (observed with a calcite dichroscope), hydrostatic SG and fluorescence to standard long-wave (366 nm) and short-wave (254 nm) UV radiation. Refractive indices were measured on the 50 cut samples with a refractometer, and the RI of an additional rough sample was measured with a Freiberger Präzisionmechanik double-wheeled goniometer using the method of minimal deviation in sodium light. The cut gems were examined with a Leica polarizing microscope, a Krüss trinocular microscope and an Optika horizontal immersion microscope.

Identical-appearing inclusions in two samples were identified by optical microscopy (in a faceted stone) and by X-ray diffraction using a Siemens X'Pert Pro diffractometer (in a thin sample plate). The measurement conditions were Cu$K\alpha$ radiation, 40 kV, 30 mA and 0.02° step size, under both air-dried and glycolated (with ethylene glycol) conditions. X'Pert HighScore software was used to identify the inclusions from the obtained XRD spectra.

Raman analysis of 10 faceted samples was performed using a GL Gem Raman PL532 instrument with a spectral range of 175–1500 cm^{-1} and a resolution of ~16 cm^{-1} FWHM. Spectra were compared to the RRUFF database (www.rruff.info). Semi-quantitative chemical analyses of the same 10 sekaninaite samples (65 spots total) were obtained with a Tescan MIRA3 GMU scanning electron microscope equipped with an Oxford Instruments EDS microanalytical system.

Ultraviolet-visible–near infrared (UV-Vis-NIR) spectra of 30 faceted samples were collected with a GL Gem Spectrometer in the range 300–1000 nm (optimized for the 400–950 nm range). For comparison, a spectrum also was collected from

one sample of cordierite from the Babati area of the Lake Manyara region in Tanzania.

Results and Discussion

The properties of sekaninaite are summarized and compared to cordierite in Table I. The sekaninaite showed an attractive blue-violet colour and a vitreous lustre where it was unaltered. Like cordierite, sekaninaite displayed strong trichroism (pale yellow to green, violet to blue-violet and light blue). Most of the cut stones were lightly to moderately included (e.g. Figures 1 and 4). The RI values of sekaninaite (n_α = 1.561, n_β = 1.572 and n_γ = 1.576) mostly overlap those of cordierite (typically n_α = 1.527–1.560, n_β = 1.532–1.574 and n_γ = 1.538–1.578). However, the lowest RI value for sekaninaite (n_α = 1.561) is slightly higher than the n_α range for cordierite (1.527–1.560), and is therefore diagnostic for separating the two minerals. The SG measurements of sekaninaite (2.53–2.78) had a wider range than those reported for cordierite (2.53–2.66) and higher values also may be diagnostic in some cases, although SG measurements from both minerals commonly overlap. Therefore, the use of additional methods

Table I: Properties of sekaninaite and cordierite.[a]

Mineral	Sekaninaite	Cordierite
Formula	$(Fe,Mg)_2Al_3(AlSi_5O_{18})$	$(Mg,Fe)_2Al_3(AlSi_5O_{18})$
Crystal system	Orthorhombic	Orthorhombic
Optic sign	Biaxial (−)	Biaxial (+,−)
Type locality	Dolní Bory, Vysočina region, South Moravian Region, Czech Republic	Großer Arber, Bayerisch Eisenstein, Zwiesel, Lower Bavaria, Germany
Year of discovery	1968	1813
Colour	Greyish blue to bluish violet	Grey, blue, blue-violet, greenish, yellowish brown; colourless to very light blue in transmitted light
Pleochroism	*Strong:* *X = c = Pale yellow to green* *Y = a = Violet to blue-violet* *Z = b = Light blue*	Strong: X = c = Pale yellow to green Y = a = Violet to blue-violet Z = b = Light blue
Diaphaneity	Transparent, translucent	Transparent, translucent
Hardness (Mohs)	7½	7–7½
Lustre	Vitreous	Vitreous
Cleavage	{100} good	{100} imperfect/fair, {001} fair and {010} poor
Fracture	Sub-conchoidal	Sub-conchoidal
RIs	*n_α = 1.561* *n_β = 1.572* *n_γ = 1.576*	n_α = 1.527–1.560 n_β = 1.532–1.574 n_γ = 1.538–1.578
Birefringence	*0.015*	0.011–0.018
SG	*2.53–2.78*	2.53–2.66
Fluorescence	None	None
Inclusions	Chloritoid, chlorite, ferrogedrite, quartz, muscovite and orthoclase	Hematite, rutile, apatite, mica, etc. (Henn and Milisenda, 2004)
Absorption spectra[b]	*416, 456, 468, 486, 508, 553 and 627 nm*	426, 436, 456, 492, 535, 585, 593 and 645 nm (O'Donoghue, 2006); *416 and 627 nm also recorded in this study*
Essential elements	Al, Fe, O, Si	Al, Mg, O, Si
Common impurities	*Mg, Mn, Ti, Ca, Na, K,* H_2O[c]	Mn, Fe, Ti, Ca, Na, K

[a] Data in italics indicate the results of our measurements; data not from this study are from www.mindat.org and http://rruff.info/doclib/hom/sekaninaite.pdf, unless otherwise cited.
[b] Absorption spectra vary with pleochroic direction, and in the direction of the violet-blue colour, some bands may be masked by general absorption.
[c] H_2O is from Staněk (2009) and J. Staněk, pers. comm. (2012).

Figure 4: These faceted samples of sekaninaite (left 0.78 ct and right 0.86 ct) show the colour range of the material; both stones are moderately included. Photos by R. Hanus.

such as X-ray diffraction (XRD) or quantitative chemical analysis may be necessary to separate the two minerals.

The alteration (pinitization) of sekaninaite typically follows the abundant fractures in the material, and may even surround entire masses of rough sekaninaite. The inclusions in our faceted samples most commonly consisted of fractures and wispy linear aggregates of microcrystalline chloritoid (Figure 5) and chlorite. Chloritoid was previously documented by Staněk (2009), but the mineral could not be confirmed in the present study because it was not possible to separate a completely 'clean' inclusion for XRD analysis. However, chlorite inclusions were identified in the current study. The chlorite and smectite groups have nearly the same position of the first basal peak measured by XRD. However, expandable structures such as those exhibited by Ca-Mg smectites form intercalates that shift the position of the first basal diffraction peak from 14–15 Å to 17–18 Å. No shift in the first basal peak was observed in the analysed sekaninaite inclusion, confirming it as a chlorite mineral (14.40 Å in spectra of both air-dried and glycolated samples). Other mineral inclusions present in the sekaninaite—identified visually and by their geological association—consisted of ferrogedrite (Figure 5), quartz, muscovite and orthoclase. Also present were minute fluid inclusions. No colour zoning was seen.

Raman Spectroscopy

The Raman spectra of the studied samples showed major peaks at 251.4, 293.8, 560.1 and 665.1 cm^{-1}, with or without additional peaks at 718.2, 901.1, 965.5 and 1006.5 cm^{-1}. These are comparable to spectra of both cordierite and sekaninaite in the RRUFF database (Figure 6). The peak positions were similar, although differences in the spectra were exhibited by the width and intensity of some peaks. These differences were probably due to orientation effects. In addition, sekaninaite and cordierite do not have a fixed chemical composition, as they constitute an isomorphous series. Further deviations may result from admixtures, inclusions or disorders in the crystal lattice. In addition, Raman spectra should be interpreted with respect to the technical limits of the instrumentation (resolution, range, signal/noise ratio, etc.). Therefore, routine Raman spectra cannot be used to distinguish between sekaninaite and cordierite.

Figure 5: Fractures and wispy linear aggregates of microcrystalline chloritoid and/or chlorite form conspicuous inclusions in these sekaninaite gemstones (left magnified 5× and right 3×). The stone on the left also contains ferrogedrite (see arrow). Photomicrographs by R. Hanus.

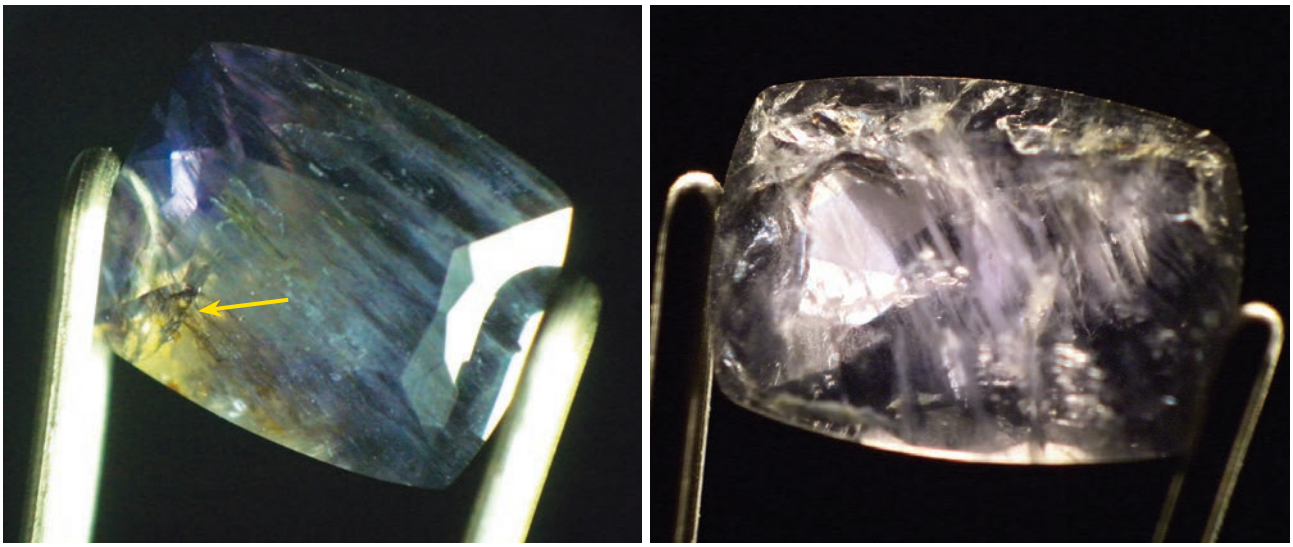

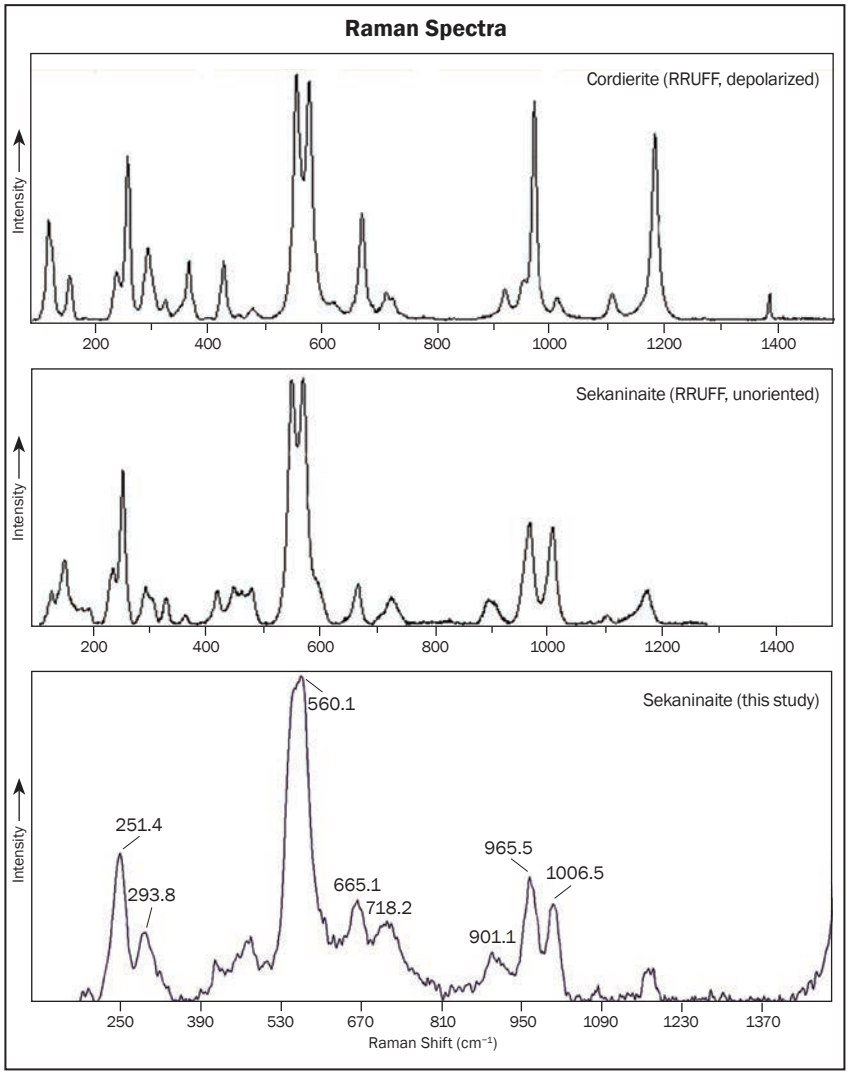

Figure 6: Raman spectra are shown for cordierite and sekaninaite from the RRUFF database, and also for a sekaninaite from this study. The spectra generally have overlapping features, with differences in peak intensities that are probably due mostly to orientation effects.

Chemical Composition

On average, sekaninaite from Dolní Bory contained 16.8 wt.% FeO, 0.8 wt.% MnO and 2.1 wt.% MgO. By comparison, sekaninaite from Winklarn, Germany (as reported by Keck et al., 2010) contained more Fe (average 17.1 wt.% FeO) and Mn (2.5 wt.% MnO), and less Mg (0.2 wt.% MgO). Keck et al. (2010) reported that the Winklarn sekaninaite contained the lowest known Mg concentration, and this remains true. Therefore, the German sekaninaite is slightly closer to end-member composition than the material from Dolní Bory.

UV-Vis-NIR Spectroscopy

The spectra for sekaninaite showed main absorptions at 416, 456, 468, 486, 508, 553 and 627 nm (Figure 7). By comparison, a spectrum for cordierite had main absorptions at 416, 436, 456 and 627 nm. Measured spectra of both sekaninaite and cordierite can vary according to the pleochroic orientation of the sample, with some peaks not occurring in certain orientations.

Figure 7: UV-Vis-NIR spectra of sekaninaite and cordierite show similar absorption features, which may vary according to the pleochroic orientation of the sample.

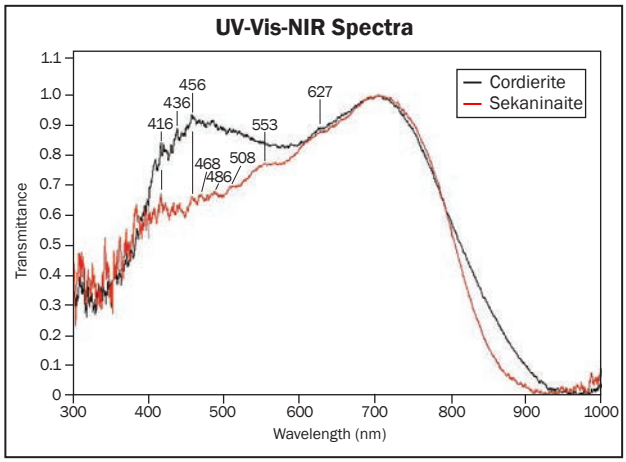

Conclusion

Sekaninaite is a rare collectors' stone that has gemmological properties similar or identical to cordierite, with which it forms a solid-solution series. The two minerals can sometimes be separated by careful RI readings (paying attention to the lowest RI value) and SG measurements, while advanced techniques such as XRD or quantitative chemical analysis will provide a definitive identification.

It is highly unlikely that gem-quality sekaninaite will be produced in a larger scale in the future. Yet, the type locality of Dolní Bory in the Czech Republic will probably continue to yield a limited amount of this attractive gem material.

References

Duda J., 1986. Pegmatity v borském granulitovém masivu. *Sborník geologických věd. Ložisková geologie, mineralogie*, **27**, 157–202.

Fleischer M. and Jambor J., 1977. New mineral names. *American Mineralogist*, **62**(2), 395–397.

Geiger C.A. and Voigtländer H., 2000. The heat capacity of synthetic anhydrous Mg and Fe cordierite. *Contributions to Mineralogy and Petrology*, **138**(1), 46–50, http://dx.doi.org/10.1007/PL00007661.

Grapes R., Korzhova S., Sokol E. and Seryotkin Y., 2011. Paragenesis of unusual Fe-cordierite (sekaninaite)-bearing paralava and clinker from the Kuznetsk coal basin, Siberia, Russia. *Contributions to Mineralogy and Petrology*, **162**(2), 253–273, http://dx.doi.org/10.1007/s00410-010-0593-0.

Henn U. and Milisenda C.C., 2004. *Gemmological Tables*. German Gemmological Association, Idar-Oberstein, Germany.

Jaroš Z., 1936. Příspěvek k otázce původu pseudomorfos v dolnoborských pegmatitech. *Věda přírodní Ročník*, **17**(6–8), 160–164.

Keck E., Mücke A., Kronz A. and Staněk J., 2010. Sekaninait aus einem Pegmatitgang im Serpentinit von Galgenberg bei Winklarn in der Oberpfalz. *Der Aufschluss*, **61**(1), 1–16.

Korchak Y.A., Men'shikov Y.P., Pakhomovskii Y.A., Yakovenchuk V.N. and Ivanyuk G.Y., 2011. Trap formation of the Kola Peninsula. *Petrology*, **19**(1), 87–101, http://dx.doi.org/10.1134/S0869591111010036.

Němec D., 1981. Ein Pegmatit mit Li-Mineralisierung von Dolní Bory in Westmähren (CSSR). *Chemie der Erde*, **40**, 146–177.

O'Donoghue M., Ed., 2006. *Gems*, 6th edn. Butterworth-Heinemann, Oxford.

Staněk J., 1952a. Mineralogie a petrografie pegmatitových žil u Dolních Borů na západní Moravě. Ph.D. thesis, Faculty of Science, Masaryk University, Czech Republic.

Staněk J., 1952b. Petrografie a mineralogie pegmatitových žil u Dolních Borů na západní Moravě. Ph.D. thesis, Faculty of Science, Masaryk University, Czech Republic.

Staněk J., 1991. Parageneze minerálů pegmatitových žil z hatí u Dolních Borů na západní Moravě [The mineral parageneses of the Dolní Bory-Hatě pegmatite dykes, western Moravia, Czechoslovakia]. *Acta Musei Moraviae, Scientiae naturales (Časopis Moravského muzea, Vědy přírodní)*, **76**(1–2), 19–49.

Staněk J., 2009. *Minerály Borů a Cyrilova u Velkého Meziříčí*. Obec Bory, Bory, Czech Republic, 102 pp.

Staněk J. and Miškovský J., 1975. Sekaninaite, a new mineral of the cordierite series, from Dolní Bory, Czechoslovakia. *Scripta Facultatis Scientiarum Naturalium Universitatis Purkinianae Brunensis, Geologie,* **1**(5), 21–30.

Yakubovich O.V., Massa V., Pekov I.V., Gavrilenko P.G. and Chukanov N.V., 2004. Crystal structure of the Na-, Ca-, Be-cordierite and crystallochemical regularities in the cordierite–sekaninaite series. *Crystallography Reports*, **49**(6), 953–963, http://dx.doi.org/10.1134/1.1828139.

The Authors

Dr Radek Hanus, Ivana Kusá and Jana Kasíková
e-gems.cz
Vysoký Újezd 47, Beroun
267 16 Czech Republic
Email: kakt@centrum.cz

Acknowledgements

The authors thank Prof. Jean-Marie Dereppe and Dr Jan Stubna for kindly performing Raman spectroscopy, and Aleš Vít Sr. for his help with preparing some of the photos. We also thank Justin Velner for proofreading the article.

An innovator in gemstone reporting

• Identification of colored gemstones • Country of origin determination • Full quality and color grading analysis

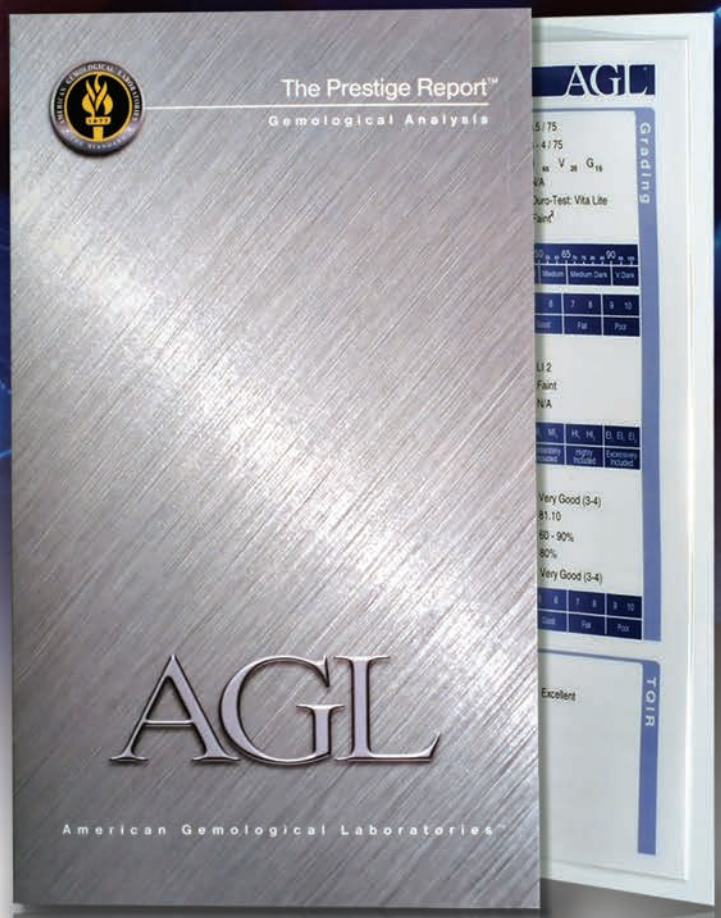

AMERICAN GEMOLOGICAL LABORATORIES AGL

580 5th Ave • Suite 706 • New York, NY 10036, USA
www.aglgemlab.com • +1 (212) 704 - 0727

Phase Transformation of Epigenetic Iron Staining: Indication of Low-Temperature Heat Treatment in Mozambique Ruby

Tasnara Sripoonjan, Bhuwadol Wanthanachaisaeng and Thanong Leelawatanasuk

In the past several years, Mozambique has emerged as one of the world's most important sources of ruby, and unheated stones from this country are in particularly strong demand. Nevertheless, it is common for these rubies to undergo low-temperature heating (~1,000°C or below) to slightly improve their colour. The treated stones may show very subtle or no alteration of internal features (e.g. mineral inclusions, 'fingerprints', needles, 'silk', etc.). However, 'iron-stained' surface-reaching fractures in the rubies commonly display a noticeably more intense colour after heating. Raman and FTIR spectroscopy were used to document a transition from goethite to hematite within stained fractures in samples heated to 500°C and 600°C. The identification of hematite within such fractures provides key evidence for the low-temperature heat treatment of Mozambique ruby.

The Journal of Gemmology, **35**(2), 2016, pp. 156–161, http://dx.doi.org/10.15506/JoG.2016.35.2.156

Introduction

Mozambique is currently a globally important source of gem-quality ruby (e.g. Figure 1). Since the late 2000s, various ruby deposits have been discovered in the country, particularly around the Montepuez district (e.g. GIT-GTL, 2010). The stones show a range of colours and qualities, from pinkish red to purplish red with low-to-high clarity. The red colour is commonly inhomogeneous, with bluish zoning being commonly visible. Heat treatment is the most commonly used method to improve the colour so that it is acceptable to the gem trade. In late 2014, the Gem and Jewelry Institute of Thailand's Gem Testing Laboratory (GIT-GTL) learned about the low-temperature heat treatment of corundum, particularly of ruby from Mozambique. Low-temperature heating was subsequently documented as effective for improving the appearance of this material and removing bluish overtones (Pardieu et al., 2015). Typically the treatment process involves heating in air to at least 550°C, and then the temperature is increased by 100°C to a maximum of 750°C; however, the temperature at which the colour change occurs is not known to the present authors.

Heat treatment of corundum has been performed for centuries, and initially gem burners used firewood or charcoal as a heat source, sometimes with a blowpipe. Such treatments were performed

Figure 1: Mozambique has emerged as an important ruby source, as shown by these untreated stones (1.02–5.93 ct). Photo by T. Sripoonjan.

at relatively low temperatures compared to some current heating methods, although more recently these low-temperature conditions have been applied using modern electric furnaces. The identification of such treatments by gem laboratories is problematic—particularly for labs that rely only on the appearance of inclusions—resulting in inconsistencies in identification reports. While in some cases careful microscopic observation of inclusions may indicate that a ruby underwent low-temperature heating, the application of Fourier-transform infrared (FTIR) spectroscopy may provide additional proof by detecting the alteration of inclusions such as diaspore (Smith, 1995, 2010). Furthermore, the effects of heating may be detected in weathering-related minerals such as kaolinite (C. Smith, pers. comm., 2016). The systematic study of samples before and after heating is necessary to understand the temperatures under which transformations may occur.

One of the most prominent internal features in both rough and faceted rubies from Mozambique is iron-oxide staining, seen as yellow-to-orange epigenetic residues along surface-reaching fractures. The colour saturation of the iron staining tends to be intensified by heating (Kammerling and Koivula, 1989; de Faria and Lopes, 2007; Koivula, 2013; Pardieu et al., 2015). This study further investigates the changes that occur in iron-stained fractures within Mozambique rubies, and provides criteria for detecting their low-temperature treatment.

Materials and Methods

Ten representative unheated rough samples of ruby from Mozambique (0.11–0.41 g) were used in this study, and all work was carried out at GIT-GTL. Each sample was cut in half, and one piece was used for heating experiments while the other was retained for reference (Figure 2). All

Figure 2: Ten rough ruby samples from Mozambique were sliced in half, and the right-hand portion of each sample was subjected to heating experiments (to 500 °C, and then to 600 °C), while the other half was kept for reference and colour comparison. Photo by T. Sripoonjan.

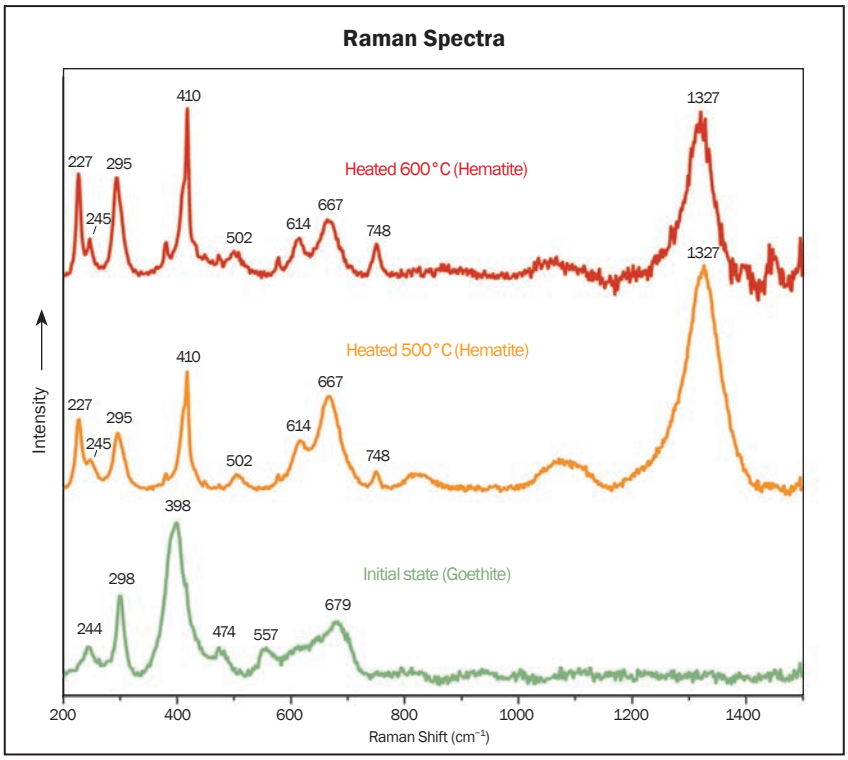

Figure 3: Raman spectra of iron-stained residues within fractures in the Mozambique rubies indicated the presence of goethite in the unheated stones and hematite in samples that were heated to 500 °C and 600 °C.

of the rubies contained prominent iron-stained fractures. The test samples were placed within an alumina crucible in an electric resistance furnace and thermally treated in air for a dwell time of two hours. The samples were initially heated to 500°C and allowed to cool slowly before being analysed. Then they were heated again, to 600°C, and more data were collected.

The iron-stained residues in the unheated reference samples and in the treated rubies were analysed with a Renishaw inVia Raman microscope, and the spectra were compared to GIT-GTL's gemstone and mineral databases and Renishaw's minerals and inorganic material database. In addition, FTIR spectroscopy of all samples was performed with a Thermo Scientific Nicolet 6700 instrument (128 scans, 4 cm^{-1} resolution and 4000-400 cm^{-1} range, using a DTGS detector and KBr beam splitter). The beam was directed through areas of the samples containing iron-stained fractures.

Results and Discussion

Raman spectroscopy of the unheated ruby samples (e.g. Figure 3, bottom) identified the epigenetic iron-stained residues as goethite, α-$Fe^{3+}O(OH)$. This compound precipitated in surface-reaching fractures after iron-bearing groundwater dried out under oxidizing conditions (Kennedy, 1990; Koivula, 2013).

After the samples were heated to 500°C and 600°C, the colour of the iron stains appeared more saturated, as shown in Figures 4 and 5. Raman

Figure 4: The iron-stained fractures in this representative sample of Mozambique ruby display a noticeable increase in orangey red coloration in the heated half (right side) compared to the untreated portion (left side). Photos by Y. Lhongsomboon.

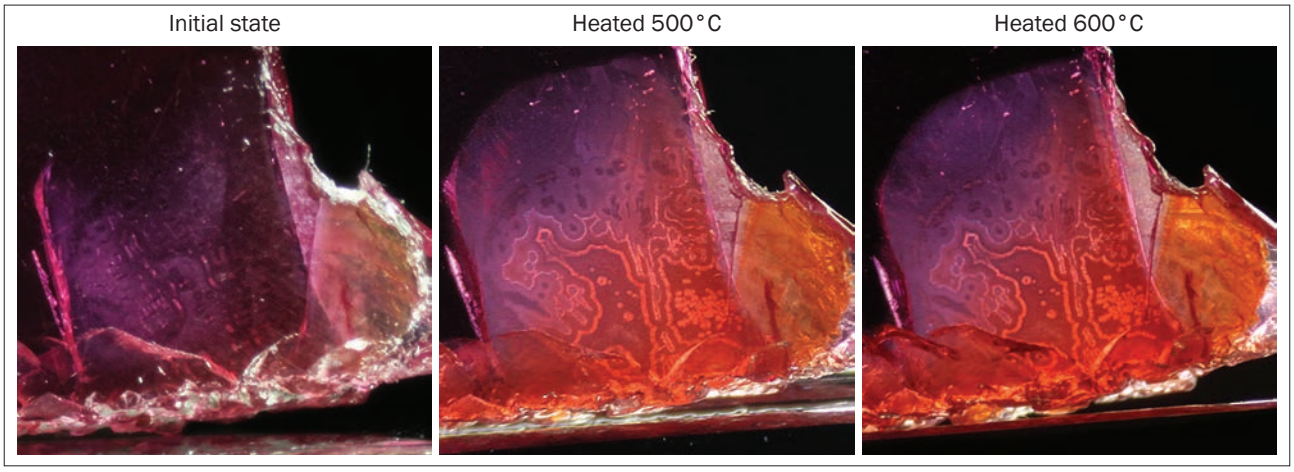

Figure 5: Heating of this Mozambique ruby produced a distinct change in the appearance of epigenetic iron staining within a fracture. Photomicrographs by Y. Lhongsomboon; image width 4.65 mm.

spectra of the iron-stained residues after heating identified them as hematite, Fe_2O_3 (Figure 3, centre and top). The characteristic Raman peaks of hematite at approximately 227, 245, 295 and 410 cm^{-1} were clearly evident after treatment at 500°C. Further heating to 600°C caused the Raman peaks to become slightly narrower, which may be due to increased crystal size and crystallinity of the hematite (Liu et al., 2013). Similar results were found in all samples, indicating that the transformation and dehydration of goethite to hematite in the iron-stained fractures easily occurs below 500°C, as suggested by Koivula (2013) and Liu et al. (2013). The appearance of other internal features (e.g. mineral inclusions) in the samples remained unchanged after heating to both 500°C and 600°C (Figure 6).

Infrared spectroscopy is useful for investigating absorption features related to structural OH groups in rubies, and can reveal trace impurities of diaspore, boehmite and/or kaolinite (Smith, 1995; Beran and Rossman, 2006). The spectra are commonly dominated by O-H stretching frequencies related to boehmite and/or kaolinite impurities, particularly in the 4000–3000 cm^{-1} region (e.g. Figure 7) that is useful for determining if a ruby or sapphire has been heated (Smith, 1995). However, low-temperature heat treatment may not cause boehmite and kaolinite to completely decompose (cf. Glass, 1954; Wanthanachaisaeng,

Figure 6: These inclusion scenes in Mozambique ruby (top: diaspore; bottom: amphibole) show no significant changes in appearance after heating to 500 °C and 600 °C. Photomicrographs by Y. Lhongsomboon; image width 1.8 mm.

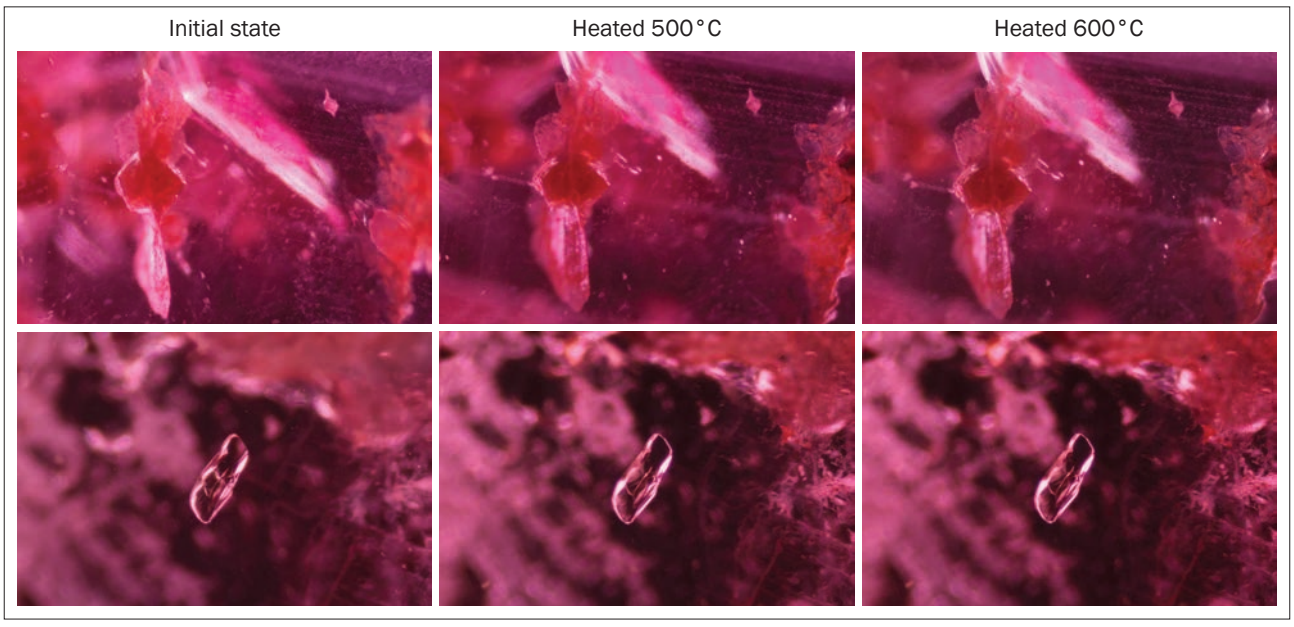

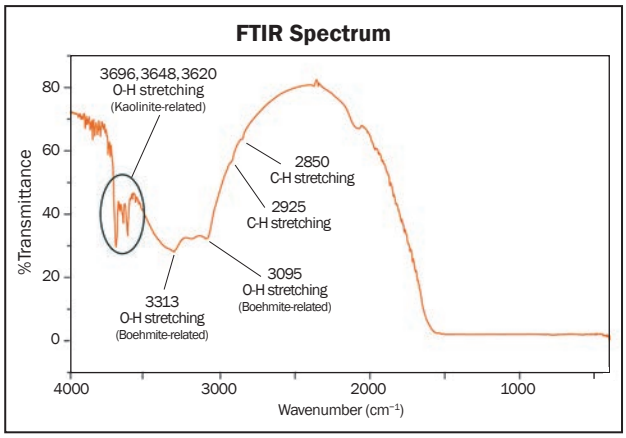

Figure 7: FTIR spectroscopy of OH-related features in ruby and sapphire can help gemmologists determine whether stones have undergone heat treatment. Frequently, the identification of low-temperature heating (i.e. below 600 °C) cannot be precisely achieved because the OH-related features may not have completely decomposed. (The peaks at ~2925 and 2850 cm^{-1} are probably due to contamination from finger oils or cutting residues; Cartier, 2009.)

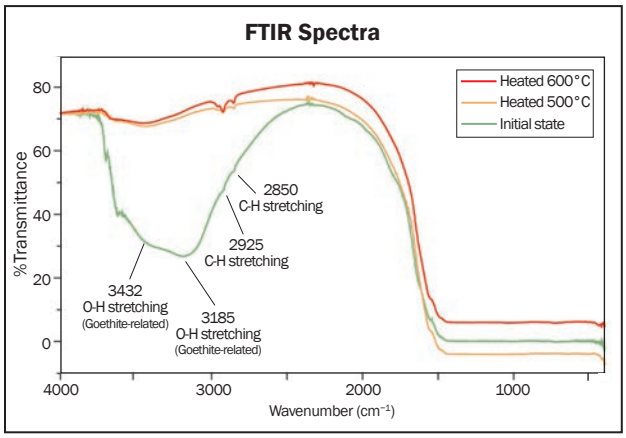

Figure 8: FTIR spectra are shown for a representative sample of Mozambique ruby before treatment and after heating to 500 °C and 600 °C. Goethite-related absorptions in the 3600–3000 cm^{-1} region are evident before heat treatment, but they nearly disappear after treatment.

2007). Unheated samples of Mozambique ruby in this study occasionally showed FTIR absorption bands associated with iron hydroxides (i.e. goethite, as identified by Raman spectroscopy), although only when the ruby samples were analysed in particular directions and positions (cf. Cambier, 1986). In the spectral range of 3600–3000 cm^{-1}, which is important for the detection of hydroxyl bonds (including goethite), the absorption bands in the unheated samples were slightly broadened rather than appearing as sharp peaks. After treatment at 500°C or 600°C, these absorption bands became barely visible due to dehydroxylation and recrystallization of goethite into hematite (Liu et al., 2013; Figure 8). Heating of goethite causes a gradual dehydration that begins at 260°C (Kammerling and Koivula, 1989; de Faria and Lopes, 2007; Koivula, 2013; Liu et al., 2013). It continues with the transformation of the yellow-to-orange goethite (orthorhombic) to dark orange-red hematite (trigonal), through the chemical reaction:

$$2\alpha\text{-FeO(OH)} + \text{Heat} \rightarrow \alpha\text{-Fe}_2\text{O}_3 + \text{H}_2\text{O}$$

Goethite — Hematite — Water

Conclusions

Although the low-temperature heating of ruby and sapphire has been conducted for centuries, the detection of such treatment remains difficult. For ruby in particular, low-temperature treatment of material from Myanmar and Vietnam is well known (e.g. Smith, 2010; Wathanakul et al., 2011; Pardieu et al., 2015), but conclusive identification criteria remain elusive in many cases.

In recent years, Mozambique ruby has become important in the gem and jewellery market. Low-temperature heat treatment is successful for improving the colour of this material, but unfortunately many unethical traders have sold these heated stones as untreated. Microscopic observation of inclusions in such rubies is not reliable for identifying this treatment. However, heating intensifies the coloration of epigenetic iron-stained fractures, providing visual evidence of treatment. This change in appearance is due to the transformation of goethite to hematite by a dehydration mechanism that takes place during the heating process. Raman and FTIR spectroscopy are useful for detecting the presence of hematite residues in the iron-stained fractures, which is a key criterion to indicate heat treatment at relatively low temperatures in Mozambique ruby.

References

Beran A. and Rossman G.R., 2006. OH in naturally occurring corundum. *European Journal of Mineralogy*, **18**(4), 441–447, http://dx.doi.org/10.1127/0935-1221/2006/0018-0441.

Cambier P., 1986. Infrared study of goethites of varying crystallinity and particle size: II. Crystallographic and morphological changes in series of synthetic goethites. *Clay Minerals*, **21**(2), 201–210, http://dx.doi.org/10.1180/claymin.1986.021.2.09.

Cartier L.E., 2009. Ruby and sapphire from Marosely, Madagascar. *Journal of Gemmology*, **31**(5-8), 171–179.

de Faria D.L.A. and Lopes F.N., 2007. Heated goethite and natural hematite: Can Raman spectroscopy be used to differentiate them? *Vibrational Spectroscopy*, **45**(2), 117–121, http://dx.doi.org/10.1016/j.vibspec.2007.07.003.

GIT Gem Testing Laboratory, 2010. New ruby deposits in Mozambique. Gem and Jewelry Institute of Thailand, Bangkok, 8 pp, www.git.or.th/2014/eng/testing_center_en/lab_notes_en/glab_en/2010/new_ruby_deposits_mozambique.pdf.

Glass H.D., 1954. High temperature phases from kaolinite and halloysite. *American Mineralogist*, **39**, 193–207.

Kammerling R.C. and Koivula J.I., 1989. Thermal alteration of inclusions in 'rutilated' topaz. *Gems & Gemology*, **25**(3), 165–167, http://dx.doi.org/10.5741/gems.25.3.165.

Kennedy B.A., Ed., 1990. *Surface Mining*, 2nd edn. Society for Mining, Metallurgy, and Exploration Inc., Baltimore, Maryland, USA, 1,206 pp.

Koivula J.I., 2013. Useful visual clue indicating corundum heat treatment. *Gems & Gemology*, **49**(3), 160–161, http://dx.doi.org/10.5741/gems.49.3.160.

Liu H., Chen T., Zou X., Qing C. and Frost R.L., 2013. Thermal treatment of natural goethite: Thermal transformation and physical properties. *Thermochimica Acta*, **568**, 115–121, http://dx.doi.org/10.1016/j.tca.2013.06.027.

Pardieu V., Saeseaw S., Detroyat S., Raynaud V., Sangsawong S., Bhusrison T., Engniwat S. and Muyal J., 2015. "Low temperature" heat treatment of Mozambique ruby—Results report. GIA Thailand, Bangkok, www.gia.edu/gia-news-research-low-temperature-heat-treatment-mozambique-ruby.

Smith C.P., 1995. A contribution to understanding the infrared spectra of rubies from Mong Hsu, Myanmar. *Journal of Gemmology*, **24**(5), 321–335, http://dx.doi.org/10.15506/jog.1995.24.5.321.

Smith C.P., 2010. Heated corundum: What inclusions can tell us. *World of Gems Conference II*, Rosemont, Illinois, USA, 9–10 October, 61–63.

Wanthanachaisaeng B., 2007. The influence of heat treatment on the phase relations in mineral growth systems. PhD dissertation, University of Mainz, Germany, 79 pp.

Wathanakul P., Monarumit N., Leelawatanasuk T., Ingavanija S., Sriprasert B. and Atichat W., 2011. A contribution to indicating the low temperature heat treatment of ruby samples from Myanmar and Vietnam. *7th European Conference on Mineralogy and Spectroscopy*, 4–7 September, Potsdam, Germany.

The Authors

Tasnara Sripoonjan and Thanong Leelawatanasuk
The Gem and Jewelry Institute of Thailand (Public Organization), 4th Floor, ITF Tower, Silom Rd., Bangrak, Bangkok 10500, Thailand. Email: lthanong@git.or.th

Dr Bhuwadol Wanthanachaisaeng
Division of Materials Science (Gems & Jewelry), Department of General Science, Faculty of Science, Srinakharinwirot University, Sukhumvit 23, Wattana, Bangkok 10110, Thailand

Acknowledgements

This research was funded by The Gem and Jewelry Institute of Thailand. The authors thank all staff members of GIT-GTL for their support during the research. We also thank C. Smith for providing useful comments during the review of this paper.

Letters

Digital Manipulation of Gem Photos

I noticed that summaries of papers from *The Journal of Gemmology* are once again being included in *Gems&Jewellery*, and these will enable *Journal* articles to have broader trade exposure.

However, a point niggled me regarding the photo in the summary of *The Journal* article on inclusions in cat's-eye, star and other chrysoberyls that appeared in the current issue of *G&J* (May/June 2016, p. 21); this photo was reprinted from p. 26 of *The Journal* (Vol. 35, No. 1, 2016). It is the matter of showing two photos of the same gem in daylight and in incandescent or other light, which demonstrates a colour change. This particular example illustrates the change in colour of a cat's-eye alexandrite, which according to the caption "... is shown in daylight (left) and incandescent light (right)". Now, the point is, the two photos are one and the same, except one has had the centre gem digitally altered in colour to represent the different lighting environment. From the reflections on the gem, I would say the incandescent one is the actual photo and the daylight one, therefore, is the manipulated one. I suggest that photos manipulated in this way are labelled as such, possibly with 'rendered to simulate daylight appearance'. I know it is often difficult, sometimes impossible, to capture a correct colour (i.e. the photo image does not match what the eye sees), and I am perfectly happy for such manipulation to be carried out in order to represent for us what the photographer was actually seeing. I just want it stated as such, especially in a paper that includes scientific evidence and records of testing.

This subject also arose with *Gems & Gemology* some years ago and they did, finally, admit that such colour manipulation was used and they would alter the description to say so.

It also would help with believability if two photos could be taken, perhaps of slightly differing angles, even if one is then altered.

I hope that this letter will encourage future authors to indicate when photo manipulation has occurred in articles that include such images.

Grenville Millington
Knowle, West Midlands

Reply

Thank you, Mr Millington, for your good suggestion. In the future we will be sure to indicate that such photos are modified to simulate daylight appearance.

Brendan M. Laurs
Editor-in-Chief

Interpretation of Colours Seen Between Crossed Polarizers

I was very interested to read the Gem Note by Candice Caplan and Franck Notari titled "A Lalique quartz pendant, in polarized light" (Vol. 35, No. 1, 2016, pp. 13–15). The accompanying photographs of the lovely quartz pendant dramatically illustrate the beauty of gem materials when viewed in cross-polarized light. However, the reasons stated for some of the optical effects observed by the authors are not completely accurate.

Judging from the interference figure, some of the colours seen in the untwinned areas of the quartz are due to optical activity that results from *rotatory dispersion of light* travelling parallel to the optic axis, and some are due to a *combination of optical activity and interference*. They are not "due to a combination of diffusion and diffraction", nor are they caused by "its crystallographic orientation versus the polarization direction of the light."

Thickness does affect the colours resulting from rotatory dispersion. It also affects the colours due to interference when the optic axis is inclined to the direction the light is travelling,

a condition that seems to be the case in Figure 14, which shows the optic figure slightly askew. And, as stated above, colours can result from a combination of these two phenomena.

Optical activity in quartz is a complicated subject, and because it is rarely treated in any depth in gemmological and mineralogical literature, observations can be easily misconstrued. Clear understanding of the underlying cause of optical activity and its resulting optical effects can be important for interpreting differences in synthetic versus natural quartz, as well as for understanding the nature of quartz itself. For more information on this phenomenon, please see the 2015 booklet by E. A. Skalwold and W. A. Bassett titled *Quartz: A Bull's Eye on Optical Activity*, which is freely available at www.minsocam.org/msa/openaccess_publications/#Skalwold_02. The discussion of optical activity, the nature of the bull's-eye optic figure and, in particular, the quartz monochromator's ability to produce various colours, will give gemmologists a background for interpreting the unique optical effects seen in quartz gems.

Elise A. Skalwold
Ithaca, New York, USA

Authors' Reply

We are thankful to Ms Skalwold for providing the link to her publication and for the explanation regarding the rotatory dispersion of light that we missed including as a possible mechanism. Nevertheless, the purpose of the entry was to draw attention to the differences between the front and back views of the carved figures in the pendant with cross-polarized light, as well as the colours observed during rotation of the object between crossed polarizers, for which we found no explanations in gemmological publications.

Candice Caplan and Franck Notari
GGTL Laboratories, Geneva, Switzerland

Conferences

AGA Las Vegas

The Accredited Gemologists Association's 2016 Las Vegas conference took place on 2 June, just prior to the JCK Las Vegas Show in Nevada, USA. Attended by 62 people, the event was chaired by AGA past-president Donna Hawrelko, and featured seven speakers.

Peter Shemonsky (Peter Jon Shemonsky, San Francisco, California, USA) discussed imitations of high-end jewellery and how to avoid them. Some of the tips he gave were (1) learn variations in hallmarks and signatures, and where to find them on jewellery items; (2) ensure that hallmarks are consistent with the country of manufacture; (3) check for correct assembly, as well as the ease of disassembly for repairs; (4) observe the back of the item, which should be finished as well as the front; and (5) familiarize yourself with the various models that were released over time by some manufacturers. **Art Samuels** (Estate Buyers, Miami, Florida, USA) gave examples of various gem and jewellery frauds he has encountered, including a large mounted light blue diamond that was colour-enhanced with a blue substance on the girdle, HPHT-treated diamonds cut to match laboratory grading reports of untreated diamonds and overinflated appraisals used as collateral for money loans.

John King (Gemological Institute of America, New York, New York) reviewed GIA's system for grading coloured diamonds. He stressed that each colour grade represents a range of appearances, and that differences between them are not consistent throughout colour space. Therefore extensive experiments have been done to assess the amount of difference between colour grade boundaries (referred to as 'stepping') throughout the hue circle. Next, **Thomas Gelb** (Natural Color Diamond Association, New York), **José Batista** (Rio Diamond, New York) and **Scott West** (LJ West Diamonds, New York) explored value factors of natural-colour diamonds. Special considerations for these gems include their extreme rarity, high value, fragmented middle market, opaque pricing (with the exception of stones sold at auction) and complex quality grading. In general, the rarer the colour, the less important are the clarity, cut and carat weight in determining their value.

Eric Braunwart (Columbia Gem House, Vancouver, Washington, USA) discussed transparent sourcing of coloured stones (Figure 1). His criteria for fair trade gems include environmental protection, product integrity, fair labour conditions and worker rights, cultural appreciation, supply chain transparency, fair value and full information for consumers. He reported that recent surveys showed that many consumers are willing to pay ~10% more for a fair trade gemstone compared to one with no origin information.

Brendan M. Laurs

Figure 1: Eric Braunwart discusses fair trade gems at the AGA Las Vegas conference. Photo by Ya'akov Almor.

China Gems & Jewelry Academic Exchange Conference

This biannual conference was held on 30 November 2015 in Beijing. It was organized by the National Gems & Jewelry Technology Administrative Center (NGTC, Beijing) and the Gems & Jewelry Trade Association of China (Beijing). About 500 representatives from the UK, USA, Switzerland, Thailand, Poland, Hong Kong, Taiwan, and many Chinese jewellery testing centres, institutes, companies and appraisal agencies attended the conference. Invited presentations were given by 13 speakers (see, e.g., Figure 2 and summaries below). A proceedings volume published by *China Gems* (November–December 2015, 460 pages) contains extended abstracts covering most of the talks, as well as numerous short papers that were not actually presented at the conference.

Dr David Fisher (De Beers Technologies Research Centre, Maidenhead, Berkshire) reported on recent developments in the detection of currently available HPHT- and CVD-grown synthetic diamonds. **Dr Ewa Wagner-Wysiecka** (Gdańsk University of Technology, Poland) discussed the identification of natural and treated ambers using spectroscopic techniques. **Dr Daniel Nyfeler** (Gübelin Gem Lab, Lucerne, Switzerland) reviewed recent applications of LA-ICP-MS to gem testing and dating. **Dr Pornsawat Wathanakul** (Gem and Jewelry Institute of Thailand, Bangkok) described the low-temperature heat treatment of ruby and its detection. **Dr Wuyi Wang** (GIA, New York) explained the application of carbon isotopes for separating CVD and natural type IIa diamonds. **Sterling Foutz** (Sterling Turquoise, Tempe, Arizona, USA) reported on the principles, methods and identification of turquoise enhanced by the Zachery process.

A number of researchers from China also described their research. **Dr Taijin Lu** (NGTC) reported on various instrument development efforts at his laboratory. **Hua Chen** (NGTC) proposed a naming convention for silicic aggregates sold as 'jade' in China (including, but not limited to, quartzite and chalcedony). **Yan Lan** (NGTC) reported progress in the development of various precious metal analytical standards. **Profs. Guanghai Shi** and **Xuemei He** (China University of Geosciences, Beijing) described the origin and appearance of Myanmar jadeite and the coloration of 'Zhangguohong' agate, respectively. **Prof. Lijian Qi** (Tongji University) discussed the characteristics of various colours of sugilite (i.e. light to dark blue and light pink to dark violet) and their associated trade names in the Chinese market. **Author AHS** reported on the geographic origin of nephrite using a novel statistical method involving the LA-ICP-MS analysis of trace elements.

Yilang Huang, Qijuan Wan and
Prof. Andy H. Shen (ahshen1@live.com)
China University of Geosciences, Wuhan

Figure 2: This photo shows some of the invited presenters of the 2015 China Gems & Jewelry Academic Exchange Conference. Photo courtesy of conference staff.

2nd Mediterranean Gemmological & Jewellery Conference

On 6–9 May 2016, the 2nd Mediterranean Gemmological & Jewellery Conference (MGJC) took place in Valencia, Spain. The MGJC is held annually, each time in a different Mediterranean location. The theme of this year's event was diamond treatments, but other topics also were covered. The conference attracted 80 gemmologists, jewellery appraisers and scientists from 20 countries.

Figure 3: The 2nd Mediterranean Gemmological & Jewellery Conference included a panel discussion on diamond treatments moderated by John Chapman (far left) and comprising (from left to right) Branko Deljanin, Gaetano Cavalieri, Gail Brett Levine, Mikko Åström, Sonny Pope and Dusan Simic. Photo by Anastasiya Shramko.

Dr Gaetano Cavalieri (CIBJO, The World Jewellery Confederation, Milan, Italy) delivered the opening address and described the role of his organisation in protecting consumers, as specified in CIBJO's 'Blue Book' series, which defines grading standards and nomenclature. He provided examples of fraudulent and misleading conduct in the gem trade that have been acted upon by CIBJO.

Dr David Fisher (De Beers Technologies Research Centre, Maidenhead) recounted recent research toward understanding colour defects in diamond (particularly brown) and their response to HPHT treatment. Then, **Sonny Pope** (Suncrest Diamonds, Orem, Utah, USA) explained commercial HPHT and irradiation treatments of diamonds done by his company. He emphasized opportunities for transforming low-value brown diamonds into fancy-coloured gems, showing a chart of possible treated colours that depend on the starting colour and nitrogen content coupled with the processing conditions.

Dusan Simic (Analytical Gemology & Jewelry, New York) described instances of laboratories reporting 'natural' for synthetic or treated diamonds. He discussed useful indicators of treatment in FTIR and photoluminescence spectra (e.g. the width of the 741 nm irradiation peak). He also noted that improvements in laboratory techniques and interpretations are lessening instances of misidentification. With analytical tools being a key to detection, **Mikko Åström** (M&A Gemological Instruments, Jarvenpaa, Finland) described the principles and practicalities of IR spectroscopy. He described examples of IR features pertaining to diamonds and coloured stones, including the detection of emerald fillers and synthetic amethyst.

Besides treatments, the source traceability of gemstones is another consumer concern. This was addressed by **Jean Claude Michelou** (International Colored Gemstone Association, New York), who highlighted difficulties in tracing 17 varieties of coloured stones sourced from 47 countries with undeclared or under-declared reports at international borders.

Jeffrey Bergman (Primagem, Bangkok, Thailand) showed examples of how geographic origin and various visible characteristics influence the value of opals, star sapphires and trapiche gems.

Lisa Elser (Custom Cut Gems, Vancouver, British Columbia, Canada) provided her personal experiences of buying gem rough in the field, including offerings of synthetics at mine sites and other deceptive seller tactics.

Independent gemmologist **Dr Rui Galopim de Carvalho** (Lisbon, Portugal) discussed Portuguese jewellery, with examples from the royal collection that demonstrate how exploration of the New World affected the availability of different gems through history and had a strong influence on jewellery design.

The Koh-i-Noor diamond was the topic of a presentation by **Alan Hart** (The Natural History Museum, London). He traced its history using casts of the stone from the Museum's collection, and examined how the polishing anisotropy of diamond had a strong influence on the shape of such Mogul-style cuts. Hart noted the availability for scientific research of more than 1,000 diamonds and almost 5,000 coloured stones in the Museum's collection, all untreated.

The final conference session consisted of a panel discussion on diamond treatments, moderated by **this author** (Figure 3). Experts from various fields explored technologies, detection and consumer aspects of treatments, and the audience offered their questions and viewpoints.

The MGJC also included three workshops on diamonds, during which 85 participants put their learning to the test by identifying synthetics and treatments in 50 samples with the aid of microscopes and UV lamps, while UV-Vis, Raman and FTIR spectrometers provided by M&A Gemological Instruments facilitated further testing.

A conference dinner completed the weekend, and a guided city tour provided visitors with a deeper appreciation of the host city of Valencia. The theme of next year's conference is coloured diamonds, and further details will be announced in due course at www.gemconference.com.

John G. Chapman (john@gemetrix.com.au)
Gemetrix Pty. Ltd., Perth, Western Australia, Australia

Scottish Gemmological Association

The 21st Scottish Gemmological Association's annual conference took place from 29 April to 2 May 2016 in Peebles, Scotland. It was attended by approximately 85 delegates and students.

Dr Karl Schmetzer (Petershausen, Germany) gave two presentations as the keynote speaker of the conference. He first recounted synthetic emerald production in Germany between 1911 and 1962. He traced the different companies and production methods involved, and highlighted the use of platinum containers and lithium molybdate and lithium molybdate-vanadate fluxes in certain production processes. His second presentation covered historical garnets spanning 300 BC to 700 AD, and considered their origins based on chemical analyses (e.g. ratios of MgO and CaO).

Dr Thomas Hainschwang (GGTL Laboratories, Balzers, Liechtenstein) described his experiences in testing coloured diamonds and the limited availability of known untreated samples, which requires reliance on historical museum collections with documented provenance. He also highlighted the difficulties and technicalities of transporting a complete lab set-up to the relevant museums to undertake the analyses on-site, usually within a constrained timeframe.

Dr Çiğdem Lüle (Gemworld International, Glenview, Illinois, USA) described the geological occurrence of Turkish diaspore and the cause of its colour-change effect. Gem-quality diaspore is inferred to have formed during a second generation of crystal growth, and contains relatively higher contents of Cr and rare-earth elements.

Dr Rui Galopim de Carvalho (Lisbon, Portugal; Figure 4) reviewed the use of Brazil-sourced gemstones in Portuguese jewellery from the 16th century onward. He also documented a transition from traditional-worked gold styles (in which gems were used to accent the overall design) and engraving to designs showing minimal setting (commonly with foil-backed stones).

Joanna Whalley (Victoria & Albert Museum, London) described a recent V&A exhibition titled 'Bejewelled Treasures: The Al Thani Collection', which featured over 100 items of Mughal jewellery. She explained the difficulties and technical requirements of setting up such an exhibition, and also highlighted the skills of the setters and designers in manufacturing these exquisite pieces.

Figure 4: Dr Rui Galopim de Carvalho answers questions from the audience on the use of Brazil-sourced gemstones in historical Portuguese jewellery during the Scottish Gemmological Association Conference. Photo by A. Fellows.

Clare Dorrell (consultant in fine antiques and jewellery, Edinburgh) discussed the life and works of Scottish gem engraver James Tassie, who perfected the style of resin cameo work that now bears his name, and who was also responsible for producing glass imitations of many carved gem cameos at his workshop in London.

The conference also included the following workshops:

- **Kerry Gregory** (H&T Group, Sutton, Surrey) covered the range of tests available to the practising gemmologist when confronted with mounted gems and the limitations thereof.
- **Dr Çiğdem Lüle** reviewed coatings on gemstones and their detection.
- **Sarah Steele** (Ebor Jetworks, Whitby, North Yorkshire) highlighted the differences between Whitby jet and its alternatives and imitations.
- **Claire Mitchell** (Gem-A, London) reviewed diamond treatments.
- **David Callaghan** (Society of Jewellery Historians, London) highlighted fakes and imitations in the jewellery trade, showing the difference between those created as 'reproductions' and those designed to deceive.

The conference closed with a field trip to the Celts exhibition (National Museum of Scotland, Edinburgh), which features works of art, both jewellery and other, that were created by the Celts in a timeframe spanning over 2,500 years, covering a shared Celtic heritage across ancient Europe.

Andrew S. Fellows FGA DGA
(andrewfellows@gem-a.com) Gem-A, London

Swiss Gemmological Society

On 17–19 April 2016, the Swiss Gemmological Society (SGS) held its 74th annual conference in Magglingen, which is beautifully situated in the Jura Mountains above Lake Biel in western Switzerland. The lectures were attended by 83 SGS members and a few guests. The meeting was chaired by **the authors** and by **Hans Pfister**, SGS president. The main theme of the conference was the specific gemmological challenges and requirements of the Swiss watch industry, although other topics were explored in several presentations.

Jean-Pierre Chalain (Swiss Gemmological Institute SSEF, Basel) introduced his laboratory's testing procedures for the identification and quality control of melee-sized diamonds for the watch industry. In addition to describing in detail the working procedures at SSEF, he also showed how the Automated Spectral Diamond Inspection (ASDI) instrument is used as an efficient tool for diamond identification and sorting.

Cédric Bérruex and **Guillaume Chautru** (Piaget, Geneva, Switzerland) explained the importance of authenticating diamond melee (such as with the ASDI) and of maintaining internal quality control on the stones used in Piaget's gem-set luxury watches and high-end jewellery.

Daniel Haas (Haas Zifferblätter, Pieterlen, Switzerland) focused on how his company follows the highest quality standards during the production of watch dial plates made of ornamental stones for luxury watch brands. He detailed the process from the selection of the raw material (e.g. at the Tucson gem shows, where he is a regular visitor) to the design and high-precision cutting of the stones into watch dial plates. The price for such an exclusive dial plate may easily exceed 10,000 Swiss Francs.

Dr Thomas Hainschwang (GGTL Laboratories, Balzers, Liechtenstein) discussed the challenges and possibilities of sorting synthetic from natural diamonds in parcels of melee using his DFI fluorescence microscopy and spectroscopy system. He explained how synthetic and natural diamonds can be distinguished by photoluminescence and other spectroscopic characteristics, and sometimes also by metallic inclusions and fluorescent growth patterns (i.e. cubic or cuboctahedral sectors being typical for HPHT-grown synthetics).

Figure 5: Dr Walter Balmer demonstrates the heat treatment of zircon using a charcoal furnace during a barbecue at the SGS conference. Photo by M. Hügi.

Edward Johnson, (GIA, London) gave an overview of GIA's international activities and services, focusing on their mission and current infrastructure, with over 3,000 employees worldwide.

Dr Walter Balmer (Chulalongkorn University, Bangkok, Thailand) and **Sebastian Hänsel** (Swiss Gemmological Institute SSEF) gave a detailed report on a field excursion by a group of SGS members to Mogok, Myanmar, in early 2015. With a video and many photos they illustrated how gems are mined in Mogok; the audience was especially impressed by their accounts of underground mining for ruby in karstic marble host rock. In addition, Dr Balmer gave a practical demonstration of the heat treatment of zircon during an evening barbecue social event. Using a charcoal furnace similar to those seen in mining areas in Southeast Asia (Figure 5), he successfully changed the colour of brown Cambodian zircon to an attractive blue by heating the rough material in a reducing atmosphere at approximately 1,000°C for about one hour.

Antoinette Starkey (Exclusive Personal Jewellery & Gemstones, Geneva, Switzerland) gave an overview on the market situation for ruby, sapphire, emerald, spinel and other coloured stones. For more than a year there has been a substantial slowdown in the demand for luxury goods (including gemstones), due to economic and political factors in China, Russia and

the Middle East. The resulting effects on the pricing of gemstones are very different depending on the quality and origin of the material. For example, prices for heat-treated sapphire from Sri Lanka or Madagascar have remained stable or have declined slightly, while those of top-quality unheated Burmese rubies and sapphires have skyrocketed in recent years due to their extreme scarcity.

Dr Claudio Milisenda (German Foundation for Gemstone Research, Idar-Oberstein) gave a detailed report on his visits to ruby, emerald and amethyst mines operated by Gemfields in East Africa. He explained the geology of the deposits, as well as how the gems are mined and quality-sorted prior to being offered at Gemfields' auctions (in the case of ruby and emerald). The Montepuez ruby mine in northern Mozambique was discovered in 2009 and is probably the most consistent-producing source of ruby today.

Dumortierite is typically known to the gemmologist as a blue ornamental stone, often forming fine-grained intergrowths with quartz. **Author MH** presented other aspects of this boron silicate, for example its occurrence as nano-sized fibres responsible for the colour of rose quartz. Also, at the Vaca Morta quarry in Brazil's Bahia State, attractive blue dumortierite quartzite (sold as Azul Macaubas) is cut into large slabs for architectural applications and interior design. Near this quarry, a relatively new discovery has yielded specimens of rock crystal with inclusions of dumortierite providing a beautiful micro-world of transparent, idiomorphic blue crystals.

Willy Bieri (GRS Gemresearch Swisslab AG, Lucerne) presented the current status of emerald mining in Colombia, such as at the famous Muzo mine and the nearby Cunas mine, as well in Chivor. His presentation also showed possibilities for the use of new technologies in field exploration, including aerial surveys of the mining area made with a drone.

In his first talk, **author MK** discussed new non-destructive methods for pearl analysis: X-ray phase contrast and X-ray scattering (dark field) imaging, and neutron radiography and tomography. These techniques are complementary to traditional X-radiography and tomography, and provide new and additional insights into the inner structure of pearls. His second talk provided an annual update of news from the SSEF laboratory, ranging from challenging analytical problems to exceptional or amusing items that the lab has encountered. These specimens included the 'Sleeping Lion pearl', a fake 'Imperial Chinese pearl necklace', exceptional rubies from Mozambique (i.e. the Rhino ruby and a matched pair called Eyes of the Dragon), and a 16 ct musgravite and 10 ct taaffeite.

René Lauper (Frieden AG Creative Design, Thun, Switzerland) provided his annual report on the cultured pearl market. The pearl industry still has not recovered from the challenges of the recent years, particularly because of China's economic difficulties. Nevertheless, today's market offers a much broader variety of qualities and prices of cultured pearls than ever before. Whereas the prices of commercial qualities of cultured pearls have remained stable or weakened in certain ranges, prices for the top qualities are expected to rise due to relatively strong demand, especially for Akoya and high-end round freshwater cultured pearls.

Klemens Link (Gübelin Gem Lab, Lucerne) presented 10 years' experience with the gemmological application of LA-ICP-MS at his laboratory. The main advantages of this sophisticated method of chemical analysis are the large range of elements that can be measured and the low detection limit for trace-element concentrations. The data are particularly useful for origin determination of coloured stones, and in some cases it is even possible to determine the age of surface-reaching zircon inclusions by measuring the isotope ratios of uranium and lead.

Dr Laurent Cartier (Swiss Gemmological Institute SSEF) reviewed the use of corals in the gem trade. He described the species that are economically important and how they are incorporated into jewellery. With photos from a recent visit to Taiwan, he showed the importance of coral as a gem material in the Far East and in many other cultures since antiquity. He also addressed the significance and application of the Convention on International Trading in Endangered Species (CITES) regulations when trading coral internationally.

Karl Vogler (Gemtrade AG, Hergiswil, Switzerland) gave a short overview about the diamond market. The diamond trade is currently going through a difficult period due to political and economic factors in major producing and consuming countries.

Helen Molesworth (Gübelin Academy, Lucerne) reviewed the historical significance and iconography of gems. She traced mankind's knowledge about coloured stones throughout history, the sources of this knowledge and the psychology of adornment. Gems from ancient burials and hoards were discussed, ranging from ancient Egypt to Britain in the 17th century, and she also examined more modern glamorous and royal collections to illustrate the value and status of wearing jewels.

Michael Hügi (michael.huegi@gemmologie.ch)
Swiss Gemmological Society, Bern, Switzerland

Dr Michael S. Krzemnicki
Swiss Gemmological Institute SSEF
Basel, Switzerland

Gem-A Notices

GIFTS TO THE ASSOCIATION

The Association is most grateful to the following for their gifts for research and teaching purposes:

Brian Cook, Tucson, Arizona, USA, for 17 rough untreated Paraíba tourmalines from the Batalha mine, São José da Batalha, Paraíba, Brazil; and 22 garnets consisting of spessartine from the Alto Mirador mine, Rio Grande do Norte, Brazil, and chrome pyrope from the Navajo reservation, Arizona.

John Garsow, Murrieta, California, USA, for two parcels of rough amethyst from Rwanda.

Mohamed Fahmy Mohamed Hilmy, Harrow, Middlesex, for a rough and a faceted sample of ruby from Greenland.

E. Alan Jobbins FGA, Caterham, Surrey, for over 4,000 slides depicting gemstones, photomicrography and gemmological trips, and copies of *The Mirror of Stones* by Camillus Leonardus, published in 1750, and *Glossary of Geology* (2011).

A. D. Moth, High Wycombe, Buckinghamshire, for an impregnated red and white coral cabochon.

Mark Olm, Tucson, Arizona, USA, for two samples of rough amber weighing 70.11 g in total.

Patricia Stoecklein FGA, Trafalgar, Indiana, USA, for danburite crystals from San Luis Potosí, Mexico.

Jason Williams FGA DGA, G. F. Williams & Co., London, for three carved garnets and five cubic zirconia briolettes.

MEMBERSHIP

The Council of the Association have elected the following to membership:

Associate Membership

Achikalova, Anna, *Kowloon, Hong Kong*
Hann, Janet, *Dubai, UAE*
Hughes, Billie, *Bangkok, Thailand*
Lee, Vanessa Hena, *London*
Luca, Alexander, *Göttingen, Germany*
Ozdil, Ozlem, *Enfield, Middlesex*
Poulson, Majken, *Nuuk, Greenland*
Segura, Olivier, *Paris, France*
Van Maris Dijk, Michele, *Oxshott, Surrey*

GENERAL MEETINGS

The Annual General Meeting of the Gemmological Association of Great Britain will be held on Friday 9 September 2016. The venue is to be announced.

A report of the Extraordinary General Meeting scheduled for 30 June 2016 will be published in the next issue of *The Journal*.

OBITUARIES

It is with great sadness that we announce the death of **Michael J. O'Donoghue FGA,** Sevenoaks, Kent. Michael died on 16 June 2016 and a full tribute will be published in the next issue of *The Journal*.

June Ive FGA, Waltham Abbey, Essex, died on 5 June 2016. June qualified for her Gemmology Diploma in 1966 and has been a Fellow of the Association ever since.

Learning Opportunities

CONFERENCES AND SEMINARS

2nd Eugene E. Foord Symposium on Pegmatites
15–19 July 2016
Golden, Colorado, USA
www.colorado.edu/symposium/pegmatite

Northwest Jewelry Conference
12–14 August 2016
Seattle, Washington, USA
www.northwestjewelryconference.com

46th ACE IT Annual Mid-Year Education Conference
13–16 August 2016
Newport Beach, California, USA
www.najaappraisers.com/html/conferences.html

Dallas Mineral Collecting Symposium
19–21 August 2016
Dallas, Texas, USA
www.dallassymposium.org

35th International Geological Congress
27 August–4 September 2016
Cape Town, South Africa
www.35igc.org
Sessions of Interest: Gems: Bringing the World Together; The Dynamic Earth and Its Kimberlite, Cratonic Mantle and Diamond Record Through Time; Diamonds and Crustal Recycling into Deep Mantle

International Conference on Diamond and Carbon Materials
4–8 September 2016
Le Corum, Montpellier, France
www.diamond-conference.elsevier.com

ASA 2016 International Appraisers Conference
11–14 September 2016
Boca Raton, Florida, USA
www.appraisers.org/Education/conferences/asa-conference
Session of interest: Gems & Jewelry

2nd European Mineralogical Conference (emc2016)
11–15 September 2016
Rimini, Italy
http://emc2016.socminpet.it
Sessions of Interest: Gem Materials; Inclusions in Minerals as a Record of Geological Processes; New Analysis Methods and Application

Compiled by Georgina Brown and Brendan Laurs

49th Annual Denver Gem & Mineral Show
16–18 September 2016
Denver, Colorado, USA
www.denvermineralshow.com
Note: Includes a seminar programme.

IRV Loughborough Conference
17–19 September 2016
Loughborough
www.jewelleryvaluers.org/Loughborough-Conference

Geological Society of America Annual Meeting & Exposition
25–28 September 2016
Denver, Colorado, USA
http://community.geosociety.org/gsa2016/home
Session of interest: Gemological Research in the 21st Century: Characterization, Exploration, and Geological Significance of Diamonds and other Gem Minerals

42nd Pacific Northwest Chapter Friends of Mineralogy Symposium
14–16 October 2016
Longview, Washington, USA
www.friendsofmineralogy.org/symposia.html

CIBJO Congress 2016
26–28 October 2016
Yerevan, Armenia
www.cibjo.org/congress2016

The Munich Show
28–30 October 2016
Munich, Germany
www.mineralientage.de
Note: Includes a seminar programme.

MJSA ConFab
30 October 2016
Fashion Institute of Technology, New York, New York, USA
www.mjsa.org/eventsprograms/mjsa_confab

The Wonder of Fabergé: A Study of the McFerrin Collection
3–4 November 2016
Houston Museum of Natural Science, Texas, USA
www.hmns.org/education/adults/faberge-symposium

Gem-A Conference
5–8 November 2016
London, UK
www.gem-a.com/news--events/gem-a-conference-2016.aspx

37th Annual New Mexico Mineral Symposium
12–13 November 2016
Socorro, New Mexico, USA
https://geoinfo.nmt.edu/museum/minsymp/home.cfml

Gem and Jewelry Institute of Thailand Conference (GIT 2016)
14–15 November 2016
Pattaya, Thailand
www.git.or.th/2014/index_en.html

3rd European Congress on Jewellery: The Jewel in Art and Art in Jewel
17–18 November 2016
Barcelona, Spain
www.museunacional.cat/en/jewel-art-and-art-jewellery

AGA Tucson Conference
1 February 2017
Tucson, Arizona, USA
http://accreditedgemologists.org

Amberif International Fair of Amber, Jewellery and Gemstones
22–25 March 2017
Gdańsk, Poland
www.amberif.amberexpo.pl/title,Jezyk,lang,2.html
Note: Includes a seminar programme.

14th Annual Sinkankas Symposium (Sapphire)
8 April 2017
Carlsbad, California, USA
www.sinkankassymposium.net

11th International Conference on New Diamond and Nano Carbons
28 May–2 June 2017
Cairns, Queensland, Australia
http://ndnc2017.org

Swiss Gemmological Society Conference
8–11 June 2017
Zermatt, Switzerland
www.gemmologie.ch

11th International Kimberlite Conference
18–22 September 2017
Gaborone, Botswana
www.11ikc.com
Note: Pre- and post-conference field trips will visit diamond deposits in Botswana and neighbouring countries.

EXHIBITS

Asia

Van Cleef & Arpels, the Art and Science of Gems
Until 14 August 2016
ArtScience Museum, Marina Bay Sands, Singapore
www.marinabaysands.com/museum/van-cleef-and-arpels.html

Europe

Charlotte De Syllas
Until 22 July 2016
Goldsmiths' Hall, London
www.thegoldsmiths.co.uk/company/today/events/2016/charlotte-de-syllas-exhibition

Une Education Sentimentale
Until 24 September 2016
Le Musée Ephémère of Chaumet, Paris, France
www.chaumet.com/news/the-musee-ephemere-of-chaumet-presents-une-education-sentimentale

Celts
Until 25 September 2016
National Museum of Scotland, Edinburgh
www.nms.ac.uk/national-museum-of-scotland/whats-on/celts

Fabergé—The Tsar's Jeweller and the Connections to the Danish Royal Family
Until 25 September 2016
Museet på Koldinghus, Kolding, Denmark
www.koldinghus.dk/uk/exhibitions/exhibitions-2016/faberge.html

Heavenly Bodies—The Sun, Moon and Stars in Jewellery
Until 30 October 2016
Schmuckmuseum, Pforzheim, Germany
www.schmuckmuseum.de/flash/SMP_en.html

Elements: From Actinium to Zirconium
Until 26 February 2017
Ulster Museum, Belfast, Northern Ireland
http://nmni.com/um/What-s-on/Elements

Smycken: Jewellery. From Decorative to Practical
Ongoing
Nordiska Museet, Stockholm, Sweden
www.nordiskamuseet.se/en/utstallningar/jewellery

North America

Tourmaline Treasures
Until 1 September 2016
Houston Museum of Natural Science, Texas, USA
www.hmns.org/exhibits/special-exhibitions/tourmaline-treasures

Thunderbirds: Jewelry of the Santo Domingo Pueblo
Until 5 September 2016
Abby Aldrich Rockefeller Folk Art Museum, Williamsburg, Virginia, USA
http://tinyurl.com/zgyd54k

Fabergé from the Matilda Geddings Gray Foundation Collection
Until 27 November 2016
The Metropolitan Museum of Art, New York, New York, USA
www.metmuseum.org/exhibitions/listings/2011/faberge

Glitterati: Portraits & Jewelry from Colonial Latin America
Until 27 November 2016
Denver Art Museum, Denver, Colorado, USA
www.denverartmuseum.org/exhibitions/glitterati

Jewelry, from Pearls to Platinum to Plastic
Until 1 January 2017
Newark Museum, Newark, New Jersey, USA
www.newarkmuseum.org/jewelry

Arts of Islamic Lands: Selections from The al-Sabah Collection, Kuwait
Until 29 January 2017
Museum of Fine Arts, Houston, Texas, USA
www.mfah.org/exhibitions/arts-islamic-lands-selections-al-sabah-collection-/

American Mineral Heritage: Harvard Collection
Until February 2017
Flandrau Science Center & Planetarium, Tucson, Arizona, USA
http://flandrau.org/exhibits/harvard

Gold and the Gods: Jewels of Ancient Nubia
Until 8 January 2017
Museum of Fine Arts, Boston, Massachusetts, USA
www.mfa.org/exhibitions/gold-and-gods

Amber Secrets: Feathers from the Age of Dinosaurs
Ongoing
Houston Museum of Natural Science, Texas, USA
www.hmns.org/exhibits/special-exhibitions/amber-secrets-feathers-from-the-age-of-dinosaurs

City of Silver and Gold: From Tiffany to Cartier
Ongoing
Newark Museum, New Jersey, USA
www.newarkmuseum.org/SilverAndGold.html

Fabergé: From a Snowflake to an Iceberg
Ongoing
Houston Museum of Natural Science, Texas, USA
www.hmns.org/exhibits/special-exhibitions/faberge-a-brilliant-vision

Gemstone Carvings
Ongoing
Houston Museum of Natural Science, Texas, USA
www.hmns.org/exhibits/special-exhibitions/gemstone-carvings

Gilded New York
Ongoing
Museum of the City of New York, New York, USA
www.mcny.org/content/gilded-new-york

Mightier than the Sword: The Allure, Beauty and Enduring Power of Beads
Ongoing
Yale Peabody Museum of Natural History, Yale University, New Haven, Connecticut, USA
http://peabody.yale.edu/exhibits/mightier-sword-allure-beauty-and-enduring-power-beads

OTHER EDUCATIONAL OPPORTUNITIES

Gem-A Workshops and Courses
Gem-A, London
www.gem-a.com/education/course-prices-and-dates.aspx

Gemstone Safari to Tanzania
11–28 July 2016
Morogoro, Umba, Arusha, Longido, Merelani and Lake Manyara, Tanzania
www.free-form.ch/tanzania/gemstonesafari.html

American Society of Appraisers and Shanghai BETTER Institute of Gemology's Advanced Gemological Appraisal Course
19–30 September 2016
Shanghai, China
http://tinyurl.com/j5dh4lk

Lectures with The Society of Jewellery Historians
Society of Antiquaries of London, Burlington House, London
www.societyofjewelleryhistorians.ac.uk/current_lectures

27 September 2016
Galina Korneva—The Grand Duchess Maria Pavlovna's Contacts with Paris Jewellers and Her Collection of Treasures

25 October
Robert Baines—Bogus or Real: Jewellery and the Capture of Human Drama

22 November
Kieran McCarthy—Fabergé and London

New Media

Rough Diamonds, a Practical Guide

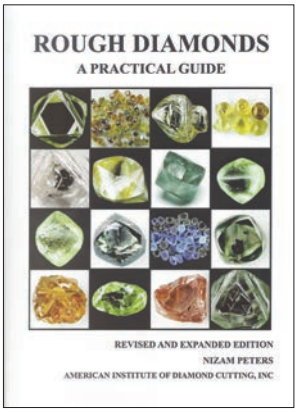

By Nizam Peters, 2016. American Institute of Diamond Cutting, Deerfield Beach, Florida, USA, 274 pages, ISBN 978-0966585490, http://diamondschool.com/books. US$165.00 hardcover.

This book is a revised and expanded edition of the previous version published in 1998. My first impression was that the book is for those who know little about diamonds and want to get involved in rough diamond trading and/or cutting. This assumption was validated by the final sentence in the introduction: "The author's intention is to keep this work free from cumbersome technical language and present an educational format that will be easily understood by anyone."

Chapter 1 is titled 'Overview of the Rough Diamond Market', but it actually deals with a variety of subjects like mining, deposit types, prospecting, recovery, classification and production. These are all valid topics, but they are somewhat incoherent and misplaced in this section.

Chapter 2 covers 'Rough Diamond Structure, Shape and Orientation'. Noticeably absent in this chapter is any mention or illustration of the atomic structure of diamond and its crystallography. The images of the various crystal shapes are, on the other hand, of high photographic quality, and are varied enough to allow the reader to get a good idea of what rough diamonds look like. The captions 'Elongated Irregular' and 'Irregular Diamond' for elongated dodecahedra are, however, vague at best. The images of twinned crystals and macles are comprehensive. The portion on 'orienting the rough for weight retention and yield' seems out of place, as it forms part of cutting and polishing (covered in Chapter 7).

Chapter 3 comprehensively reviews the surface features of diamonds. This reviewer noted one surface feature is missing: the flattened or inverted cube faces seen on some diamonds.

Chapter 4 deals with the internal characteristics of diamonds. The images are of high quality and informative, although colour photomicrographs of mineral inclusions would have added more depth to the chapter. The author also digresses by including content on twinned and multiply twinned crystals that should have appeared in Chapter 2. The portion on 'stress and strain' lacks any reference to the detection of stress using a polariscope, which is vital in the planning and marking process.

The title of Chapter 5, 'Fundamentals of Rough Diamond Proportions', is misleading since it only covers polished diamonds and not rough material. The chapter is, however, informative for those who want to learn about polished diamonds.

Chapter 6 includes some very interesting high-quality images showing diamond colour, colour zoning and colour saturation.

The content of Chapter 7 on 'Manufacturing Rough Diamonds' is somewhat dated, but still relevant. Technology changes constantly and staying up to date is a challenge to any author. This reviewer found it interesting to read about the author's concept of a 'Master Diamond Cutter', which was described but not defined. There is no academy where a person can get a master's degree in diamond cutting. The title 'Master Diamond Cutter' is indeed earned and reflects the title holder's ability to purchase, plan, cut and polish as well as grade the finished diamond to the highest standards.

Chapter 8, 'Introduction on Valuing Rough Diamonds', deals with the ability of a buyer to determine an appropriate dollar value by measuring and determining the projected colour, clarity, size and shape of the finished diamond(s).

Chapter 9 provides an introduction to alluvial diamond mining with some relevant images. It also covers the Kimberley Process scheme that is designed to monitor the movement of rough diamonds between countries.

Chapter 10 is a bonus chapter that provides many high-quality images of rough and polished diamonds

The author succeeds in using language that is easily understandable, particularly to those who have done or are familiar with diamond cutting. Despite the need for an editor, there is some good content in the book for persons who want to 'wet their toes' by getting an understanding of rough diamonds, mining and recovery, and cutting and polishing as well as the diamond industry in general.

Mike Botha
Embee Diamonds, Prince Albert, Saskatchewan, Canada

OTHER BOOK TITLES

Coloured Stones

Canteras—Mexican Opals in Matrix
By Jack Hobart, 2015. Self-published, 88 pages, ISBN 978-1944564001. US$25 softcover.

Collector's Guide to the Amphibole Group
By Robert Lauf, 2015. Schiffer Publishing Ltd., Atglen, Pennsylvania, USA, 96 pages, ISBN 978-0764348709. US$19.99 softcover.

***Colored Gemstones: The Antoinette Matlins Buying Guide—How to Select, Buy, Care for & Enjoy Sapphires, Emeralds, Rubies and Other Colored Gems with Confidence and Knowledge*, 4th edn.**
By Antoinette Matlins, 2016. Gemstone Press, Woodstock, Vermont, USA, 256 pages, ISBN 978-0990415275. US$18.99 softcover.

Diamond

Brilliance and Fire: A Biography of Diamonds
By Rachelle Bergstein, 2016. Harper Collins, New York, New York, USA, 400 pages, ISBN 978-0062323774. US$29.99 hardcover.

***Diamonds: The Antoinette Matlins Buying Guide—How to Select, Buy, Care for & Enjoy Diamonds with Confidence and Knowledge*, 4th edn.**
By Antoinette Matlins, 2016. Gemstone Press, Woodstock, Vermont, USA, 228 pages, ISBN 978-0990415268. US$19.99 softcover.

Gem Localities

***Northeast Treasure Hunter's Gem and Mineral Guide: Where and How to Dig, Pan and Mine Your Own Gems and Minerals*, 6th edn.**
By Kathy J. Rygle and Stephen F. Pederson, 2016. Gemstone Press, Woodstock, Vermont, USA, 240 pages, ISBN 978-0997014501. US$16.99 softcover.

***Northwest Treasure Hunter's Gem and Mineral Guide: Where and How to Dig, Pan and Mine Your Own Gems and Minerals*, 6th edn.**
By Kathy J. Rygle and Stephen F. Pederson, 2016. Gemstone Press, Woodstock, Vermont, USA, 208 pages, ISBN 978-0990415282. US$16.99 softcover.

***Southeast Treasure Hunter's Gem and Mineral Guide: Where and How to Dig, Pan and Mine Your Own Gems and Minerals*, 6th edn.**
By Kathy J. Rygle and Stephen F. Pederson, 2016. Gemstone Press, Woodstock, Vermont, USA, 214 pages, ISBN 978-0997014518. US$16.99 softcover.

***Southwest Treasure Hunter's Gem and Mineral Guide: Where and How to Dig, Pan and Mine Your Own Gems and Minerals*, 6th edn.**
By Kathy J. Rygle and Stephen F. Pederson, 2016. Gemstone Press, Woodstock, Vermont, USA, 224 pages, ISBN 978-0990415299. US$16.99 softcover.

General Reference

Gem Hunter
By George Frangoulis, 2015. Self-published using www.lulu.com, 60 pages, ISBN 978-1329075634. US$35.00 softcover.

Gemstones: Species & Varieties
By Charleen Kiefer, 2015. Self-published using www.lulu.com, 454 pages, ISBN 978-1312943803. US$39.99 softcover.

Instrumentation

Infrared Spectroscopy of Minerals and Related Compounds
By Nikita V. Chukanov and Alexandr D. Chervonnyi, 2016. Springer, New York, New York, USA, 1,120 pages, ISBN 978-3319253473. US$329.00 hardcover or $259.00 eBook.

Jewellery and *Objets d'Art*

Glitterati: Portraits and Jewelry from Colonial Latin America
By Donna Pierce and Julie Wilson Frick, 2016. Denver Art Museum, Denver, Colorado, 96 pages, ISBN 978-0914738756. US$14.95 softcover.

Jewelry International: Volume 6
By Caroline Childers and Tourbillon International, 2016. Rizzoli International Publications, New York, New York, USA, 576 pages, ISBN 978-0847848423. US$50.00 hardcover.

The Other Mountain: Contemporary Jewellery from China
By Norman Cherry, 2016. National Centre for Craft and Design, Sleaford, Lincolnshire, 96 pages, ISBN 978-1526200600. £10.00 softcover.

René Lalique: The Forgotten Years
By Bernard Williams, 2016. Self-published using CreateSpace Independent Publishing Platform, 132 pages, ISBN 978-1523372003. £22.00 softcover.

Compiled by Georgina Brown and Brendan Laurs

Literature of Interest

Coloured Stones

Back to black [Whitby jet]. S. Steele, *Gems& Jewellery*, **25**(3), 2016, 16–20.

A bicolour feldspar. A. Hodgkinson, *Gems& Jewellery*, **25**(3), 2016, 14–15.

La calcédoine bleue d'Ambilobe: Une introduction aux colorations par diffusion [The blue chalcedony of Ambilobe: An introduction to diffusion colorations]. D. Peyresaubes, J. Raoul, O. Beyssac, I. Estève, M. Schoor and J.-C. Boulliard, *Revue de Gemmologie A.F.G.,* **195**, 2016, 15–20.

Characteristics of inclusions in topaz from Serrinha pegmatite (Medina granite, Minas Gerais State, SE Brazil) studied by Raman spectroscopy. M. Dumańska-Słowik, T. Toboła, L. Natkaniec-Nowak and A.C. Pedrosa-Soares, *Vibrational Spectroscopy*, **85**, 2016, 196–201, http://dx.doi.org/10.1016/j.vibspec.2016.04.019.

Chrysoberyl recovered with sapphires in the New England placer deposits, New South Wales, Australia. K. Schmetzer, F. Caucia, H.A. Gilg and T.S. Coldham, *Gems & Gemology*, **52**(1), 2016, 18–36, http://dx.doi.org/10.5741/GEMS.52.1.18.*

Colour analysis of turquoise using uniform chromaticity coordinate. Z. Dai, X. Lyu, X. Gu and D. Chen, *Journal of Gems & Gemmology*, **18**(2), 2016, 9–14 (in Chinese with English abstract).

Coloration of yellow and red colored quartzite jade. Y. Zhang, R. Wei, J. Ke, H. Chen and T. Lu, *Acta Petrologica et Mineralogica*, **35**(1), 2016, 139–146 (in Chinese with English abstract).

Corundum (sapphire) and zircon relationships, Lava Plains gem fields, NE Australia: Integrated mineralogy, geochemistry, age determination, genesis and geographical typing. F.L. Sutherland, R.R. Coenraads, A. Abduriyim, S. Meffre, P.W.O. Hoskin, G. Giuliani, R. Beattie, R. Wuhrer and G.B. Sutherland, *Mineralogical Magazine*, **79**(3), 2015, 545–581, http://dx.doi.org/10.1180/minmag.2015.079.3.04.

Emerald deposits around the world, their similarities and differences. G. Giuliani, Y. Branquet, A.E. Fallick, L.A. Groat and D. Marshall, *InColor*, special issue from the 1st World Emerald Symposium, December 2016, 56–69.

Ethiopian opals: Facts, fears and fairytales. J. Bergman with B. Wheat, *Australian Gemmologist*, **25**(11–12), 2016, 393–402.

Fe^{2+} and Fe^{3+} oxidation states on natural sapphires probed by X-ray absorption spectroscopy. N. Monarumit, W. Wongkokua and S. Satitkune, *Procedia Computer Science*, **86**, 2016, 180–183, http://dx.doi.org/10.1016/j.procs.2016.05.053.*

Gem-quality morganite from Monte Capanne pluton (Elba Island, Italy). F. Caucia, L. Marinoni, A.M. Callegari, A. Leone and M. Scacchetti, *Neues Jahrbuch für Mineralogie - Abhandlungen: Journal of Mineralogy and Geochemistry*, **193**(1), 2016, 69–78, http://dx.doi.org/10.1127/njma/2015/0293.

Gem-quality serpentine from Val Malenco, central Alps, Italy. I. Adamo, V. Diella, R. Bocchio, C. Rinaudo and N. Marinoni, *Gems & Gemology*, **52**(1), 2016, 38–49, http://dx.doi.org/10.5741/GEMS.52.1.38.*

Gemmological characteristic of Nanhong agate and formation of red stripe. L. Zhu, M. Yang, J. Tang and X. Yang, *Journal of Gems & Gemmology*, **17**(6), 2015, 31–38 (in Chinese with English abstract).

The geographic origin determination of emeralds. D. Schwarz, *InColor*, special issue from the 1st World Emerald Symposium, December 2016, 98–105.

Identification of amber and its imitation. M. Ouyang, S. Yue and K. Gao, *Journal of Gems & Gemmology*, **18**(1), 2016, 24–34 (in Chinese with English abstract).

Identification of nephrite gravel with organic imitated skin. C. Tang, Z. Zhou, Z. Liao and Q. Zhong, *Journal of Gems & Gemmology*, **17**(6), 2015, 1–7 (in Chinese with English abstract).

Identification of turquoise and treated turquoise. W. Ou, S. Yue and K. Gao, *Journal of Gems & Gemmology*, **18**(1), 2016, 6–14 (in Chinese with English abstract).

The influence of Vietnam and Sri Lanka spinel mineral chemical elements on colour. A. Kleišmantas and A. Daukšytė, *Chemija*, **27**(1), 2016, 45–51, www.lmaleidykla.lt/publ/0235-7216/2016/1/45–51.pdf.*

Luminescence behavior and Raman characterization of rhodonite from Turkey. N. Can, J.J. Garcia Guinea, R. Kibar and A Cetin, *Spectroscopy Letters*, **44**(7-8), 2011,566–569, http://dx.doi.org/10.1080/00387010.2011.610656.

* Article freely available for download, as of press time

Mineralogy and petrology of gneiss hosted corundum deposits from the Day Nui Con Voi metamorphic range, Ailao Shan–Red River shear zone (north Vietnam). N.N. Khoi, C.A. Hauzenberger, D.A. Tuan, T. Häger, N.V. Nam and N.T. Duong, *Neues Jahrbuch für Mineralogie - Abhandlungen: Journal of Mineralogy and Geochemistry*, **193**(2), 2016, 161–181, http://dx.doi.org/10.1127/njma/2016/0300.

Moldavite, a gemmological relevant natural glass. G. Pearson, *Australian Gemmologist*, **25**(11–12), 2016, 403–409.

Reading pegmatites—Part 2: What tourmaline says. D. London, *Rocks & Minerals*, **91**(2), 2016, 132–149, http://dx.doi.org/10.1080/00357529.2016.1113464.

Preseli bluestone. S. Steele, *Gems&Jewellery*, **25**(2), 2016, 25–27.

Spectroscopic and microstructural studies of ruby gemstones of Sinapalli, Odisha. J.K. Sinha and P.K. Mishra, *Journal of the Geological Society of India*, **86**(6), 2015, 657–662, http://dx.doi.org/10.1007/s12594-015-0357-6.

Standards and protocols for emerald analysis in gem testing laboratories. T. Hainschwang and F. Notari, *InColor*, special issue from the 1st World Emerald Symposium, December 2016, 106–114.

Study on the relationship between the relative content of moganite and the crystallinity of quartzite jade by Raman scattering spectroscopy, infrared absorption spectroscopy and X-ray diffraction techniques. D. Zhou, H. Chen, T. Lu, J. Ke and M. He, *Rock and Mineral Analysis*, **34**(6), 2015, 652–658 (in Chinese with English abstract).

Trapiche: The rising star. J. Bergman, *InColor*, **31**, 2016, 32–44.

'Trapiche' vs 'trapiche-like' textures in minerals. G. Giuliani and I. Pignatelli, *InColor*, **31**, 2016, 45–46.

An unusual occurrence of iron sulphide and baryte in Coober Pedy opal. B.A. Grguric, A. Pring and J. Zhao, *Australian Gemmologist*, **25**(11–12), 2016, 410–411.

Value factors, design, and cut quality of colored gemstones (non-diamond) [Part 5: Craftsmanship and Summary]. A. Gilbertson, *GemGuide*, **35**(3), 2016, 2–9.

Variscite from central Tajikistan: Preliminary results. A.K. Litvinenko, E.S. Sorokina, S. Karampelas, N.N. Krivoschekov and R. Serov, *Gems & Gemology*, **52**(1), 2016, 60–65, http://dx.doi.org/10.5741/GEMS.52.1.60.*

Diamonds

Blue, reds and primrose: A diamond and a dancer [Mouawad-Tereschenko blue diamond]. J. Ogden, *Gems&Jewellery*, **25**(2), 2016, 32–33.

Diamond detectives. M. Rapaport, *Rapaport Magazine*, **39**(4), 2016, 50–53.

Diamond formation through metastable liquid carbon. T.G. Shumilova, S.I. Isaenko and S.N. Tkachev, *Diamond and Related Materials*, **62**, 2016, 42–48, http://dx.doi.org/10.1016/j.diamond.2015.12.015.

Eclogitic diamonds from variable crustal protoliths in the northeastern Siberian craton: Trace elements and coupled $\delta^{13}C$–$\delta^{18}O$ signatures in diamonds and garnet inclusions. D. Zedgenizov, D. Rubatto, V. Shatsky, A. Ragozin and V. Kalinina, *Chemical Geology*, **422**, 2016, 46–59, http://dx.doi.org/10.1016/j.chemgeo.2015.12.018.

An introduction to photoluminescence spectroscopy for diamond and its applications in gemology. S. Eaton-Magaña and C.M. Breeding, *Gems & Gemology*, **52**(1), 2016, 2–17, http://dx.doi.org/10.5741/GEMS.52.1.2.*

Low temperature spectroscopy of single colour centres in diamond—The silicon-vacancy centre in diamond. K.D. Jahnke, PhD dissertation, Ulm University, Ulm, Germany, 2015, 141 pages, https://oparu.uni-ulm.de/xmlui/handle/123456789/3356.*

Multiple carbon and nitrogen sources associated with the parental mantle fluids of fibrous diamonds from Diavik, Canada, revealed by SIMS microanalysis. D.C. Petts, T. Stachel, R.A. Stern, L. Hunt and G. Fomradas, *Contributions to Mineralogy and Petrology*, **171**(2), 2016, 17 pages, http://dx.doi.org/10.1007/s00410-016-1231-2.

Nitrogen isotope systematics and origins of mixed-habit diamonds. D. Howell, R.A. Stern, W.L. Griffin, R. Southworth, S. Mikhail, T. Stachel, *Geochimica et Cosmochimica Acta*, **157**, 2015, 1–12, http://dx.doi.org/10.1016/j.gca.2015.01.033.

Plastic deformation in natural diamonds: Rose channels associated to mechanical twinning. M. Schoor, J.C. Boulliard, E. Gaillou, O. Hardouin Duparc, I. Estève, B. Baptiste, B. Rondeau and E. Fritsch, *Diamond and Related Materials*, **66**, 2016, 102–106, http://dx.doi.org/10.1016/j.diamond.2016.04.004.

Red luminescence decay kinetics in Brazilian diamonds. F.A. Stepanov, V.P. Mironov, A.L. Rakevich, V.S. Shatsky, D.A. Zedgenizov and E.F. Martynovich, *Bulletin of the Russian Academy of Sciences: Physics*, **80**(1), 2016, 74–77, http://dx.doi.org/10.3103/s1062873816010238.

Temperature effects on radiation stains in natural diamonds. S.C. Eaton-Magaña and K.S. Moe, *Diamond and Related Materials*, **64**, 2016, 130–142, http://dx.doi.org/10.1016/j.diamond.2016.02.009.

X-ray topographic study of a diamond from Udachnaya: Implications for the genetic nature of inclusions. G. Agrosì, F. Nestola, G. Tempesta, M. Bruno, E. Scandale and J. Harris, *Lithos*, **248–251**, 2016, 153–159, http://dx.doi.org/10.1016/j.lithos.2016.01.028.

Gem Localities

Delineation of potential sites for gemstone mining in Kuru Ganga catchment, Ratnapura: A GIS approach. R.G.C. Jaliya, A.H.T.T.B. Thotahewa, C.R. Palihakkara, P.R.R. Siriwardena, H.M.R. Pre-masiri, S.P. Chaminda, P.G.R. Dharmaratne and I.P. Senanayake, *ERE Research Conference 2015 on Earth Resources Management*, 2015, 46–51.

Distribution and chronological framework for Iberian variscite mining and consumption at Pico Centeno, Encinasola, Spain. C.P. Odriozola, R.V. García, C.I. Burbidge, R. Boaventura, A.C. Sousa, O. Rodríguez-Ariza, R. Parrilla-Giraldeza, M.I. Prudêncioc and M.I. Dias, *Quaternary Research*, **85**(1), 2016, http://dx.doi.org/10.1016/j.yqres.2015.11.010.

The emerald mines of the Panjshir Valley, Afghanistan. G. Bowersox, *InColor*, special issue from the 1st World Emerald Symposium, December 2016, 70–77.

Emeralds in Russia: The geology and gemology of the Malyshev mine. W.F. Boyd and M.S. Alferova, *InColor*, special issue from the 1st World Emerald Symposium, December 2016, 78–87.

European precious opal from Červenica-Dubník – An historical and gemmological summary. P. Semrád, *Australian Gemmologist*, **25**(11–12), 2016, 372–388.

Flying into the heart of the Colombian emerald-mining region. A. Peretti and W. Bieri, *InColor*, special issue from the 1st World Emerald Symposium, December 2016, 32–42.

In search of Colombia's green dreams. C. Unninayar, *InColor*, special issue from the 1st World Emerald Symposium, December 2016, 22–31.

Investigating the Montana sapphire deposits. J. Clanin and C. White, *InColor*, **31**, 2016, 21–25.

Progress on the study of parameters related to the origin of Colombian emeralds. C.J.C. Ochoa, M.J.H. Daza, D. Fortaleche and J.F. Jiménez, *InColor*, special issue from the 1st World Emerald Symposium, December 2016, 88–97.

Trace elements in corundum, chrysoberyl, and zircon: Application to mineral exploration and provenance study of the western Mamfe gem clastic deposits (SW Cameroon, Central Africa). N.S. Kanouo, E. Ekomane, R.F. Yongue, E. Njonfang, K. Zaw, C. Ma, T.R. Ghogomu, D.R. Lentz and A.S. Venkatesh, *Journal of African Earth Sciences*, **113**, 2016, 35–50, http://dx.doi.org/10.1016/j.jafrearsci.2015.09.023.

Instrumentation

The foundation of a color-chip evaluation system of jadeite-jade green with color difference control of medical device. G. Ying, W. Huan and D. Hongmei, *Multimedia Tools and Applications*, **75**(7), 2016, 1–12, http://dx.doi.org/10.1007/s11042-016-3291-8.

Provenance determination of sapphires and rubies using laser-induced breakdown spectroscopy and multivariate analysis. K.A. Kochelek, N.J. McMillan, C.E. McManus, and D.L. Daniel, *American Mineralogist*, **100**(8–9), 2015, 1921–1931, http://dx.doi.org/10.2138/am-2015-5185.

Miscellaneous

Assessment of mine ventilation systems and air pollution impacts on artisanal tanzanite miners at Merelani, Tanzania. L.P. Mayala, M.M. Veiga and M.B. Khorzoughi, *Journal of Cleaner Production*, **116**, 2016, 118–124, http://dx.doi.org/10.1016/j.jclepro.2016.01.002.

Early adoption dynamics of private sustainability governance initiatives: A case study of the marine cultured-pearl industry. J. Nash, Ph.D. thesis, University of Vermont, Burlington, Vermont, USA, 2015, 172 pages.

Education and the mine-to-market story. A. Lucas, *InColor*, special issue from the 1st World Emerald Symposium, December 2016, 44–48.

Gemstone 2016 price level trends. R.B. Drucker, *InColor*, **31**, 2016, 48–53.

The Kimberley Process Certification System - KPCS and diamond production changes in selected African countries and Brazil. E. Gomes dos Santos, *REM: Revista Escola de Minas*, **68**(3), 2015, 279–285, http://dx.doi.org/10.1590/0370-44672015680024.*

The magnificent mineral and gem collections of the Royal Ontario Museum in Toronto. S. Robinson, *Rocks & Minerals*, **91**(2), 2016, 154–163, http://dx.doi.org/10.1080/00357529.2016.1113467.

The one who controls the diamond wears the crown! The politicization of the Kimberley Process in Zimbabwe. N. Munier, *Resources Policy*, **47**, 2016, 171–177, http://dx.doi.org/10.1016/j.resourpol.2016.02.001.

Tanzanite processing in Tanzania: Challenges and opportunities. W.E.N. Mbowe, N. Yabu and M. Lugobi, *Applied Economics and Finance*, **3**(3), 2016, 236–257, http://dx.doi.org/10.11114/aef.v3i3.1640.

Written in stone: Remembering master faceter Art Grant. E.A. Skalwold, *InColor*, **30**, 2016, 22–29.

News Press

The big three jewels: Why ruby, sapphire and emerald top the list of precious gems. C. Besler, *Forbes*, 11 March 2016, www.forbes.com/sites/carolbesler/2016/03/11/the-big-three-why-ruby-sapphire-and-emerald-top-the-list-of-precious-gems/#6679d9f83804.*

The blood rubies of Montepuez. E. Valoi, *Foreign Policy*, 3 May 2016, http://foreignpolicy.com/2016/05/03/the-blood-rubies-of-montepuez-mozambique-gemfields-illegal-mining.*

Could more acidic oceans mean less pearls? N. Rohaidi, *Asian Scientist*, 29 January 2016, www.asianscientist.com/2016/01/in-the-lab/acidic-oceans-pearls.*

Diamonds suffer from oversupply, price falls in new era. J. Wilson, *Financial Times*, 16 March 2016, www.ft.com/cms/s/2/9f937268-c35b-11e5-808f-8231cd71622e.html#axzz4396f9KWz.*

Greed, corruption and danger: A tarnished Afghan gem trade. M. Mashal, *New York Times*, 6 June 2016, www.nytimes.com/2016/06/06/world/asia/afghanistan-lajwardeen-mining-lapis-lazuli.html?_r=0.*

How a ragtag gang of retirees pulled off the biggest jewel heist in British history. M. Seal, *Vanity Fair*, March 2016, www.vanityfair.com/culture/2016/03/biggest-jewel-heist-in-british-history.*

Inside the world's richest diamond mine [Jwaneng, Botswana]. P. Guest, CNN, 3 December 2015, http://edition.cnn.com/2015/12/03/africa/botswana-diamonds-jwaneng.*

Koh-i-Noor: India says it still wants return of priceless diamond. BBC News, 20 April 2016, www.bbc.com/news/world-asia-india-36088749.*

The shine is off diamonds and gold. E. Paton, *New York Times*, 20 March 2016, www.nytimes.com/2016/03/19/fashion/diamonds-gold.html?_r=1.*

Organic Gems

Bioactivity of Baltic amber – fossil resin. P. Tumilowicz, L. Synoradzki, A. Sobiecka, J. Arct, K. Pytkowska and S. Safarzynski, *Polimery*, **61**(5), 2016, 347–356, http://dx.doi.org/10.14314/polimery.2016.347.

A catalogue of the collections of Mexican amber at The Natural History Museum, London and National Museums Scotland, Edinburgh, UK. A.J. Ross, C.J.T. Mellish, B. Crighton and P.V. York, *Boletín de la Sociedad Geológica Mexicana*, **68**(1), 2016, 45–55, http://boletinsgm.igeolcu.unam.mx/bsgm/vols/epoca04/6801/(7)Ross.pdf.*

Examination of amber and related materials by NMR spectroscopy. J.B. Lambert, J.A. Santiago-Blay, Y. Wu and A.J. Levy, *Magnetic Resonance in Chemistry*, **53**(1), 2015, 2–8, http://dx.doi.org/10.1002/mrc.4121.

Pearls

Identification of high-luster and lusterless freshwater-cultured pearls by X-ray absorption spectroscopy. N. Monarumit, N. Noirawee, A. Phlayrahan, K. Promdee, K. Won-in and S. Satitkune, *Journal of Applied Spectroscopy*, **82**(4), 2015, 677–680, http://dx.doi.org/10.1007/s10812-015-0163-3.

Identification of "pistachio" colored pearls treated by Ballerina Pearl Co. C. Zhou, J.W.Y. Ho, S. Chan, J.Y. Zhou, S.D. Wong and K.S. Moe, *Gems & Gemology*, **52**(1), 2016, 50–59, http://dx.doi.org/10.5741/GEMS.52.1.50.*

Microstructure of iridescence-lacking pearl formed in *Pinctada fucata*. M. Suzuki, H. Mukai, H. Aoki, E. Yoshimura, S. Sakuda, H. Nagasawa and T. Kogure, *Journal of Crystal Growth*, **433**, 2016, 148–152, http://dx.doi.org/10.1016/j.jcrysgro.2015.10.014.

Relationship between luster and microstructure of seawater cultured pearl. Q. Li, E. Zhang and X. Tu, *Acta Petrologica et Mineralogica*, **35**(1), 2016, 225–230 (in Chinese with English abstract).

Synthetics and Simulants

Characterization of interfaces in mosaic CVD diamond crystal. A.B. Muchnikov, D.B. Radishev, A.L. Vikharev, A.M. Gorbachev, A.V. Mitenkin, M.N. Drozdov, Y.N. Drozdovc and P.A. Yunin, *Journal of Crystal Growth*, **442**, 2016, 62–67, http://dx.doi.org/10.1016/j.jcrysgro.2016.02.026.

Crystallization of HPHT diamond crystals in a floatage system under the influence of nitrogen and hydrogen simultaneously. G. Huang, Y. Zheng, L. Peng, Z. Li, X. Jia and H. Ma, *CrystEngComm*, **17**(34), 2015, 6504–6511, http://dx.doi.org/10.1039/c5ce01225b.

High-pressure synthesis and characterization of Ge-doped single crystal diamond. Y.N. Palyanov, I.N. Kupriyanov, Y.M. Borzdov, A.F. Khokhryakov and N.V. Surovtsev, *Crystal Growth & Design*, **16**(6), 2016, 3510–3518, http://dx.doi.org/10.1021/acs.cgd.6b00481.

HPHT synthesis of N–H co-doped diamond single crystals. C. Fang, X. Jia, N. Chen, Y. Li, L. Guo, L. Chen, H. Ma and X. Liu, *Journal of Crystal Growth*, **436**, 2016, 34–39, http://dx.doi.org/10.1016/j.jcrysgro.2015.11.042.

Méthode HPHT à température constante pour petits diamants synthétiques de forme sub-octaédrique [HPHT method at constant temperature for making small sub-octahedral synthetic diamonds]. J.C.C. Yuan, *Revue de Gemmologie A.F.G.,* **195**, 2016, 23–24.

Padparadscha or pretender: Examination of an unusual pink-orange sapphire. E.B. Hughes, C. Chankhantha, A. Burkhardt, W. Manorotkul and R.W. Hughes, *Australian Gemmologist*, **25**(11–12), 2016, 389–392.

Silicon-doped CVD synthetic diamond with photochromic effect. Z. Song, T. Lu, J. Su, B. Gao, S. Tang and N. Hu, *Journal of Gems & Gemmology*, **18**(1), 2016, 1–5 (in Chinese with English abstract).

Structure ordonnée d'une imitation d'œil-de-chat en fibres de verre: Arrangement hexagonal [Ordered structure of an imitation cat's-eye made of glass fibres: Hexagonal arrangement]. J.-P. Gauthier, A. Laurent and J. Fereire, *Revue de Gemmologie A.F.G.,* **195**, 2016, 4–8.

Swarovski joins the man-made diamond market. C. Even-Zohar, *Diamond Intelligence Briefing,* **32**(875), 2016, 1–8, www.idexonline.com/DIB_875.pdf.*

Synthesis and characterization of $NaAlSi_2O_6$ jadeite under high pressure from 4.0 GPa to 5.5 GPa. F.B. Wang, G.H. Zuo, L.J. Wang, Y.J. Zheng, X.P. Jia and H.A. Ma, *Modern Physics Letters B*, **30**(10), 2016, article 1650124, 8 pages, http://dx.doi.org/10.1142/s0217984916501244.

The synthetic diamond scam. M. Rapaport, *Rapaport Magazine*, **39**(4), 2016, 34–38.

The technology of lab-grown diamonds. M. Rapaport, *Rapaport Magazine*, **39**(4), 2016, 44–48.

Treatments

Analysis on chemical composition and heat treatment result of light yellow scapolite. Q. Ren, M. Chen, X. Li and J. Jiang, *Journal of Gems & Gemmology*, **18**(2), 2016, 34–39 (in Chinese with English abstract).

Beautifying emeralds—The perennial debate… K. Scarratt, *InColor*, special issue from the 1st World Emerald Symposium, December 2015, 50–55.

Investigation of the magnetic properties of proton irradiated type Ib HPHT diamond. N. Daya, E. Sideras-Haddad, T.N. Makgato, M. García-Hernández, A. Climent-Font, A. Zucchiatti and M.A. Ramos, *Diamond and Related Materials*, **64**, 2016, 197–201, http://dx.doi.org/10.1016/j.diamond.2016.02.019.

A simple ion implanter for material modifications in agriculture and gemmology. S. Singkarat, A. Wijaikhum, D. Suwannakachorn, U. Tippawan, S. Intarasiri, D. Bootkul, B. Phanchaisri, J. Techarung, M.W. Rhodes, R. Suwankosum, S. Rattanarin and L.D. Yu, *Nuclear Instruments and Methods in Physics Research Section B: Beam Interactions with Materials and Atoms*, **365**, 2015, 414–418, http://dx.doi.org/10.1016/j.nimb.2015.07.066.

Conference Proceedings

Amberif 2016—The 23rd Seminar on Baltic Amber in the Kaleidoscope of Time. E. Wagner-Wysiecka and B. Kosmowska-Ceranowicz, Eds., 18 March 2016, Gdańsk, Poland, 39 pages, http://amberif.amberexpo.pl/mtgsa2010/library/File/AMBERIF/2016/Amberif_2016_en_EWW_2.pdf.*

43rd Rochester Mineralogical Symposium. Rochester, New York, USA, 14–17 April 2016, 28 pages, www.rasny.org/minsymp/43rd%20RMS%20Program%20Notes.pdf.*

Compilations

***G&G* Micro-World.** Dolomite with unusual inclusions • Olivine in Oregon labradorite • Epigenetic 'footprint' in rose quartz • Phase changes in a sapphire fluid inclusion • Iridescent inclusions in scapolite • Halo in taaffeite • Lazulite in quartz. *Gems & Gemology*, **52**(1), 2016, 77–81, www.gia.edu/gems-gemology.*

Gem News International Tucson report • Notable coloured stones • Fracture-filled tourmaline • Fordite paint • Imperial topaz sculpture • Scorpion mine tsavorite update • Jewelry Television in Tucson • Paula Crevoshay collections • Wheel of Light pendant • GILC 2016 • Blue sapphires from Andranondambo, Madagascar • Red cordierite from Madagascar • Corundum from Muling, China • 'Star of David' spinel • Colourless HPHT synthetic diamonds from China • Polymer-treated hessonite. *Gems & Gemology*, **52**(1), 2016, 82–102, www.gia.edu/gems-gemology.*

Lab Notes. Rare coloured stones • Monazite inclusion in diamond with radiation halo • Screening yellow diamond melee • Emerald/emerald doublet • Oil- and Opticon-treated hydrophane • 5.03 ct blue HPHT-grown synthetic diamond • Ring with CVD synthetic diamond melee • Quench-crackled blue synthetic spinel. *Gems & Gemology*, **52**(1), 2016, 68–76, www.gia.edu/gems-gemology.*

Gem-A
THE GEMMOLOGICAL ASSOCIATION OF GREAT BRITAIN

PRESENTING

GEMSTONE PHOTOGRAPHER OF THE YEAR 2016

Have you got what it takes to be Gem-A's gemstone photographer of the year? Enter Gem-A's NEW photo competition and you could win a year's free Membership and a *Photoatlas of Inclusions in Gemstones*.

THERE ARE THREE CATEGORIES FOR ENTRY:

THE INTERNAL
Including photomicrography, gemscapes and unusual inclusions.

THE EXTERNAL
The external world of gemstones, e.g. shots of unusually cut or faceted gemstones, carvings and *objets d'art*.

THE HUMANITY IN GEMS
This category covers the life around gemstones, including mining, dealing, gemmologists at work or studying.

SUBMISSIONS
Members and current students of Gem-A only. Please submit a maximum of three entries to editor@gem-a.com, specifying your membership or student number, captions for each photo and each category of entry. Photos should be a minimum of 300 ppi. Please send files larger than 10 MB via Dropbox. Closing date for entries is Friday 2 September 2016.

WINNERS
A Member Award and a Student Award will be given. Honourable mentions will also be given for each category. Winners will be announced at the 2016 Gem-A Conference. For full terms and conditions please see our website.

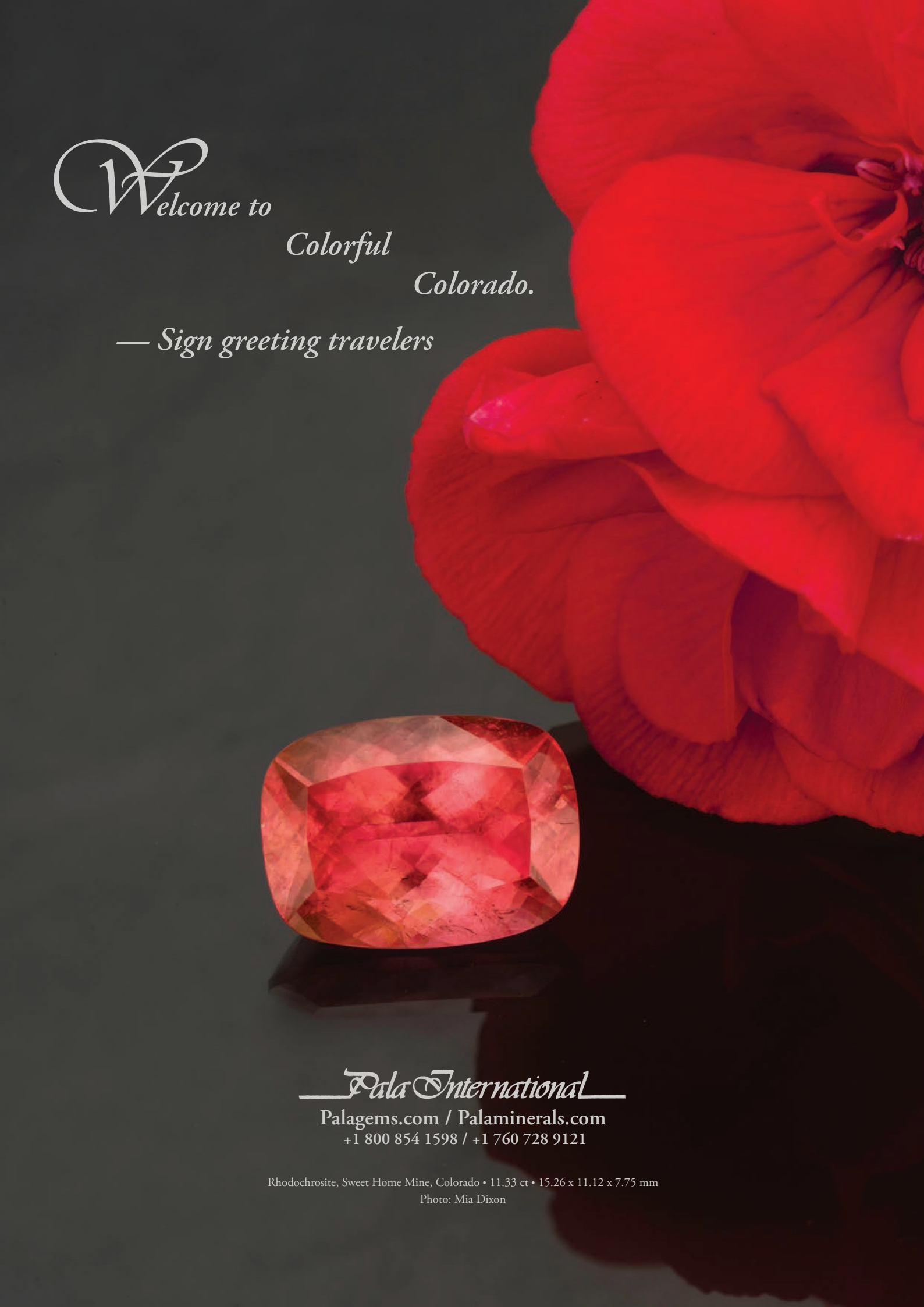

Rhodochrosite, Sweet Home Mine, Colorado • 11.33 ct • 15.26 x 11.12 x 7.75 mm
Photo: Mia Dixon